WIRELESSLY POWERED ELECTROWETTING-ON-DIELECTRIC (EWOD)

by

Sang Hyun Byun

B.S. in Materials Science & Engineering, Korea University, 2001

M.S. in Electrical Engineering, Pennsylvania State University, 2004

Submitted to the Graduate Faculty of

Swanson School of Engineering in partial fulfillment

of the requirements for the degree of

Doctor of Philosophy

University of Pittsburgh

2013

UNIVERSITY OF PITTSBURGH

SWANSON SCHOOL OF ENGINEERING

This dissertation was presented

by

Sang Hyun Byun

It was defended on

June 04, 2013

and approved by

Jung-Kun Lee, PhD, Associate Professor,
Department of Mechanical Engineering and Materials Science

C. Isaac Garcia, PhD, Full Research Professor,
Department of Mechanical Engineering and Materials Science

Zhi-Hong Mao, PhD, Associate Professor,
Department of Electrical and Computer Engineering

Dissertation Director: Sung Kwon Cho, PhD, Associate Professor,
Department of Mechanical Engineering and Materials Science

WIRELESSLY POWERED ELECTROWETTING-ON-DIELECTRIC (EWOD)

Sang Hyun Byun, PhD

University of Pittsburgh, 2013

Electrowetting-on-dielectric (EWOD) allows us to control wettability of droplets on a solid surface using electrical inputs and has been used in a wide range of applications including microfluidics, optical displays, lenses, and others. To date, however, they all have been powered in wired connections, limiting their further employments in hard-to-reach area particularly for implantable EWOD devices. One way to deal with the presented issue, a wireless EWOD system is studied and developed.

Due to compatibility of EWOD with AC (less than 1 kHz), a wireless powering as prompt method is achieved by a magnetic induction which essentially utilizes AC signal. The wireless powering with droplets actuation is verified in both using spool-type coils and planar coils. In the spool-type wireless EWOD study, the induced voltage at the receiver is much higher (~390 V) than typically required EWOD voltages (at least >50 V), which is sufficient to actuate the droplets. For reliable wireless EWOD actuation, the voltage induction has to be higher than the conventional EWOD while the current does not have to be necessarily high. Since the voltage induction is proportional to the transmission frequency, a higher voltage can be obtained by increasing the transmission frequency. However, if the transmission frequency is too high, the actuation of droplets might be limited. For an efficient EWOD actuation even at such a high transmission frequency, the system might need to be incorporated with an external demodulation circuit. This issue is addressed in the planar wireless EWOD system in which the powering

devices and EWOD electrodes are integrated by standard photolithography process. To oscillate droplets while in lateral actuation irrespective of the coil type, amplitude modulation (AM) technique is applied to the wirelessly transmitted signal. Droplet oscillations are often introduced in many applications and beneficial to reduce the contact angle hysteresis. Eventually, by employing the compact wireless EWOD system into particle collecting and mini-boat propulsion, the unnecessary and cumbersome wire connections between the device components are significantly reduced, and more convenient and flexible EWOD operation is achieved with less constraint of the space and equipment.

TABLE OF CONTENTS

LIST OF TABLES

LIST OF FIGURES

1.0 INTRODUCTION

Microfluidics deals with the precise control and manipulation of micro or even nano scale volumes of fluids. Especially, droplet-based microfluidics (sometimes referred to as digital microfluidics) in which a form of individual droplet is a basic fluid handling unit as opposed to in continuous channel flow streams, has attracted increasing attention to many researchers over the past few decades from the area of the 'lab-on-a-chip' systems for DNA and protein analysis, and biomedical diagnostics [1-4] due to its simple geometrical structure, easy operation with real-time analysis and disposability. In droplet-based microfluidics, single or multiple droplets in contact with dielectric layer are created, transported, mixed, and analyzed [5, 6] by applying DC or AC voltage across the electrodes underneath the dielectric. Droplets can be manipulated in various device geometries such that droplets are squeezed between two electrode plates (covered EWOD system) or placed on a single array of electrodes while in contact with air (open EWOD system) [4, 7, 8]. Such simplicity and versatility of EWOD can be possibly applied to a wide range of applications including optical devices such as displays [9] and liquid micro lens [10], biomedical devices such as lab-on-a-chip systems [2, 11, 12], and so on.

When the electric potential is applied across the dielectric layer, droplets tend to spread over the horizontal solid surface while the apparent contact angle at the interface (between the droplet and dielectric layer) is decreased. This change of contact angle by applying potential is well known phenomenon called electrowetting-on-dielectric (EWOD) or electrowetting [8, 13,

14]. Although droplet-based microfluidics with advances in EWOD comes into play over the extensive area prominently, there still remain several challenging tasks to be accomplished. In EWOD, as it states, the electric potential has to be applied for droplet manipulation, and most of studies have been conducted under static consideration (DC applied voltage) or low AC signal (less than 1 kHz) via a wired connection, which might limit the further applications where the wireless powering and remote control with freedom of movement is inevitably necessary (e.g., implantable passive EWOD device for drug delivery, capsule endoscope and water floating or submarine EWOD device).

There has been wireless EWOD report by Mita *et al.* [15] using commercial spool-type coils as opposed to the conventional powering method. In their study, they demonstrated that a wireless powering could be applied to a floating EWOD device to produce movement. However, the driving voltage is ~15 V (RF power transmission), which is not suitable for full droplet actuation. Generally, the voltages needed for EWOD actuations are typically very high while the current is very low, although some lower voltages have been reported [16, 17]. Simultaneously, there have been driving forces to develop a miniaturized and integrated EWOD devices that will allow reduced consumption of samples, shorter analysis times, and portability for biological or medical applications [18-20]. With aid of microfabrication techniques, such as photolithography process, that are originally from the semiconductor industry, it became possible to fabricate the integrated EWOD devices and perform more complex analysis. To our best knowledge, however, the effort of making transition from EWOD components to compact wireless EWOD device has not been intensively made yet, which will provide much simple and liberal operation of EWOD. In this regards, this study is stimulated to realize EWOD to be functional with wirelessly transmitted electric signal.

To achieve the motivated ideas, the main objective is divided into several sub-topics. Firstly, preliminary but important study of AC electrowetting in a wired powering is performed and investigated. In AC electrowetting study, voltage division of the EWOD is studied by introducing an electrical circuit model. Secondly, in-depth study of amplitude modulation (AM) technique with simple demodulating circuit is also provided and investigated to suggest an efficient way to increase the span of contact angle and oscillation at the contact line. Thirdly, in order to demonstrate successful droplet's lateral transportation (which is essentially required for further application) via wireless powering, spool-type homemade coils is introduced. The voltage required for EWOD operation is achieved by magnetic induction. To oscillate the droplet while in transportation, and thus mitigate adverse effects of friction (contact angle hysteresis), AM scheme is also employed and applied to the wirelessly transmitted signal. Fourthly, after the verification of the wireless EWOD operation via spool-type coils, a planar coil with EWOD array electrodes on a single chip are provided on printed circuit board (PCB). By employing a demodulation circuit, droplet's lateral transportation while in oscillation is demonstrated. Finally, the planar wireless powering is further applied for the particle collection and mini-boat propulsion operated by EWOD principle. The presented wireless powering with EWOD will contribute to the area where the remote control via wireless powering is essentially required for fluid operations by simple design and fabrication.

2.0 BACKGROUND

2.1 ELECTROWETTING-ON-DIELECTRIC (EWOD)

2.1.1 Principle of EWOD

Electrocapillarity, the foundation of electrowetting, was first recognized over a hundred years ago by Gabriel Lippmann [21]. In electrowetting, one is generically dealing with droplets of partially wetting liquids on planar solid substrates [22, 23]. With electrowetting a voltage is used to modify the wetting properties of a solid material. A thin dielectric layer to overcome intrinsic obstacle such as electrolytic decomposition of droplets upon applied voltages was developed by Berge [24, 25]. This is the concept that has become known as EWOD. The most basic form of a modern electrowetting structure consists of a sessile droplet, planar dielectric, a planar substrate, and DC voltage source as illustrated in Fig. 1(a).

Electrowetting deals with the use of an externally applied electric field to actuate or manipulate tiny volumes of liquid droplet by modifying solid/liquid interfacial tension and hence the apparent (macroscopic) contact angle. Especially, advances in EWOD technology combined with droplet-based microfluidics have become one of the most efficient methods for driving single or multiple droplets [1, 7].

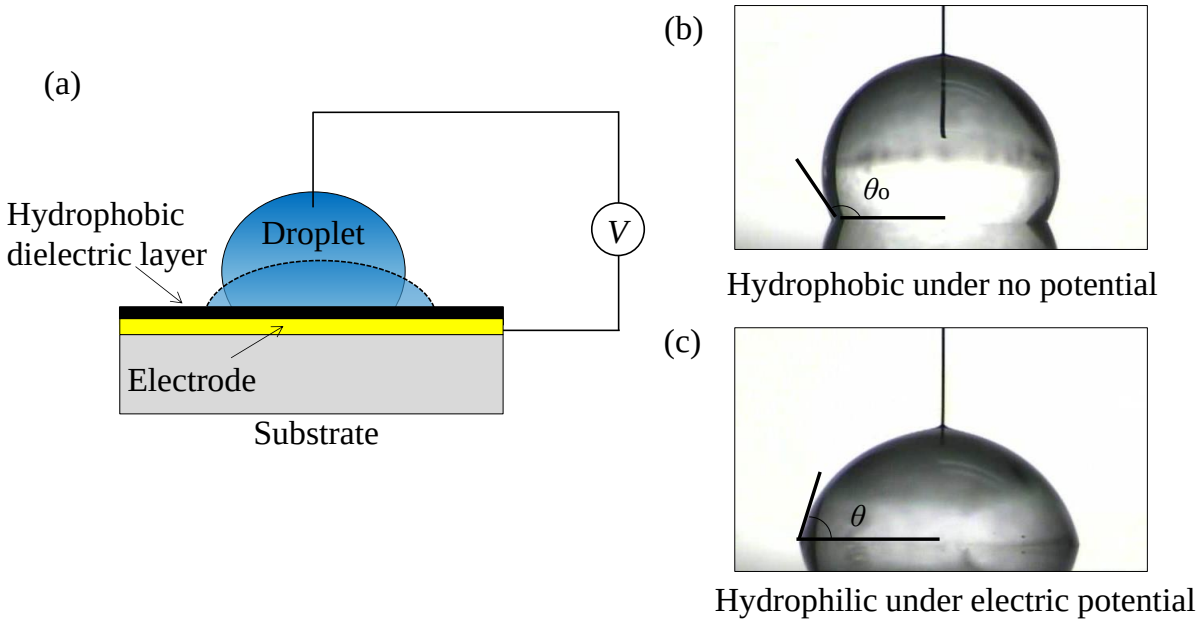

Figure 1. Principle of electrowetting on dielectric. (a) Typical configuration of EWOD. (b) Photo of a sessile droplet under no poetetial (hydrophobic). (c) Photo of a sessile droplet under electirc potential (hydrophilic, 5 µl of volume).

An example of such modified wettability is illustrated in the photos of Fig. 1(b) and (c). The photo in (b) shows a sessile droplet on a hydrophobic surface. In this stage, the water droplet is not favorable to be in contact with the surface and therefore minimizes the contact area. The droplet spreads and the wettability over the surface increases strongly, when a potential difference is applied between the electrode in the water droplet and electrode present underneath the hydrophobic dielectric layer as shown in the photo (c). When the voltage is removed, the droplet returns to the original stage as indicated in Fig. 1(b). With proper selection of dielectric materials relatively large and reversible contact angle changes could be achieved [26, 27]. EWOD can be described in the following Lippmann-Young equation [14].

$$\cos\theta = \cos\theta_o + \frac{c}{2\gamma_{LG}}V^2 \quad (1)$$

where θ_o is the initial contact angle when the applied voltage V to the dielectric layer is zero, θ is the modulated contact angle, c is the specific capacitance (F/m^2) of the dielectric layer, and γ_{LG} is the interfacial tension between air and water (~0.072 N/m). Note that $c = \varepsilon_o\varepsilon_d/t$ where ε_o is the permittivity of free space (8.85419×10^{-12} F/m), ε_d is the dielectric constant of the dielectric layer, and t is the thickness of the dielectric layer.

According to Lippmann-Young equation, the change of contact angle is a consequence of the electrostatic energy induced and stored in the capacitor formed by the droplet, dielectric layer and electrode system. In droplet-based capacitor configuration, fringe effected usually are neglected, thus all the electrostatic energy is stored in a plate capacitor (dielectric layer) formed by droplet base area and electrode [28]. Since the change in the cosine of the contact angle is directly proportional to the applied voltage, advancing and receding of the droplet can be actively made and controlled.

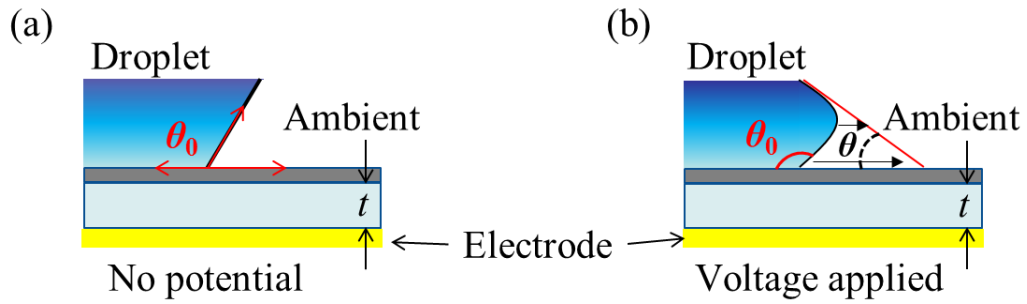

Figure 2. Diagrams of electrowetting basics in microscopic scale. Young's contact angle θ_o under no potential (a) and contact angle when potential applied (b). While electromechanical force is acting toward ambient from droplet, the Young's contact angle θ_o remains same.

Contact angle is referred as an apparent contact angle or macroscopic contact angle [29, 30]. As shown in Fig. 2, the induced charge stored under applied voltage near the contact line will provide an electric field with a partial component in parallel with solid/liquid interface direction. Application of voltage therefore results in a horizontal electromechanical force per unit length (N/m) that is directed from the water droplet toward the ambient. This electromechanical force results in the contact angle decreases (θ) to a new value of V macroscopically. However, the microscopic or local contact angle (θ_o) remains same [28, 31]. The transition between θ_o and the macroscopic contact angle θ occurs over a distance comparable to the dielectric thickness of *t*.

2.1.2 Wetting Property of Droplet

2.1.2.1 Shape of Droplet

The importance of droplets in microfluidics is obvious particularly in the presence of the capillarity and surface tension effects. More often than not, it is easily observed that relatively large droplets on surfaces take a flattened shape, whereas small droplets take a spherical shape. This simple observation give rise to fundamental questions particularly when one makes an effort to understand droplets physic.

There are two common forces acting on droplets by which droplets can take two different shapes. If the surface tension solely acts on the droplet, droplets will take a spherical shape, however on the other hands, droplets will take a flattened shape under force balance between gravity and surface tension [32, 33]. This shape transition can be better understood by the scale length or capillary length *l*. The capillary length is defined by the ratio between the Laplace pressure and the hydrostatic pressure as given in Eqn. (2) [34].

$$\frac{\Delta P_{Laplace}}{\Delta P_{hydrostatic}} = \frac{\frac{\gamma}{l}}{\rho g l} \tag{2}$$

where γ is the surface tension, ρ the density, and g the gravitational constant. The capillary length l then can be found when the Laplace and hydrostatic pressure reaches same order, that is,

$$l \approx \sqrt{\frac{\gamma}{\rho g}} \tag{3}$$

where l is the capillary length. This capillary length is useful to determine whether the droplet takes a spherical or flattened shape [34]. For example, the region where a dimension of the droplet is smaller than the capillary length, the droplet will have a shape resembling that of a spherical cap, whereas the droplet shape is flattened by gravity when a dimension of the droplet is larger than the capillary length.

In addition, a dimensionless number known as the Bond number can be also derived from the capillary length l given in Eqn. (3) yielding a similar meaning. The Bond number is expressed by

$$B_o \approx \frac{\rho g R^2}{\gamma} \tag{4}$$

where R is the radius of the droplet [32]. This dimensionless number also gives meaningful prediction. If B_o is smaller than unity, which implies that the surface tension is dominant, then the droplet takes a spherical shape, other else the gravitational force flattens the droplet on the surface. The capillary length typically is ~2 mm for most liquids.

2.1.2.2 Droplet on Rough and Inhomogeneous Surface

Unlike ideal surfaces in which Young's equation is derived, in reality, surface contains a lot of imperfections such as defects like particles, chemical residues and so on [35-37]. Even carefully micro-fabricated EWOD electrodes might have somehow surface imperfections [38]. Such surface imperfections result in textured surface (roughness: vertical deviation over the projected surface). Wenzel and Cassie models (illustrated in Fig. 3) are the well-known main models that describe the wetting property of the droplet on rough surfaces [36]. One can imagine that the rough surface can have two different conditions, one is homogeneous and the other one is inhomogeneous.

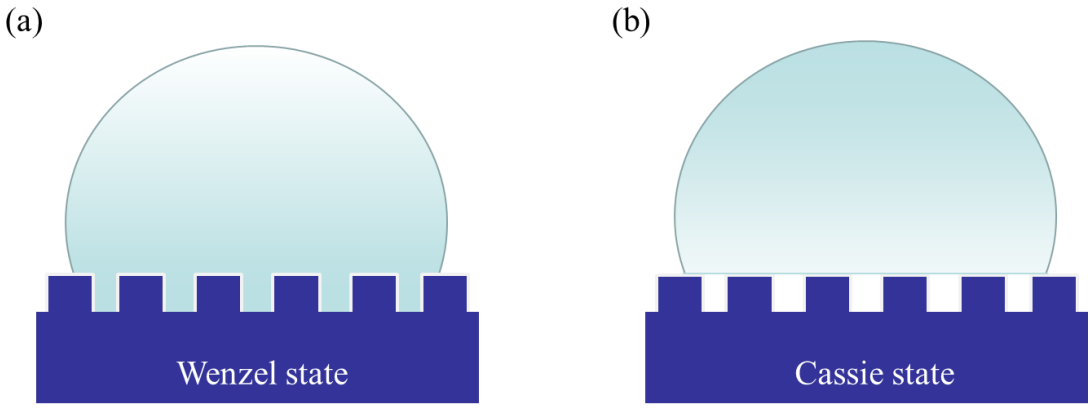

Figure 3. Droplet sitting on a rough surface (a) Wenzel state and (b) Cassie state

The Wenzel model explains the homogeneous conditions having roughness parameter *r* (*r* always greater than 1 by definition). In Wenzel state as illustrated in Fig. 3 (a), the droplet fills the trenches below the liquid and thus occupies more surface area [32, 36, 37]. According to the Wenzel's equation in the presence of roughness *r*, the contact angle θ^* is a function of Young's contact angle θ multiplied by parameter *r*.

$$\cos\theta^* = r\cos\theta \tag{5}$$

The roughness will decrease the Wenzel's contact angle θ^* when the apparent Young's angle θ is under 90° whereas will increase θ^* when the θ^* is over 90°. Thus, the increased roughness will amplify both hydrophilicity and hydrophobicity [32]. Figure 4 shows the droplet sitting on the ideal (a) and rough surface (b) respectively. For the hydrophilic wetting (top in Fig. 4), the contact angle in the presence of the roughness is smaller than Young's angle, while the contact angle is larger than Young's angle for hydrophobic wetting as illustrated in Fig. 4 bottom. However, these equations only apply when the drop size is sufficiently large compared with the surface roughness scale [32].

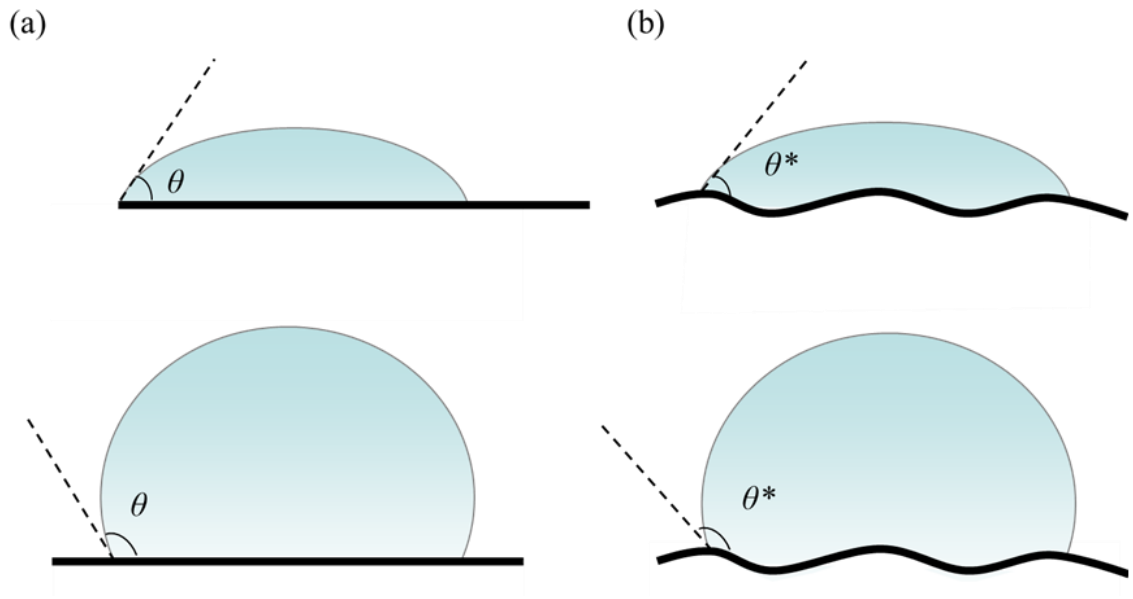

Figure 4. Contact of droplet on an ideally flat surface (a) and a rough surface (b).

In the Cassie model as illustrated in Fig. 3(b), the droplet sits on the surface without filling the trenches left air pocket below the droplet [32, 36, 37]. The surface area occupied by the droplet is less than it would be on the flat surface or the rough surface in the Wenzel state. In

the Cassie state, a different set of equations are used to define this condition. The contact angle in the Cassie state is given as [32, 36],

$$\cos\theta^{*} = \sum f_i \cos\theta_i \qquad (6)$$

where *i* denote the different chemical components of the surfaces. This is known as the Cassie–Baxter relation [32]. The Cassie–Baxter relation shows that the contact angle of the droplet sitting on a microscopically inhomogeneous surface is the summation of the cosine of the contact angles on the different chemical components of the surface. Since the Cassie–Baxter relation explains a chemically inhomogeneous surface (i.e. micro-fabricated surface coated with thin chemical layer), the wetting properties are not those that were intended, thus the wetting properties are then modified according to this relation.

2.1.3 EWOD Actuation

The concept of EWOD that is based on the modulation of surface tension is an attractive method for droplet actuation since surface tension is dominant in the micro range. An electric potential applied to the local area of the droplet base (not to the entire base area of the droplet) generates an asymmetric force balance (gradient of wettability) with interfacial tensions, whereby the droplet can be transported laterally [39]. This is the principle of the electrowetting based micro-actuation.

Typical micro droplet actuation system by EWOD is illustrated in Fig. 5 [34]. The droplet (typically less than few mm in diameter) surrounded by air or other immiscible liquid (e.g., silicone oil) is squeezed between the top and bottom plates. The top plate usually consists of a single and transparent ground electrode, while the bottom plate consists of an array of discrete

addressable EWOD electrodes. The optimal EWOD electrode and droplet size can be determined for which a droplet sitting on in the center of one electrode slightly covers all adjacent electrodes [4]. Both plates contacting the droplet are coated by a hydrophobic material (typically Teflon or Cytop).

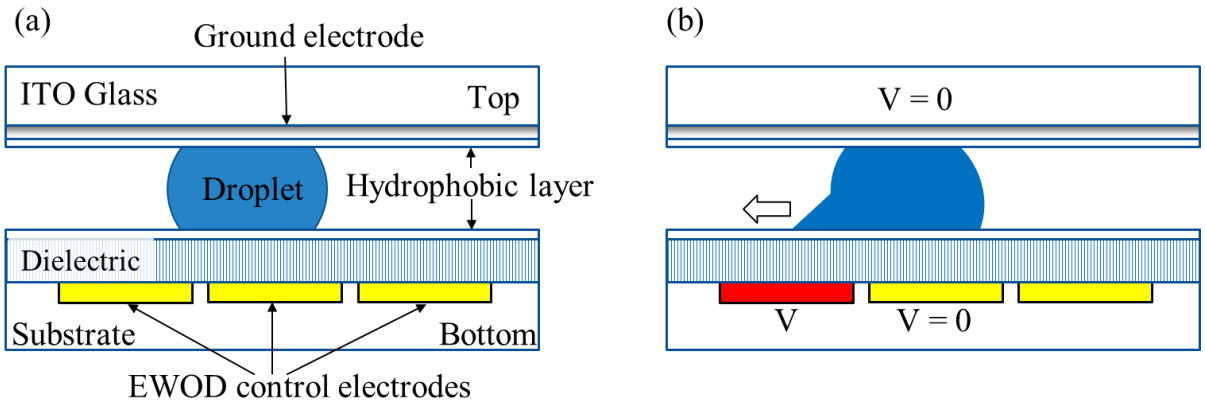

Figure 5. (a) Cross section view of typical EWOD actuation configuration. (b) The next adjacent control electrode activation to move the droplet by EWOD principle.

As illustrated in Fig. 5(b), when a voltage is applied to the bottom electrode (red colored electrode in the figure) overlapping a portion of the droplet and hydrophobic interface, the electromechanical force acting on the contact line enables for the droplet to move and re-arrange with the charged electrode. By step by step electrode activation, a droplet can be transported between two adjacent arrays of electrodes [4, 5, 7]. Electrowetting driven droplet actuation can usually be achieved by more than 40^{o} variation of contact angle change [40]. Ohmic losses are possibly prevented due to the insulating layer from the liquid [41]. Since the droplet motion is essentially governed by surface tension forces and Young's contact angle at the liquid/solid interface, the size of the EWOD electrodes is the important factor to control the droplet motion

and manipulation. Usually, when the size of the electrodes is reduced, the size effect of the EWOD electrodes will be acting even more.

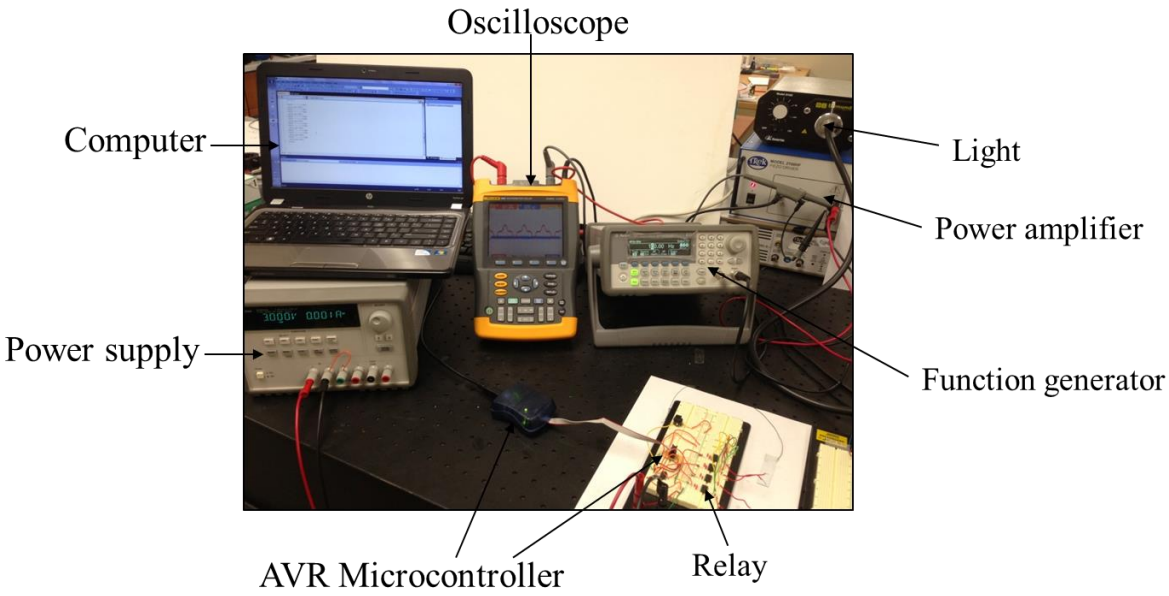

Figure 6. The typical equipment for EWOD (droplet) actuation.

When we are considering the droplet in motion, however, the electrowetting always exhibits the contact angle hysteresis at the contact line [42-44]. When the applied voltage is increased, a droplet tends to spread over the area. This situation gives rise to an advancing contact angle. In contrast, when the voltage is decreased, the droplet tends to recover its original (equilibrium) shape by reducing the contact area. This situation also give rise to a receding contact angle. By experimental observations, it is consistently observed that the advancing contact angle is always larger than the receding contact angle for a given electrowetting voltage [45, 46]. Thus, the conact angle difference between the advancing and receding situation can be defined as the conatact angle hysteresis in electrowetting [46]. The typical hysterisis angle for DI water surrounded by silicone oil is around 1.5^{o} to 2^{o} while the hysteresis DI water surrounded by

air has a much larger hysteresis angle of between 7^o and 9^o [42]. Therefore, contact anglehysteresis can have an important effect on droplet in motion and manipulation by electrowetting [43].

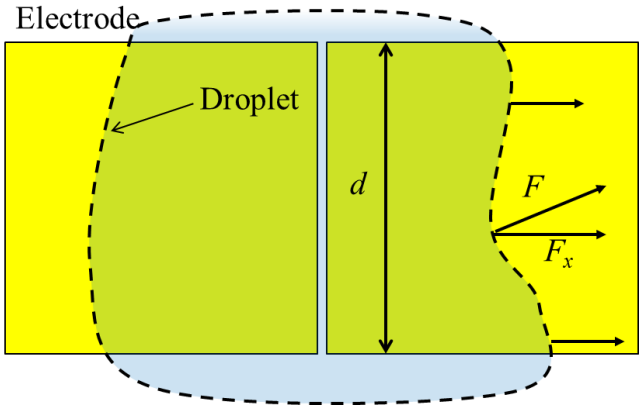

Figure 7. Droplet sitting on the electrodes.

In the presence of the hysteresis, the minimum required voltage for the droplet actuation can be calculated by considering the contact of droplet on the EWOD electrodes as sketched in Fig. 7. The capillary force acting on *x*-direction is given

$$F_x = d\gamma(\cos\theta - \cos\theta_o). \tag{7}$$

By considering the contact angle hysteresis (α) into Eqn. (7), the advancing and receding capillary forces are given as below.

$$F_x^A = d\gamma(\cos\theta + \alpha)$$

$$F_x^R = -d\gamma(\cos\theta_o - \alpha). \tag{8}$$

This equation can be re-arranged under the assumption that the contact angle hysteresis (α) is small compared to Young's value (θ and θ_o).

$$\begin{aligned} F_x^A &= d\gamma[\cos\theta - \alpha(\cos\theta + \sin\theta)] \\ F_x^R &= -d\gamma[\cos\theta_o - \alpha(\cos\theta_o - \sin\theta_o)]. \end{aligned} \tag{9}$$

Then the total capillary force acting on *x*-direction is

$$F_x = d\gamma[\cos\theta - \cos\theta_o] - d\gamma\alpha[\cos\theta + \sin\theta - \cos\theta_o + \sin\theta_o]. \tag{10}$$

By plugging the first term on the right hand side in Eqn. (10) into the Lippmann-Young equation and by the limited condition for minimum displacement of droplet, the relation can be written as

$$\frac{d}{2}cV^2 - d\gamma\alpha[\cos\theta + \sin\theta - \cos\theta_o + \sin\theta_o] > 0. \tag{11}$$

By re-arranging the Eqn. (11), it can be obtained that

$$V_{\min}^2 = \frac{2\gamma}{c}\alpha[\cos\theta + \sin\theta - \cos\theta_o + \sin\theta_o]. \tag{12}$$

Finally, Eqn. (12) can be simplified by

$$V_{\min} \approx 2\sqrt{\frac{\gamma\alpha\sin\theta_o}{c}} \tag{13}$$

As it can be seen by Eqn. (13), the contact angle hysteresis (α) is responsible for the minimum or threshold potential. In addition, a large capacitance, a low droplet surface tension, a large Young's angle can minimize the value of the voltage required to move droplets. In the absence

of contact angle hysteresis, the droplet would be able to move under the smallest of applied voltages.

2.2 WIRELESS POWERING

Historically, wireless powering traces back to Tesla's famous experiment [47] in which a 142-foot-tall, 12-million-volt electric coil in Colorado Springs transmitted electricity wirelessly across 25 miles and illuminated 200 lamps with the charge. Recently, Marin Soljacic [48] reported a remarkable wireless powering experiment. In the experiment, resonant coupling, for which the transmitting and receiving coils were tuned and resonated at the same frequency, sent wireless electricity across a room to light a 60-watt bulb over distances 2 meters with ~40% efficiency. The efficiency was much higher than Tesla's. This experiment promoted the notion of wireless powering, which is currently a hot research area.

The wireless powering technique can be divided into two main modes by the wave characteristics of an electromagnetic (EM) field [49-51]. The EM sources such as oscillating charge, antenna or coil can generate EM wave into space or media. The EM wave contains both a reactive and a radiating characteristic depending on the distance from the source. The boundary of these two modes is usually described by the wavelength λ of the source EM from the circuit [52, 53].

The reactive mode is generally regarded as in the region where the wavelength λ of the EM source is divided by 2π. Due to its close distance from the source, this region is often referred to as a near-field region. In this region, the EM source of a system only interchanges its energy with a load when it is needed, and does not radiate energy when not needed. Beyond the reactive and transition mode, (the transition mode is usually accepted a range after the reactive mode up to the region of 2λ), the radiating mode is extended from 2λ out to infinite space. Thus, this region is referred to as a far-field region. In this region, the system's energy propagates and transfers by the omni-directional radiation into the media [53]. In near-field region, EM field

generally decays with $1/r^2$ (where r is the average distance from the source), while decays with $1/r$ in the far-field region [53, 54]. Thus, if a certain operating frequency is selected far from the source, the radiating mode is more dominant due to the rapid decay of the reactive mode.

2.2.1 Magnetic Induction

An efficient wireless powering for EWOD can be accomplished by magnetic induction which essentially uses AC for power transmission and relies on non-radiative mode. Since AC frequency (typically less than 1 kHz) is usually employed for EWOD operation, AC depending magnetic induction is suitable technique to be introduced for wireless powering method for EWOD.

In this method, a power is efficiently transmitted when the receiver coil is close to the transmitter coil. The idea of magnetic induction is based on electromagnetism that interchanges energy from one coil to another [55], which is known as Faraday's law of electromagnetic induction [56]. The alternating current flow through the primary or transmitter coil (coil 1 in Fig. 8) creates a magnetic flux, which then induces a voltage in the secondary or receiver coil (coil 2 in Fig. 8). The current I_1 sets up the magnetic flux through the secondary coil when the secondary coil is placed in the magnetic field produced by the primary coil. If this flux is changed by the changing the current I_1, voltage drop (induction) appears between its terminals [57]. This voltage can be used to power a EWOD device.

The set-up for wireless powering is very similar to that of the transformer. However, the main difference is that there exists an air gap between the primary and secondary coils. The magnetic induction has been widely used for all kinds of electronic devices because it is simple, efficient, and safe.

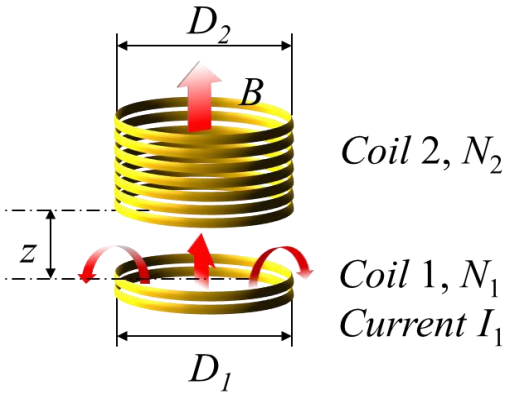

Figure 8. A schematic of wireless powering using inductive coupling. The transmitter (coil 1) carrying current I_1 induces an electromotive force in the receiver (coil 2). N_1 and N_2 denote the number of turns of each coil.

The attainable electromotive force (EMF) or voltage in the secondary coil strongly depends on the geometrical properties including N_1, N_2 (number of turns of each coils) and the size of coils (D_1 and D_2). The electromotive force (EMF) ε_{21} measured in volts in the secondary coil with the carrying current I_1 in the primary coil is given by [56, 58]

$$\varepsilon_{21} = -N_2 \frac{d\Phi_{21}}{dt} = -M \frac{dI_1}{dt} \tag{14}$$

where ϕ_{21} denotes the magnetic flux (Wb) per turn in the secondary coil generated by current I_1 in the primary coil and M is the mutual inductance (H). According to Eqn. (14), the change in the magnetic flux in coil 2 over the time is proportional to the time rate of change of the current in coil 1. This implies when the frequency of the flux is increased, the induced voltage in coil 2 will be also increased. It is obvious that high voltage induction can be achieved by selecting high transmission frequency.

The efficiency in magnetic induction depends on several parameters such as the coupling coefficient k and coil's quality factor Q [59, 60]. The coupling coefficient is determined by geometrical factors, such as the separation distance (z in Fig. 8) between the coils (transmitter and receiver coils) and the relative coil size D_1 and D_2. The coupling can be further determined by the shape of the coils and the angle between them [59]. If the receiver coil is at a proximity distance to the transmitter coil, a fraction of the magnetic flux, which is generated by the transmitter coil, links to the receiver coil and contributes to the power transmission. The more flux links to the receiver coil, the better the coils are coupled. The definition of the coupling coefficient k is given by,

$$k = \frac{M}{\sqrt{L_1 \times L_2}} \tag{15}$$

where M is the mutual inductance, L_1 and L_2 are the inductance of each coil. The coupling coefficient k can have a value between 0 and 1. For ideally perfect coupling where k = 1, all magnetic flux generated link to the receiver coil without leak flux, while k = 0, when transmitter and receiver coils are not mutually interact each other, results in no magnetic flux links.

The inductance of coil can be defined in several ways. A popular definition of inductance is made by considering the magnetic flux that is given by [58],

$$L_1 = \frac{N_1 \phi_1}{I_1} \tag{16}$$

where L_1 is the inductance (H), I_1 is the current (A), ϕ_1 is the magnetic flux (Wb), and N_1 is the number of winding turns of coil 1 (same for the coil 2). The flux produced by current in a coil (and thus the inductance of the coil) can be further increased by winding the coil around a

magnetic material. By similar way, the mutual inductances $M_{21}$and M_{12}, which describes the magnetic coupling between two coils, can be defined by:

$$M_{21} = \frac{N_1\phi_{21}}{I_2} = M_{12} = \frac{N_2\phi_{12}}{I_1} = M \tag{17}$$

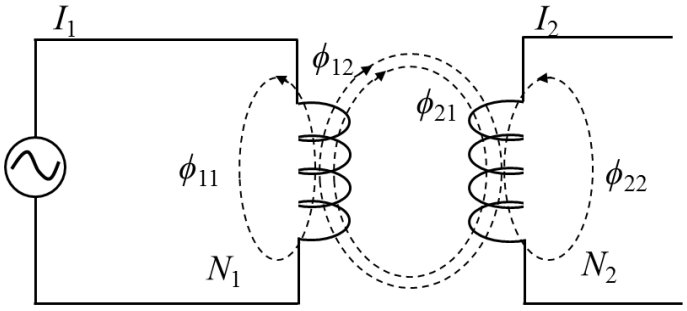

Figure 9. Magnetically coupled two coils.

For the magnetically coupled coils in Fig. 9, the currents I_1 and I_2 produce magnetic flux in each coils, where ϕ_{11} is the flux only at coil 1 produced by the current I_1, ϕ_{12} is the flux produced by the current I_1 that links both coils, ϕ_{22} is the flux only at coil 2 by the current I_2, and ϕ_{21} is the flux produced by the current I_2 that links both coils. The mutual inductance M is positive when the currents in the each coils flow in the same direction, and vice versa [61]. In practice, since not all of the flux produced links every turn of the coil, the fluxes usually refer to the effective fluxes.

Another parameter Q (quality factor) can be defined by the ratio of power stored in the coil to the power losses in the coil. For a coil having inductance L and resistance R at given frequency ω (=$2\pi f$), the quality factor Q of a coil is given by [62],

$$Q = \frac{\omega L}{R} \tag{18}$$

According to above definition, the quality factor Q can have a value between 0 and infinity. Achieving high quality factor is important especially in high frequency operating range (i.e. RF ~MHz) since Q is directly related to the loss of power. If total coil length increases to obtain high inductance, it also gives rise to the resistive loss and thus decreases the coil quality factor.

It is expected that the skin depth (δ) also plays role as the frequency increases. The skin depth can be defined to as [63]

$$\delta = \sqrt{\frac{2\rho}{\omega\mu}} \tag{19}$$

where ω is the angular frequency, ρ is the resistivity of the conductor and μ is the absolute magnetic permeability. As the frequency increases, the skin depth decreases, which implies that the effective area of the conductor is also decreased as illustrated in Fig. 10 and results in increased resistance of the conductor at given frequency. Once the conductor material and operating frequency are selected, the skin depth can be easily calculated. The skin depth of Cu with the frequency is listed in Table 1.

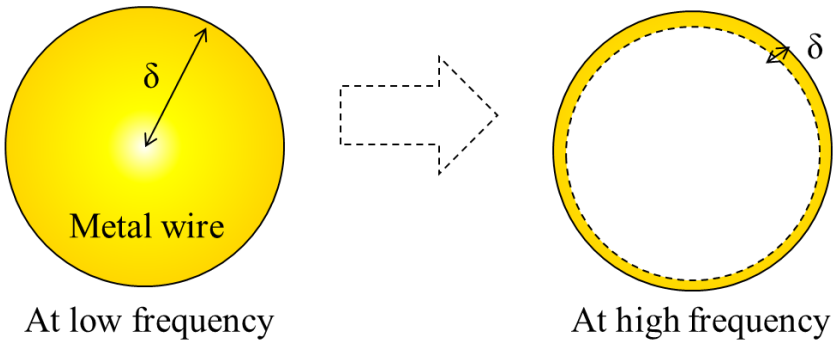

Figure 10. A schematic of skin depth effect. As frequency increases, the effective area of the conductor decreases resulting in increased effective resistane.

Table 1. Calculated skin depth of Cu wire over frequency.

Frequency	Skin depth δ [μm]
60 Hz	8470
10 kHz	660
100 kHz	210
1 MHz	66
10 MHz	21

Another way to enhance the efficiency of the wireless powering can be achieved when the transmitter and the receiver coils are tuned at the same frequency by adding charge storage devices in both sides such as capacitors [23, 24], while interacting weakly with other off-tuned frequency. The method is based on the resonant coupling of two circuits (the fact that two same-frequency resonant objects tend to be coupled), and, in particular, resonant evanescent coupling (where the coupling mechanism is mediated through the overlap of the non-radiative near-fields

of the two objects). This well-known physics leads to the result that energy can be efficiently coupled between objects in the extremely near field (e.g. within the distance < $\lambda/2\pi$) [53, 54].

The resonant frequency of L-C circuit is given by

$$f_{res} = \frac{1}{2\pi\sqrt{LC}} \tag{20}$$

where L is the inductance (H) and C is the capacitance (F). The resonant power transmission is a special but widely used method for efficient wireless non-radiative mid-range (~few m to 10 m) energy transfer [48, 52].

2.2.2 Wireless Powering Devices

2.2.2.1 Coil Design Consideration

In this study, two types of wireless powering devices are employed and designed. One is a spool-type homemade coil and the other one is a planar coil fabricated on printed circuit board (PCB) by photolithography process. Since the spool-type coil is easy with the inductance control by changing number of winding-turns and has no physical size limit, it is good to start with this type of coil as a preliminary wireless powering study. Whereas it is frequently appeared in modern EWOD structure, most of droplet-based EWOD devices have a planar structure for the droplet transportation along the discrete electrodes. For the planar coil, therefore, the EWOD device can be possibly integrated with the planar coils on PCB simultaneously since the fabrication process for both devices are compatible with the standard photolithography.

Regardless of the coil type employed in this study, in EWOD operation point of view, the attainable induction voltage across the dielectric layer in the EWOD which is placed at the

receiver has to be high (at least > 50 V). At the same time, in the transmission frequency point of view, the higher transmission frequency is favorable to attain a higher induction voltage at the receiver. More importantly, however, the major portion of the induction voltage at the receiver should be applied to the dielectric layer to guarantee a significant change in the contact angle of the droplet. Therefore, it is important for reliable EWOD operation that the transmission frequency needs to be comprised with the EWOD operational voltage.

2.2.2.2 Spool-type Coil

EWOD works with AC frequency (less than 1 kHz), however, it is not clear yet whether wirelessly operated EWOD beyond upper AC frequency limit would be successfully working or not. In this regard, a type of coil easy with the inductance control (accordingly easy control of the transmission frequency) is suitable to be adopted as an initial wireless EWOD study.

Usually, the transmitter coil has less criterions limits in many applications as opposed to the receiver coil, as far as the current change upon the polarity change is rapid and the magnetic flux can be efficiently linked to the receiver coil [56]. The efficiency of magnetic flux links strongly depends on the geometrical parameters of coil such as size or distance between two coils. In order not to lose the magnetic flux into media for a better magnetic coupling between two coils, a comparable size of each coil would be preferred. In addition, if a magnetic material such as ferrite is placed in a magnetic field, the magnetic flux lines will be re-oriented through the magnetic material due to its high permeability resulting in high flux density [64].

Cu (250 μm in diameter) wire covered by insulating polymer (250 μm) is employed for both transmitter and receiver coils. The inner diameter of the coils is 2.3 cm having a cylindrical shape. The transmitter coil has 25 winding-turns around a ring shaped air-core ferrite and measured inductance is 0.055 mH. The receiver coil has 250 winding-turns around an air core

without ferrite and measured inductance is 2.93 mH. Figure 11 shows a photo of the homemade spool-type coils.

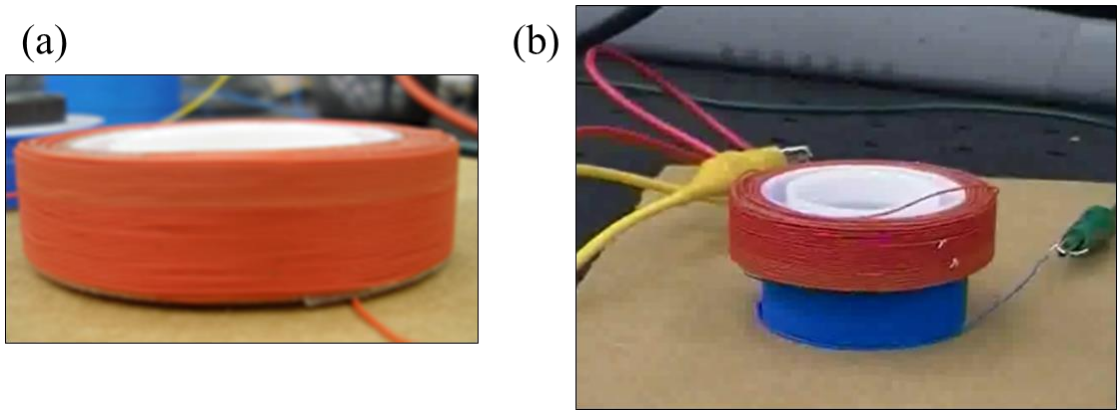

Figure 11. Homemade spool-type coils. (a) Receiver coil having 250 winding-turns, (b) Receiver coil on the top of the transmitter coil having 25 winding-turns.

2.2.2.3 Planar Coils on PCB

The design of the planar coil on PCB is restricted by its dimension (7×6.5 cm^2) which possibly drives the transmission frequency higher than that of the spool-type coils. Although higher transmission frequency will reduce component value and size, losses will also increase due to skin depth effect.

Accuracy in designing a planar coil is important because it is difficult to modify the inductance once it is built on the PCB. Numerous research works have been carried out to fabricate and integrate high *Q* coils on silicon [65-67]. However, these integrated coils on silicon have some substantial disadvantages such as large silicon area consumption, high substrate loss, and high DC resistance (several ohms) [68]. Instead, using PCB has several advantages such as the low cost and simple fabrication. Since the board substrate is nearly perfect dielectric, the resistive losses in conductors as well as dielectrics are reasonably ignored. More importantly,

planar coils and EWOD device can be simultaneously fabricated on the PCB by the standard MEMS fabrication process due to its compatibility with the photolithography process.

The inductance of planar type coil can be roughly estimated by using Wheeler's equation [69]. For rectangular (or square) shape of coil, the inductance can be estimated as below,

$$L = \frac{K_1 \mu_o n^2 d_{avg}}{1 + K_2 \rho} \tag{21}$$

where K_1=2.34, K_2=2.75 (coil shape depending coefficients), n is the number of turns. d_{avg} and ρ (fill ratio) are also given as,

$$d_{avg} = \frac{d_{out} + d_{in}}{2} \quad \text{and} \quad \rho = \frac{d_{out} - d_{in}}{d_{out} + d_{in}} \tag{22}$$

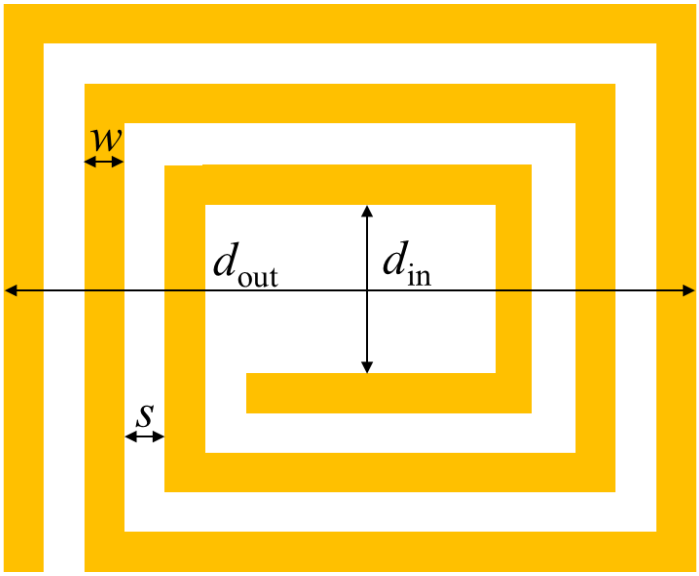

Figure 12. Rectangular planar coil having the line width of w=70 µm and line spacing of s= 0 µm. d_{in}=1.38 cm d_{out}=36 cm for 42 winding-turns of planar coil.

The rectangular shape having different number of winding-turns (20, 42 and 50) are designed while the line width (*w*) and line spacing (*s*) are same regardless of winding-turns. For the coil 42 winding-turns having the initial dimensions of 80 µm line width (*w*) and 40 µm line spacing (*s*) with 15 µm Cu thickness as illustrated in Fig. 13(a), the calculated inductance by using the Eqn. (21) is ~54 µH whereas the measured inductance is ~30 µH. The range of the inductance is several orders of magnitude smaller than that of spool-type coils implying that the transmission frequency should be increased to obtain high voltage induction at the receiver.

The discrepancy in final dimension is also observed due to the under-cut after wet-etching. As it appears in the microscope image (Fig. 13(b)), the final dimensions after the wet-etching are altered by approximately 30 µm (comparable to Cu thickness 2x) reduction in line width while increase 30 µm in line spacing compared to the initial dimensions.

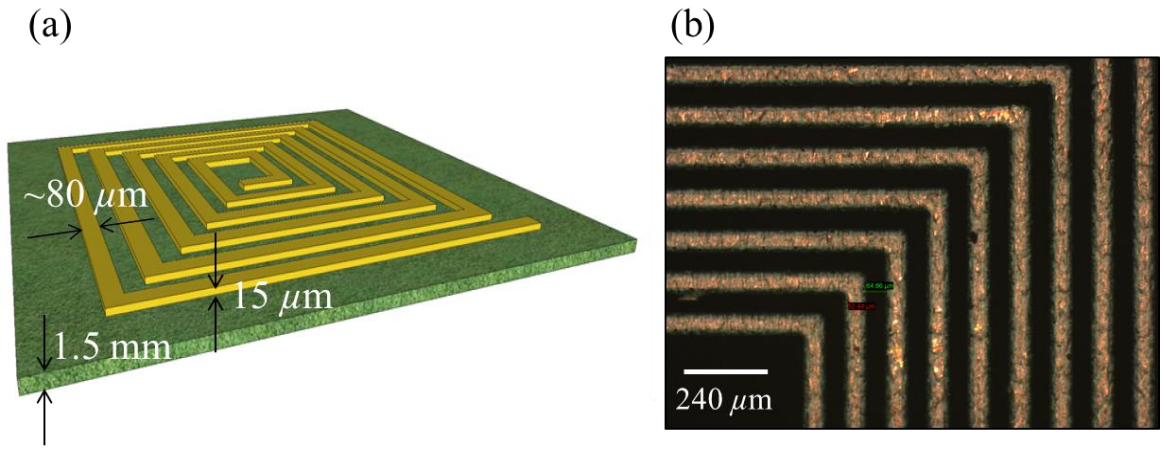

Figure 13. (a) Schematic of planar coil on PCB with 80 µm of the coil width and 40 µm of coil spacing. The copper thickness is ~15 µm and the board thickness is 1.5 mm. (b) Photo of micro-fabricated planar coil on PCB having ~50 µm of the coil width and ~70 µm of coil spacing after etching.

2.3 AC EWOD

2.3.1 Droplet Oscillation

EWOD can be performed by AC voltage as well as by DC (AC is limited to pure sine wave unless otherwise specifically stated). The distinct feature is that the droplet oscillates when the AC voltage is applied in electrowetting. In a mechanical standpoint of view, below ω_{cri} (critical frequency), the droplet oscillates in harmony with the AC frequency whereas above $\omega_{cri,}$ droplet oscillation cannot follow the applied frequency. The oscillation is mainly from the time varying electrical force acting on the three-phase contact line [70]. The shape of the droplet varies corresponding to the magnitude of the applied field as illustrated in Fig. 14. Since the droplet is subjected to the time varying force periodically, the manner of the shape deformation would be synchronized with the frequency of the applied field. Typically, the critical frequency of a millimeter-sized water droplet is in the range of a few kHz [44].

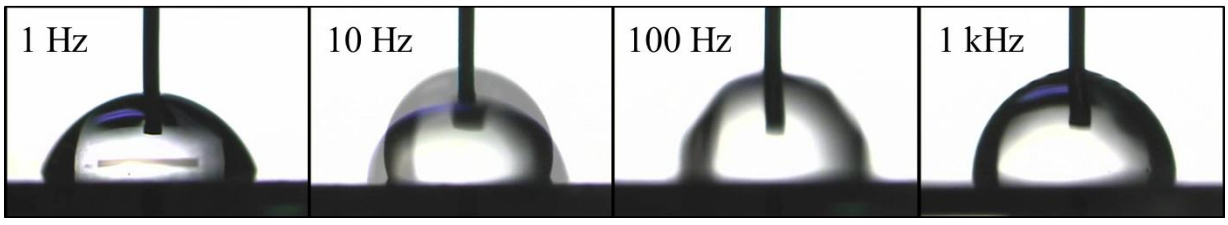

Figure 14. Instantaneous shapes of 5 µl DI water droplets oscillation at 80 V by changing the frequency.

In particular, the application of AC (less than 1 kHz) voltage to EWOD is beneficial to overcome the contact angle hysteresis. It was recently found by Mugele *et al*. that AC voltage reduces the contact angle hysteresis experienced by a droplet in electrowetting [71]. According

to their study, contact angle hysteresis is a major obstacle for the droplet movement on rough solid surfaces, and the contact angle hysteresis for sessile droplet in electrowetting can be almost disappeared with increasing alternating voltage.

The scheme of droplet's oscillation while in lateral transportation is illustrated in Fig. 15. The droplets are sitting on two different surface conditions. One is an ideal surface (a) and the other one rough surface (b) is vertically deviated from the flat surface. Since the ideal surface is flat, perfectly smooth, and chemically homogeneous, the droplet can move without experiencing the friction while in lateral motion. However, since it is expected that the chemical inhomogeneity and topographical roughness on the real surface, it would be much easier for the droplet to move with the oscillation on the rough surface.

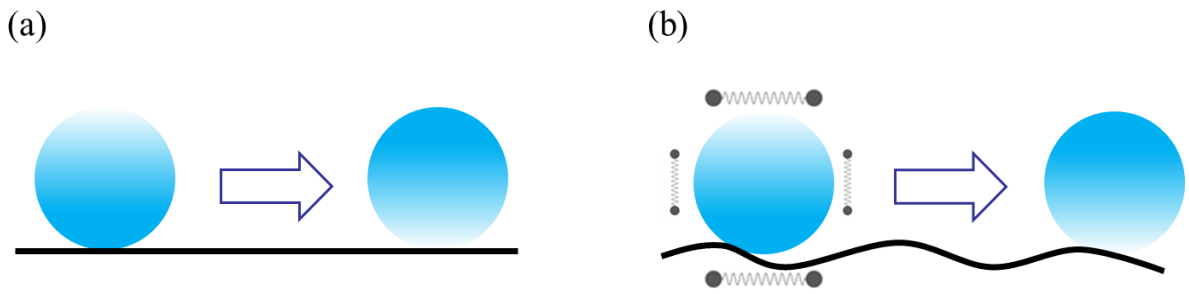

Figure 15. Liquid droplet's lateral transportation. (a) Ideally flat surface. (b) Rough surface with oscillation.

2.3.2 EWOD Circuit Model

In general, AC EWOD with the droplet shows two main modes: below the critical frequency ω_{cri}, the droplet oscillates in harmony with the AC frequency without any lag while above the critical frequency, droplet oscillation cannot follow the applied frequency and the contact angle changes and stays at the similar angle occurring at the equivalent DC voltage [44]. In the meantime,

another frequency called the cut-off frequency ω_{cut} can be defined in an electrical stand point of view [41]: far below which an liquid droplet acts as a conductor but above which the droplet acts as an electric insulator. In general, every component in the EWOD can be approximated and modeled by a resistor and capacitor, as sketched in Fig. 16.

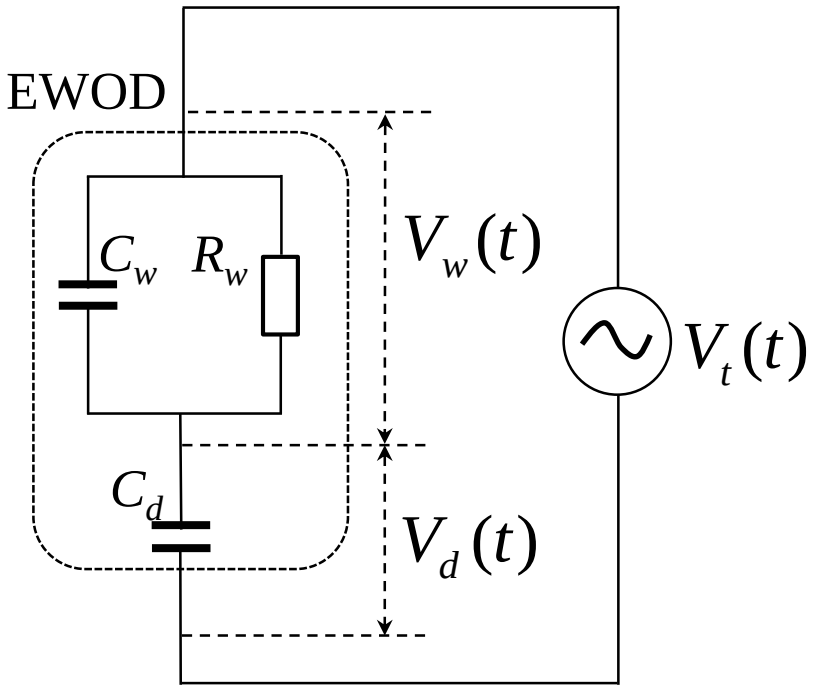

Figure 16. EWOD equivalent circuit diagram for a droplet sitting on an insulator-covered electrode. R_w is dominant at low frequency range, while C_w is dominat at high frequency range. $V_t(t)$ is overall applied voltage to EWOD. V_w and V_d denote voltage division of each component droplet and dielectric layer respectively.

EWOD with droplet is mainly divided into two components by the droplet and dielectric layer, which is connected in series. The electrical characteristics of the EWOD with droplet can be described by an equivalent R-C circuit model [72-74], where R_w and C_w denote electrical resistance and capacitance of the droplet and C_d denotes the effective capacitance of the dielectric layer. Below the hydrodynamic response limit of the droplet (e.g., low frequency or

DC) over the applied frequency, the electrical property of the droplet can be expressed by a single resistor, that is, a current pathway in serial connection with the dielectric layer, while it can be expressed by a pure single capacitor above the hydrodynamic response limit (e.g., high frequency) [71, 76-78]. Since the droplet is typically several orders of magnitude more conductive than the dielectric layers (Teflon and parylene layers), resistances of the dielectric layers are considered infinite.

There are several contributions to the droplet capacitance. For instance, the Teflon coated tip that is immersed into the droplet at the top, the electrical double layer formed at solid/liquid interface and droplet itself (analyte) can act as a capacitor [72, 73]. In most cases, however, the effect of the double layer is neglected due to its extremely small thickness compared to the dielectric layer thickness [75]. In order for the R-C model to be useful at least within our consideration, the electrical model has to be limited within the region where R_w and C_w are nearly independent of the frequency [76] (e.g. DC or low frequency) and below the contact angle saturation.

Unlike the difficulty to find the capacitance value of water droplet under limited condition (resistance is also hard to directly measure due to geometrical dependence of the R_w value), the capacitance of dielectric layer can be more easily estimated by considering droplet's base area formed at the solid/liquid interface. The base radius of the sessile depending on the contact angle θ is given as

$$R = \left(\frac{3\Delta}{\pi}\right)^{\frac{1}{3}} \frac{\sin\theta}{(2-3\cos\theta+\cos^3\theta)^{1/3}} \tag{23}$$

where Δ is the volume of the droplet and θ is the contact angle of the droplet [77]. Since the contact angle and droplet volume can be measured, the base area of the droplet can be easily

calculated. For 5 µl droplet, the base radius and corresponding area are listed in Table 2 at different contact angles.

Table 2. The base radius and base area of 5 µl droplet at different contact angles.

Contact angle [deg]	Base Radius [mm]	Base Area [mm^2]
120	0.97	2.97
110	1.09	3.8
103	1.18	4.4
97	1.25	4.9
83	1.42	6.3
74	1.53	7.3
68	1.6	8.0

The time associated parameter that is the charge relaxation time at the solid/liquid interface, denoted as $\tau_{relaxation}$ and the frequency of the input signal τ_{input} can be also considered with the R-C model. The relaxation time $\tau_{relaxation}$ is basically associated with the R-C time constant for the circuit where the droplet and dielectric layers can be modeled as resistive and capacitive components, respectively, as shown in Fig. 14. Assuming that DC voltage is applied to the EWOD with droplet, the relaxation time is [44, 78] given

$$\tau_{relaxation} = R_w(C_w + C_d) \approx \frac{1}{\omega_{cut}} \tag{24}$$

In Eqn. (24), the droplet's resistance solely contributes to the relaxation time, but in reality the EWOD circuit seems to have other resistance contributions that might need to take into account the relaxation time. The inverse of $\tau_{\text{relaxation}}$ can be used to define a cut-off frequency ω_{cut}, which is mentioned earlier in this section. Many researchers have made efforts to distinguish the low and high frequency regimes by which EWOD force is mainly responsible for the droplet's motion in the low frequency regime because the electric field is formed and concentrated only at the contact line of the dielectric layer (neglecting the fringe field at the contact line), while dielectrophoresis (DEP) force based on the redistribution of the electric field across the droplet is the responsible for the high frequency regime [78-81].

2.3.3 Voltage Drop across Droplet

The experimentally obtained frequency response of EWOD circuit can be roughly analyzed by employing a transfer function $G(s)$ to predict the voltage division in the EWOD circuit. A transfer function states the relation between the input and output of our interest in a mathematical method, and its application for AC EWOD analysis shows a good agreement with our experimental results particularly when to estimate the voltage drop across the dielectric layer [82]. Since EWOD with the droplet in the circuit model is divided into two components by the droplet and dielectric layer, the sum of voltage by each component has to be same as overall applied voltage based on the Kirchhoff's voltage law. For a given overall AC voltage $V_t(t) = \sin\omega t$ (amplitude of this signal is taken as unity for simplicity):

$$V_t(t) = Z_w I(t) + \frac{1}{C_d}\int I(t)dt \tag{25}$$

where $Z_w = \frac{R_w}{1 + C_w R_w S}$ and $S = j\omega$.

Then, the transfer function can be defined in frequency domain as below,

$$G(s): \frac{V_d}{V_t} = \frac{R_w C_w S + 1}{R_w (C_w + C_d) S + 1} \tag{26}$$

For a given input voltage $V_t(t) = \sin\omega t$, the voltage only at the dielectric layer is given as $V_d(t) = A(\omega)\sin[\omega t + \phi(\omega)]$, where the magnitude $A(\omega)$ and phase $\phi(\omega)$ are given by

$$A(\omega) = |G(j\omega)| = \sqrt{\frac{R_w^2 C_w^2 \omega^2 + 1}{R_w^2 (C_w + C_d)^2 \omega^2 + 1}} \text{ , where } \phi(\omega) = \arctan\left(\frac{\mathrm{Im}\, G(j\omega)}{\mathrm{Re}\, G(j\omega)}\right) \tag{27}$$

The validation of $A(\omega)$ can be confirmed by considering two frequency limits when $\omega \approx 0$ and $\omega \approx \infty$. For low frequency limit or DC when $\omega \approx 0$, we have $A(\omega) \approx 1$, which implies that V (total voltage applied to EWOD) would be equal to V_d (voltage across the dielectric layer). On the contrary, for high frequency limit when $\omega \approx \infty$, the $A(\omega)$ is no more unity but converged to $C_w/(C_w + C_d)$, which is only determined by the capacitances of the droplet and dielectric layer. That is, a significant voltage division occurs across the EWOD circuit. As a consequence, V_t is no more equal to V_d, possibly leading to an extremely small change in the contact angle.

2.4 AMPLITUDE MODULATION (AM)

2.4.1 AM and Demodulation

AM is one technique mostly used in wireless communication, where the carrier signal (usually radio frequency) has its instantaneous amplitude varied in accordance with the low frequency message or modulating signal [83]. In AM, the carrier signal $c(t)$ of high frequency ($\omega_c = 2\pi f_c$) is modulated by being multiplied by the enveloping signal $m(t)$ of low frequency ($\omega_m = 2\pi f_m$). The form of amplitude-modulated signal $A(t)$ is given by,

$$A(t) = c(t) \bullet m(t) = A\sin(\omega_c t) \bullet \left[1 + M\sin(\omega_m t)\right] \tag{28}$$

where A and M are the amplitude of the carrier and enveloping signal respectively [84]. The transmitted AM signal is usually demodulated by a demodulation circuit or envelope detector to recover the low frequency message signal [83]. One of the simple demodulating units, which composed of a diode and capacitor are given in Fig. 17 along with AM signal and demodulated signal. The recovering process of the low frequency envelope (also called a demodulation process) based on Fig. 17 has two main steps. AM signal is half-wave rectified by passing the diode, and the high frequency components remaining in the half-wave are by-passed through the capacitor, where the high frequency components are effectively removed. The final waveform of the demodulated signal is similar to the signal having one low frequency component (modulating signal) offset by DC component as shown in Fig. 17 on the right side.

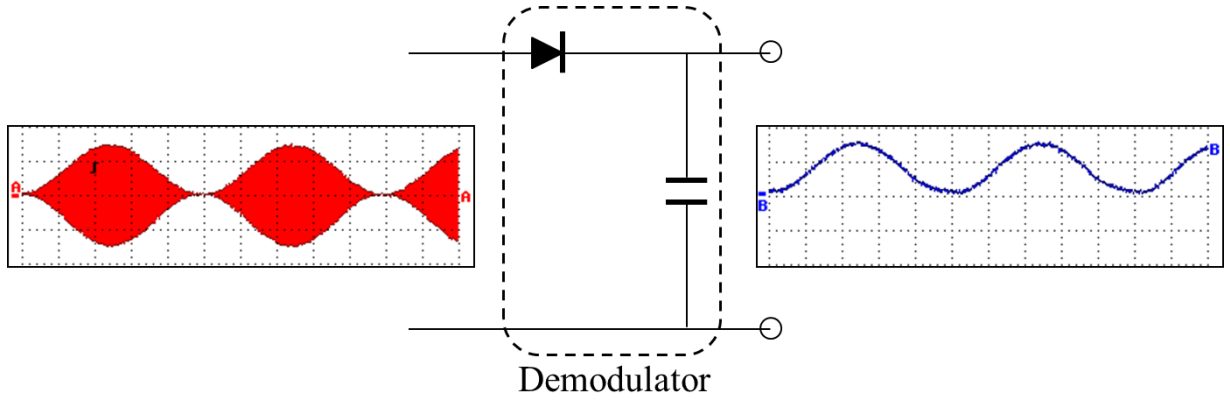

Figure 17. AM signal (waveform on the left) is demodulated to recover its envelope signal (waveform on the right)

The AM signal can be produced in the function generator after optimizing several parameters such as modulating depth and modulating frequency. The modulation index indicates how strong the modulating signal with respect to the carrier is. The modulation index should not exceed 100% in order to avoid distortion in a demodulated signal whenever an envelope detector is employed. By setting of 100% modulation depth with sinusoidal waves in function generator, for which *A* and *M* in Eqn. (28) are set equal, AM signal without distortion can be achieved.

2.4.2 AM with EWOD

As mentioned in 2.3.1, droplet oscillation by AC voltage is often used to overcome the contact angle hysteresis. However, since wirelessly transmitted signal is usually high frequency (from few hundreds kHz to few MHz range in this study) to obtain high voltage for EWOD actuation, the droplet would not be able to follow such a fast carrier frequency. This means that it is very difficult for droplet to directly oscillate in harmony with the applied carrier frequency. If the carrier frequency is below 1 kHz, the voltage at the receiver will not be high enough for the EWOD operation since the attainable voltage at the receiver through magnetic induction is

proportional to the transmission frequency [56]. Hence, AM is implemented in the wirelessly transmitted signal in order to oscillate a droplet at a lower frequency than the critical frequency.

By intuition, it is expected that the droplet will respond only to the envelope of the carrier signal. As a result, the droplet will oscillate at the frequency of the enveloping signal. This is somewhat particular application of AM scheme unlike the general application of AM in wireless communication. However, AM with wirelessly transmitted signal A(t) consists of purely high frequency components and inherits no low frequency components from the message signal m(t). This fact can be easily realized by using trigonometric identities of A(t). A(t) given in Eqn. (28) can be re-written in the form as follow.

$$A(t) = A\sin(\omega_c t) - \frac{AM}{2}[\cos(\omega_c + \omega_m)t - \cos(\omega_c - \omega_m)t] \qquad (29)$$

As it can be seen in the Eqn. (29), AM signal has only high frequency components, a carrier wave and two sinusoidal waves, whose frequencies are slightly above and below ω_c, which implies that droplet is not supposed to respond the low frequency signal m(t) due to lack of the low frequency component. However, interestingly droplets in certain conditions directly respond to the envelope signal without any external demodulation circuit.

According to Lippmann-Young's equation, the contact angle is proportional to V_d^2. The droplet's behavior responding to the envelope can be understood by theretical prediction using the transfer function given in 2.3.3. Suppose that the EWOD system in Fig. 16 is driven by the following AM signal.

$$V_t^{AM}(t) = A[1+\sin\omega_m t]\sin\omega_c t.\ \ \omega_m \langle\langle \omega_c \tag{30}$$

Then, the transfer function gives the V_d^{AM} for given $V^{AM}(t)$ as follow [82],

$$V_d^{AM}(t) = |G(s)|A[1+\sin\omega_m t]\sin\omega_c t \tag{31}$$

Then, its square value is given as,

$$(V_d^{AM})^2 = |G(s)|^2 A^2[1+\sin\omega_m t]^2 \sin^2\omega_c t$$

$$= \frac{1}{4}|G(s)|^2 A^2[3+a(t)+b(t)] \tag{32}$$

where, $a(t) = 4\sin\omega_m t - \cos 2\omega_m t$
$b(t) = -2(1+\sin\omega_m t)^2 \cos 2\omega_c t$

According to Eqn. (32), the high frequency signal $b(t)$ does not contribute to the contact angle change. Therefore, the time variation of the contact angle $\theta(t)$ will follow the slowly varying signal $a(t)$, whose dominant component contains only the low frequency envelope signal. As a consequence, droplets directly respond to the envelope signal without any external demodulation circuit. The experimental verification of this phenomenon is given in section 3.1.3.

3.0 EXPERIMENTS

3.1 AC ELECTROWETTING IN WIRED POWERING

In this chapter, the experimental measurements of the voltage division ($V_t = V_d + V_w$) of EWOD with the droplet are presented. The nature of droplets responding to the low frequency envelope in the application of AM signal is also verified experimentally. Finally, one efficient way to increase the span of contact angle ($\Delta\theta$) is presented by addition of the external demodulation circuit. All applied signals (DC, AC and AM) in experiments are generated via wired powering.

3.1.1 Experimental Set-up

AC electrowetting is performed by measuring the apparent contact angle change of the droplet in wired powering. To set up the contact angle measurement experiment, EWOD device is prepared by using Si wafers. 4-inch Si wafer is cleaved in small pieces (2×2 cm^2) and mounted in the parylene coating chamber (Speciality Coating System, PDS 2010). Parylene-C ($\varepsilon_r = 3.1$) dimers are decomposed and chemically deposited for a uniform and conformal film at room temperature. 2% Teflon AF ($\varepsilon_r = 1.93$) is also coated over the entire area of samples to increase hydrophobicity. The final film thickness is measured by the surface profiler (*Dektak* 3030). The measured thickness of the parylene layer is 1.5 μm and that of the Teflon layer is ~0.9 μm. The experimental set-up is illustrated in Fig. 18.

The 5 µl of liquid droplet with σ = 153×10^{-4} S/m (measured at 22.9 ^{o}C by Orion 3-Star pH meter) is used during this experiment and the volume of droplet is controlled by micro-pipette. For the ground electrode immersed into the droplet, a 30 µm in diameter Cu wire is used and also coated by 0.5% Teflon. The base radius of the droplet is about 1 mm. The signals (DC, AC voltage) are applied by using the function generator (Agilent 33220A) and amplified up to 50× by the high frequency piezo driver (Trek 2100HF). All applied signals are monitored by a scope meter (Fluke 199C). Apparent contact angle and change of the droplet shapes are monitored by a CCD camera and recorded real time in a PC.

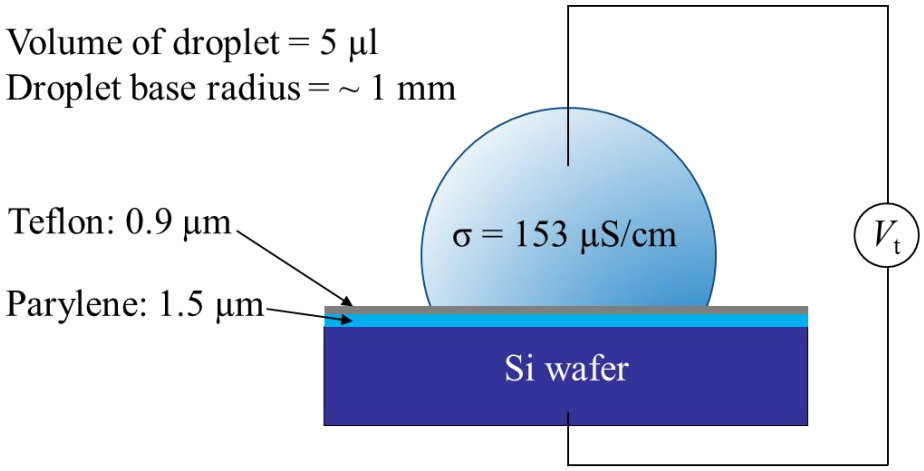

Figure 18. Experiment set-up with droplet for contact angle measurement.

In order to avoid droplet's mechanical oscillation (experimentally observed upper frequency limit was ~2 kHz in this set-up), the frequency selected in the experiment is 50 kHz. An image processing of droplet is implemented using the *Drop Shape Analysis* (*LB-ADSA*) plug-in in *ImageJ* to quantitatively read the contact angle.

3.1.2 Contact Angle Measurement

Figure 19 shows the contact angles of 5 µl sessile droplet when the voltages of DC and 50 kHz AC are applied along with Lippmann-Young curve. For the DC case, the onset of contact angle change (threshold) is noticed at 50 V with $\Delta\theta$=~8^{o} and the saturation is observed over 110 V with the saturated contact angle θ=~75^{o}. No further decrease in contact angle is achieved even at the higher voltages (known as contact angle saturation). The Lippmann-Young curve in Fig. 19 is also obtained by plugging the specific capacitance of dielectric layer into Eqn. (1). In this experiment set-up, the specific capacitance of the dielectric layer is ~9.7×10^{-6} F/m^{2} by taking both the thickness of the Teflon and parylene layer into consideration.

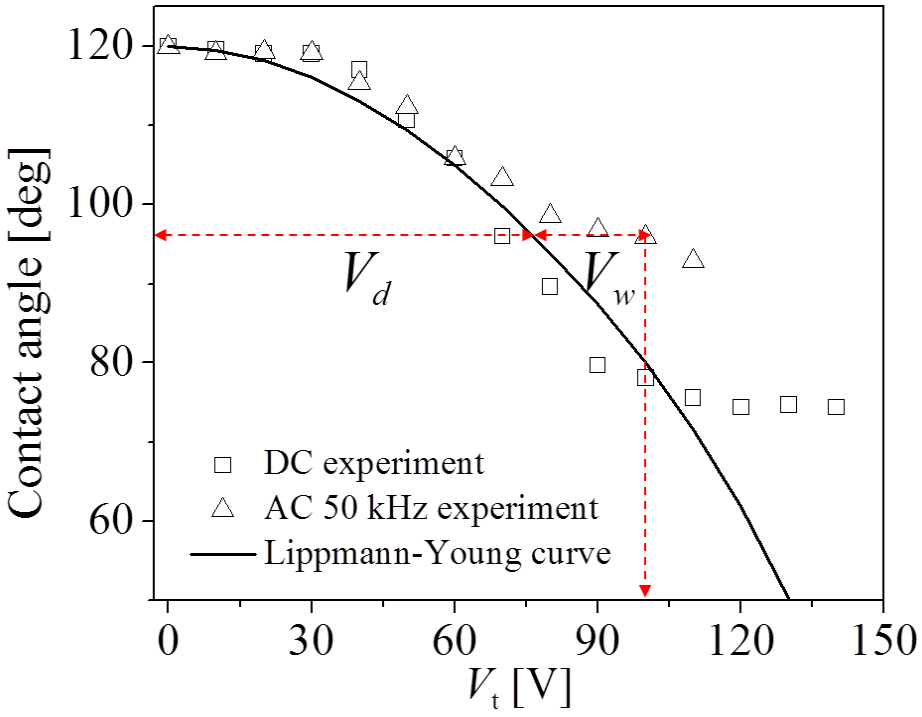

Figure 19. Contact angle of a 5 µl sessile droplet at DC and 50 kHz comparison with Lippmann-Young's curve.V_t, V_d, and V_w are the total applied voltage to EWOD, voltage only at dielectirc layer and voltage drop across the droplet, respectively.

For the AC at 50 kHz, the overall behavior of the contact angle is similar to that of the DC but larger contact angles than the DC are always observed over 70 V. This is because there exists a voltage drop across the droplet (denoted V_w in Fig. 19) in the case of AC voltage application, and thus the total applied voltage V_t is not fully delivered to the dielectric layer (denoted V_d). As a result, small contact angle variation $\Delta\theta$ is observed. For example, when V_t = 100 V, the contact angle is 78.1° in DC, thus the span of contact angle from the initial state is $\Delta\theta$=~42°, while that of AC is $\Delta\theta$=~24° at contact angle of 95.9°.

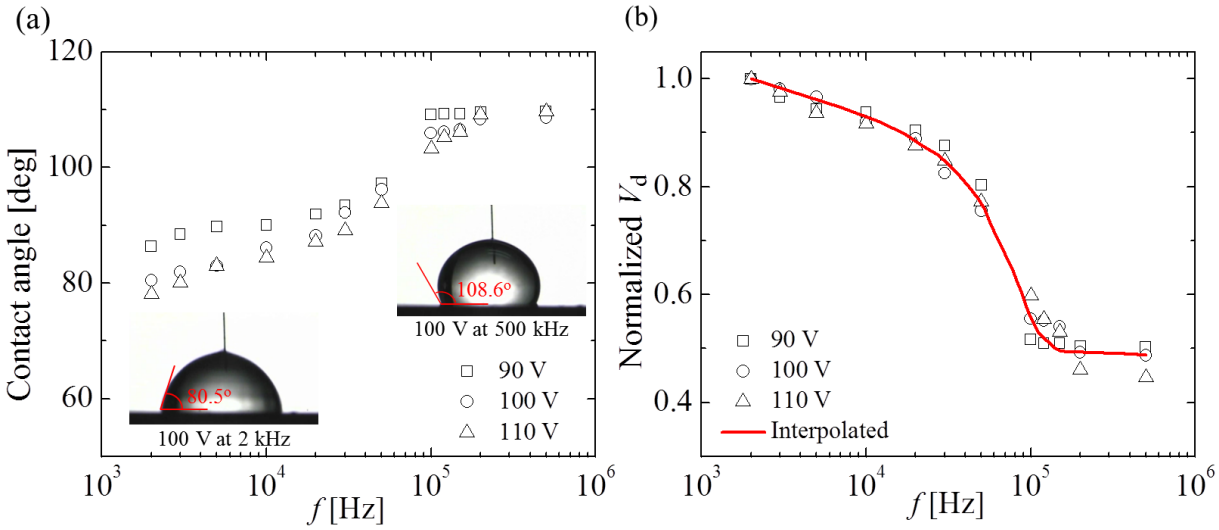

Figure 20. (a) Frequency response of contact angle at different input voltages of 90, 100, and 110 V for 5 µl sessile droplet; insets are photos of corresponding droplet shapes at 2 and 500 kHz respectively at 100 V. (b) Scattered data points are the normalized V_d at different V_t and interpolated transfer function. The measured contact angles are plugged into the DC curve in figure 18 (solid line) to calculate V_d.

The frequency response of the contact angle is further measured at different voltage inputs to investigate the voltage division at EWOD. The contact angles are measured by changing the input frequency from 2 to 500 kHz at three different RMS voltages of 90, 100, and

110 V respectively. Figure 20 represents the experimental results of contact angles vs. the frequency. Within the present frequency range, the contact angle is gradually increased up to 200 kHz (in log scale). Beyond that frequency, the contact angles remain almost unchanged.

Figure 19(b) also shows the frequency response of the normalized V_d, and the interpolated transfer function. V_d is decreased as the frequency is increased. The reduction reaches ~50% when the frequency is over 200 kHz. The contact angle beyond 200 kHz is converged to ~110^o regardless of the applied voltage. Considering that the normalized V_d is converged to $C_w/(C_w+C_d)=0.5$ above 200 kHz reading from Fig. 20(b). The change of droplet shape and base area is not so great above 200 kHz, thus, the change of the capacitance of dielectric layer would be also minimal.

3.1.3 Amplitude Modulation (AM)

3.1.3.1 Droplet Responding to Envelope

The objective of this experiment is to verify the theoretical prediction that droplets can be in harmony with the low frequency envelope driven by AM signal. The experimental set-up for AM having the same EWOD chip condition with 3.1.1 is shown in Fig. 21(a). AM signal that is 1 Hz of low frequency envelope and 50 kHz of carrier shown in Fig. 21(b) is generated by a function generator with 100% of modulation index, and applied to the droplet. AM signal has only high frequency components, that is a high frequency of the carrier and two sinusoidal waves, whose frequencies are slightly above and below the carrier frequency.

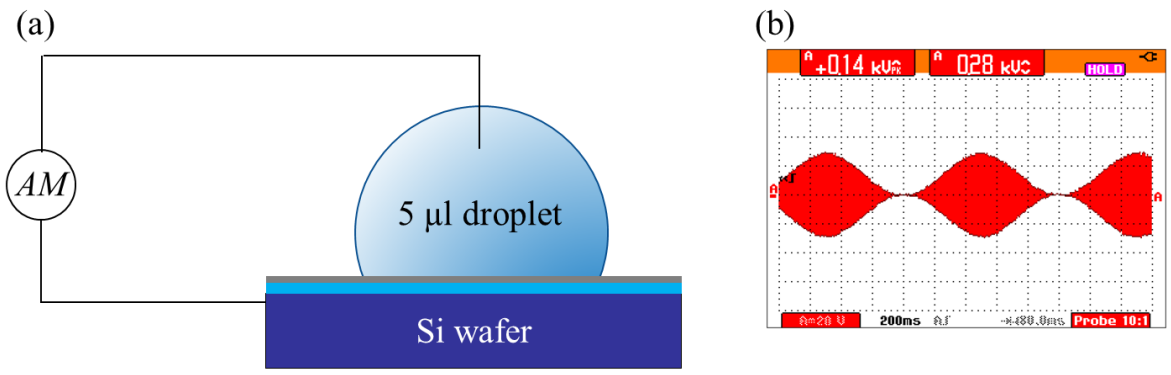

Figure 21. AM experiment set-up in wried powering (a) and the applied AM signal (1 Hz of low frequency envelope and 50 kHz of carrier from the function generator) to EWOD with droplet.

The result of the contact angle vs. time (2 periods) is shown in Fig. 22. When the AM signal is applied to the droplet, the droplet responds to the low frequency envelope while it changes its shape and contact angle as well. Droplet recovers its shape and contact angle along the given 1 Hz of envelope frequency. When the contact angle reaches at the minimum during two periods, there exists ~2^{o} of contact angle difference, which is probably from the contact angle hysteresis. However, this result is fairly in good agreement with the theoretical prediction. The contact angle variation is $\Delta\theta$=~17^{o} from the maximum to the minimum contact angle.

According to the G(s) transfer function given in Eqn. (28), a higher carrier frequency will inevitably result in more voltage drop across the droplet, since the magnitude $|G(s)|$ is decreasing with the carrier frequency. The voltage division makes the voltage across the dielectric layer smaller as the carrier frequency increases, and thus the nature of droplets responding to the envelope seems to be buried. However, this characteristic still exists even when the dielectric voltage is lowered. This issue will be also discussed in wirelessly transmitted AM signal which has a higher carrier frequency (few hundreds kHz to few MHz) than the current AM set-up.

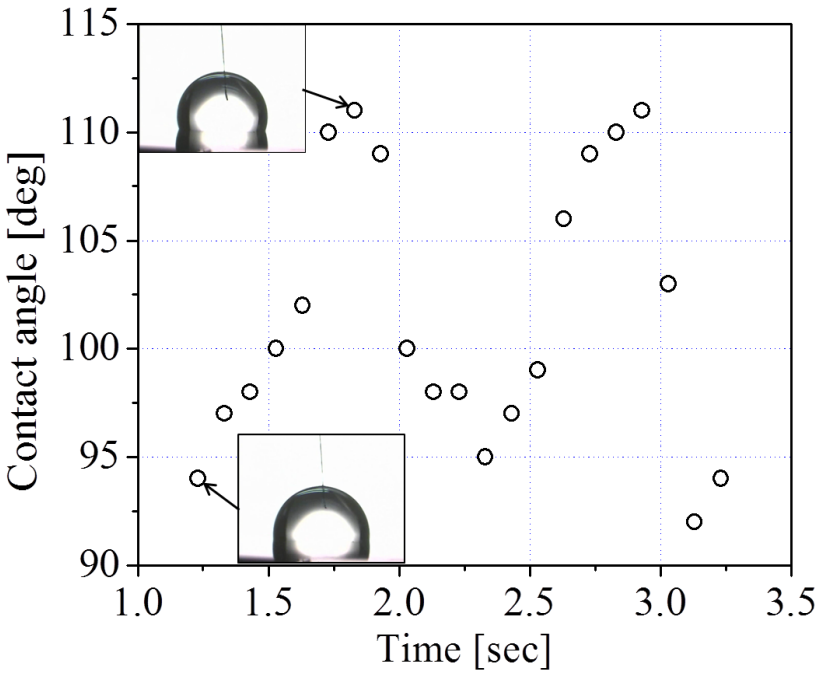

Figure 22. Contact angles under AM (1 Hz of envelope and 50 kHz of carrier frequency) signal.

3.1.3.2 External Demodulation Circuit

In contrast, from a practical point of view, a higher carrier frequency is generally desirable for the efficiency of wireless powering. However, due to significant voltage drop across the droplet with the increased frequency, EWOD would require much higher voltage than the typically required voltage. Therefore, it is good choice to install the external demodulation unit at the receiver circuit in order for the droplet not to meet any high frequency components. Fig. 23 shows AM demodulation circuit adopted in this experiment. This simple circuit is composed of single diode and capacitor (other experimental conditions such as EWOD chip, AM signal and its amplitude are remained same as 3.1.3.1).

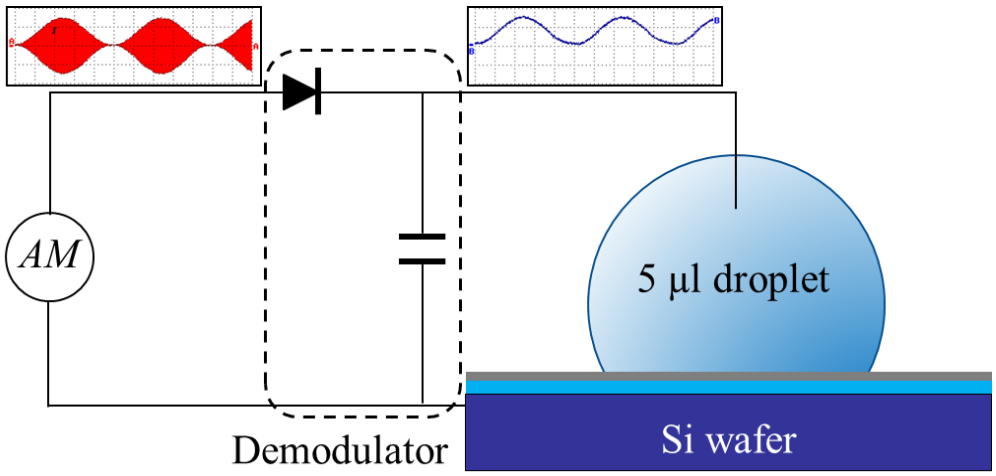

Figure 23. AM demodulation circuit composed of single diode (IN5399-E3/54) and capaciotr (10^{-8} F) in parallel connection. After the demodulator, the drolplet will see the only low frequency envelope signal.

For this demodulation circuit addition, the span of contact angle ($\Delta\theta$) is ~47^{o} as given in Fig. 24(b) and (c). Since the envelope signal is recovered by the added demodulator before reaching the droplet, the droplet meets only low frequency envelope signal. It can be clearly seen from the waveform in Fig. 24(a) (the blue waveform in the below) that the demodulated signal only contains 1 Hz of the low frequency envelope signal. As a result, there is no reduction in the dielectric layer's voltage, which occurred in the inherent demodulation of the droplet in pure AM signal. The installation of demodulation circuit is beneficial particularly when it comes with the wireless circuit via magnetic induction since this simple circuit removes the high frequency components efficiently resulting in increased $\Delta\theta$.

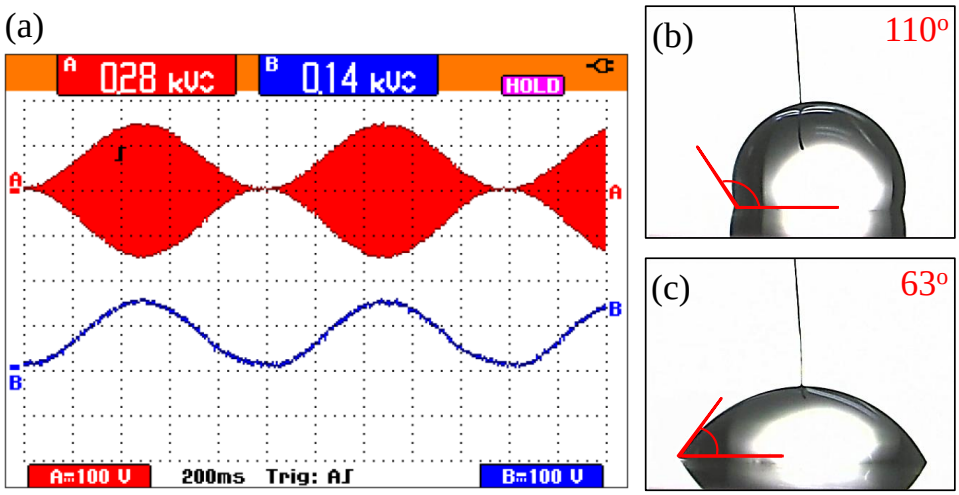

Figure 24. (a) AM signal, 50 kHz of carrier and 1 Hz of envelope (upper) and demodulated signal (below) by the external demodulation circuit. (b) and (c) are the contact angle photos captured when it reaches the maximum (b) and minimum contact angle (c).

Table 3. Comparison of the span of contact angle.

f_c at 50 kHz	θ_{min}	θ_{max}	$\Delta\theta$
without demodulator	94°	111°	17°
with demodulator	63°	110°	47°

3.1.4 Summary and Conclusion

In this chapter, the experimental verification of the voltage division ($V_t = V_d + V_w$) of EWOD in the AC input were presented. When the AC voltage is applied to EWOD with the droplet in particular above the critical frequency in which droplets cannot oscillate in harmony with the frequency, the contact angle change is reduced gradually as the frequency is increased resulting

in voltage division over the EWOD with droplet. To find the voltage across the dielectric layer, we introduced the transfer function derived from the capacitor-resistor circuit model for EWOD configuration. The prediction by the transfer function was compared with the experimentally measured results.

The low frequency (envelope) responding droplets behaviors in the AM signal were also presented. The experimental results are fairly in good agreement with the theoretical prediction. However, it is obvious that addition of the external demodulation circuit would be beneficial in practical point of view particularly when the carrier frequency is inevitably increased via a magnetic induction. Since the droplets act as capacitive component at high frequency which results in a significant voltage drop across the droplet, by addition of external demodulation circuit, it is confirmed that the voltage drop across the droplet is reduced and thus the span of contact angle is significantly increased at given AC frequency.

3.2 WIRELESS POWERING VIA SPOOL-TYPE COILS

In this chapter, we investigate wireless power transmission for EWOD utilizing magnetic induction. To meet the droplet actuation conditions by EWOD, the resonant inductive coupling method at a high resonant frequency is introduced and investigated. To optimize the transmission efficiency, we study the effects of many parameters such as the frequency, inductance and capacitance at the transmitter and receiver, the gap between the transmitter coil and receiver coil, and the droplet size by measuring the voltage at the receiver and the contact angle of the droplet placed on a wirelessly operated EWOD chip. In addition, by applying AM technique into wirelessly transmitted signal, droplet oscillations are also achieved. Finally, it is successfully demonstrated that a droplet is transported laterally by using an array of electrodes, which is also powered by the AM wireless signal.

3.2.1 Resonant Wireless Circuit Set-up

As shown in Fig. 25, the transmitter consists of a function generator, a power amplifier, a spool-type coil (0.055 mH) and a capacitor (22000 pF). The receiver also has an L-C circuit composed of a spool-type coil (2.93 mH), a capacitor (470 pF), and EWOD chip, all connected in parallel. The frequency of the transmitter and the receiver is tuned to be equal at 140 kHz based on Eqn. (20). The measured *L* and *R* values for the coils are listed in Table 4.

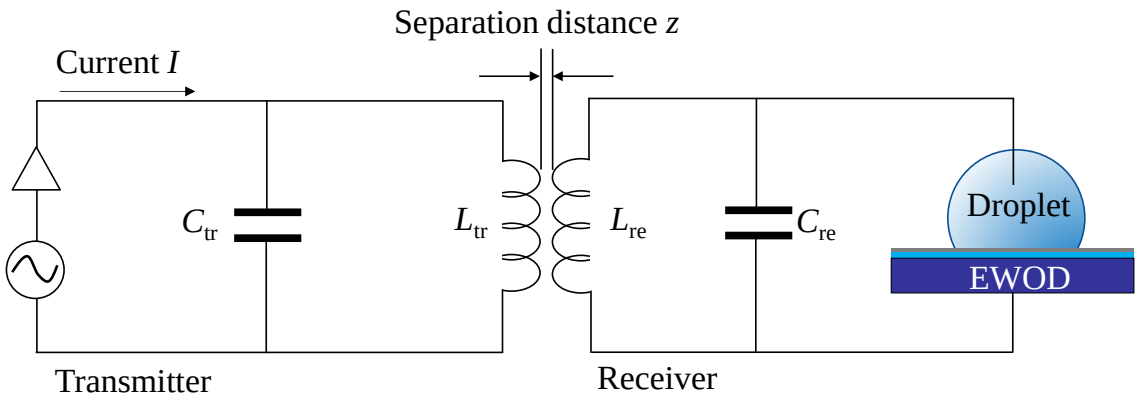

Figure 25. An equivalent electric circuit using a magnetic induction. The EWOD part (including a droplet) is connected to the receiver coil in parallel. Subscript tr and re denotes the transmitter and receiver respectively.

Table 4. The measured inductance and resistance values of spool-type coils by LCR meter (Agilent 4285A).

	Transmitter coil	Receiver coil
Number of turns	25	250
L [mH]	0.055	2.93
R [Ω]	0.17	5.7
Coil D_i [cm]	2.3	2.3
Wire D [μm]	Cu 250 μm and insulating polymer 250 μm	

3.2.2 Fabrication of EWOD Testing Device for Droplet Transporting

In order to demonstrate the droplet transportation via wireless EWOD, a testing device on a 4-inch glass substrate is fabricated with the process flow as illustrated in Fig. 26. The testing device consists of two parallel plates: top and bottom. The bottom plate shown in Fig. 26(C) has an array of EWOD driving electrodes while the top plate in Fig. 26(b) has a single electrode covering the entire area of the plate, which is used for electric grounding. A droplet is placed between the two plates. In droplet transporting, at least two neighboring EWOD electrodes placed underneath the droplet are required. The dimension of the EWOD electrode is 1.2×1.2 mm^2.

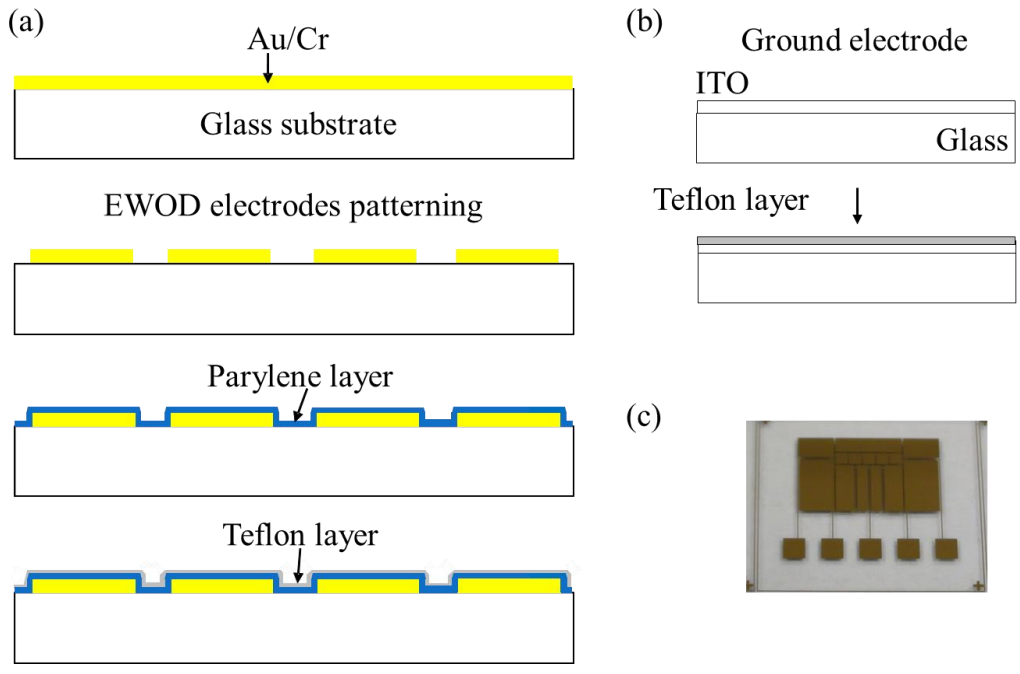

Figure 26. Fabrication process for EWOD testing device. (a) 4" glass wafer prepared for the bottom plate of the EWOD chip and Cr/Au (10/100 nm thick respectively) layer sputter-deposited and patterned by wet-etching. Dielectric layer (parylene) deposited by chemical vapor deposition process and 2% Teflon solution spin-coated. (b) Top plate: Conductive ITO glass coated with 0.5% Teflon solution. (c) Photo of fabricated EWOD testing device.

3.2.3 Experimental Results

3.2.3.1 Effectiveness of Wireless Circuit

The experiments are carried out to find the resonant frequency of the wireless circuit without the EWOD chip installed in the receiver. Both transmitter and receiver have coils and capacitors to make the resonant circuit. For the transmitter circuit, the inductance and the capacitance are 0.055 mH and 22000 pF, respectively. The receiver has the inductance of 2.93 mH and the capacitance of 470 pF. The resonant frequency according to Eqn. (22) is 140 kHz in both the transmitter and receiver.

As shown in Fig. 27(a), the resonant frequency is measured to be 137 kHz at V_t =24.9 V and 143 kHz (V_{tr}=42.3 V), respectively, slightly depending on the input voltage at the transmitter. The voltages at the receiver up to 148 V at 137 kHz and 211 V at 143 kHz are obtained when the receiver coil is placed on the transmitter coil with a zero separation distance. These voltages are much higher than the required EWOD voltage. The significant voltage reduction occurs as the frequency is off the peak frequencies, and the voltage flattens as the frequency is increased.

Figure 27(b) also shows the relation of the receiver voltage to the separation distance between the transmitter and receiver coils. As the separation distance between two coils is increased, the magnetic field reaching the receiver coil becomes weaker and eventually the measured voltage at the receiver drops monotonically as predicted. For EWOD operation in all cases, the distance should be maintained smaller than 20 mm in order for the voltage at the receiver to be higher than 50 V.

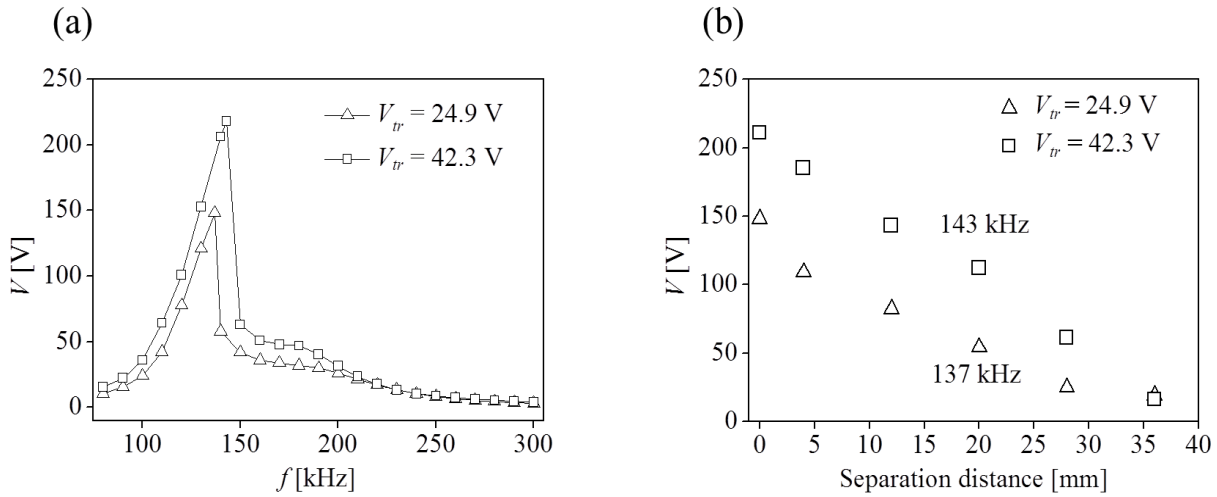

Figure 27. (a) Voltage at the receiver. Peaks in which resonance occurs are at 137 and 143 kHz for 24.9 and 42.3 input voltages, respectively. (b) Voltage at the receiver vs. distance between the transmitter and receiver coils.

In additional experiment (circuit illustrated in Fig. 28(a)), the capacitor at the receiver is removed to see whether resonating could be obtained without the capacitor. Unlike the circuit with the capacitor, two peaks appeared as shown in Fig. 28(b). Regardless of the input voltage, the first peak is at 190 kHz in which the measured voltages at the receiver are 26.1 and 40.7 V, respectively. For the second peak, the voltages are up to 44 V at 515 kHz (when V_{tr}=24.9 V) and 72.9 V at 500 kHz (when V_{tr}=42.3 V). The voltages at the peaks are much lower than those with the capacitor and thus might not be high enough to drive EWOD in some cases. Even at the off-peak frequency, the voltage behavior is slightly different. The appearance of two peaks may be attributed to the parasitic capacitance inherently existing in the receiver circuit. As the frequency increases, the reactance of the parasitic capacitance, which is inversely proportional to the frequency, decreases. Thus, the parasitic capacitance comes into play at a high frequency. Note that the voltages at the second peaks are higher than those at the first peaks. This may be

explained by the fact that the derivatives in Eqn. (14) become greater at higher frequencies, leading to a greater electromotive force and thus a higher voltage.

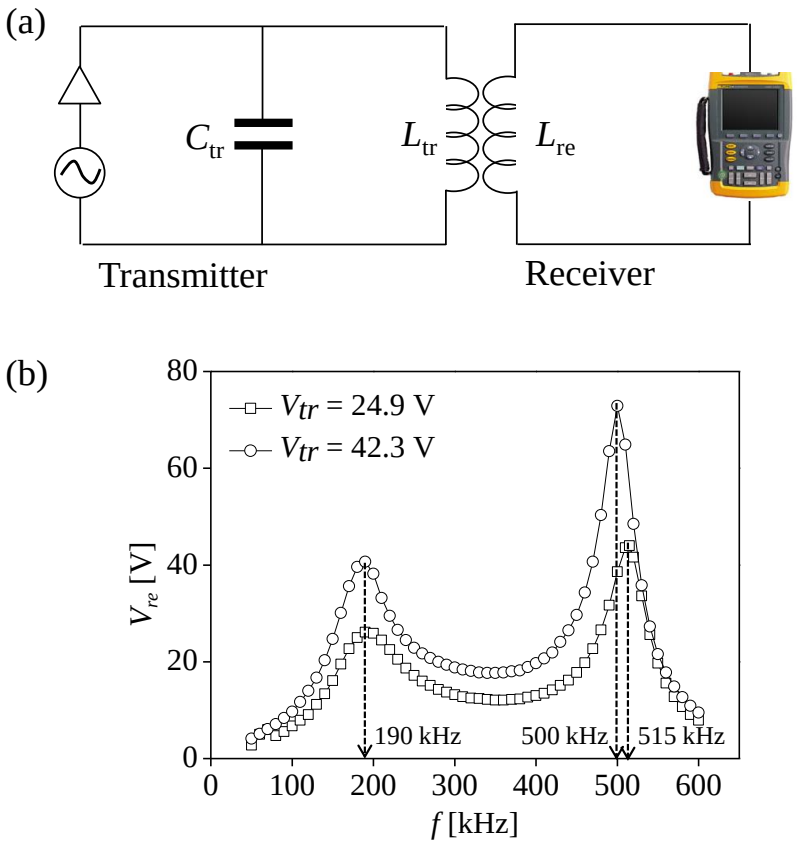

Figure 28. (a) The wireless circuit having no external capacitor at the receiver circuit. (b) Voltage at the receiver when the external capacitor is removed at the receiver. Two peaks for each case are produced.

3.2.3.2 Effects of Droplet Size

It is expected that adding EWOD chip at the receiver will change the overall capacitance of the receiver circuit and thus the resonant frequency. In this scenario, two components in the EWOD chip change the overall capacitance. The first one is the dielectric layer underneath the droplet consisting of the Teflon and parylene layers in the present EWOD chip. The second one is the droplet itself acting as a capacitor and resistor. As illustrated in the equivalent electrical circuit in

Fig. 16, it has been widely understood that EWOD dielectric layer mainly acts as a capacitor [26, 27].

For the capacitor formed by the dielectric layer, the droplet base area that interfaces with the dielectric layer serves as one electrode, while the EWOD electrode underneath the dielectric layer serves as the other electrode. Thus, the base area of the droplet is a key parameter in determining the capacitance of the dielectric layer. Assuming that the Teflon layer (~0.2 μm) is negligibly thin and thus the contribution to the total capacitance is also negligible, the total capacitance for the EWOD dielectric layer would be equal to that of the parylene layer. The parylene layer for the present chip has a thickness of 1.5 μm. Using the thickness and dielectric constant (ε =3.1) of the parylene layer and the droplet base area, the capacitance of the dielectric layer formed by three different droplet sizes is calculated and tabulated in Table 3 when the contact angle θ is 120^{o}.

Next, the droplet acts as a parallel circuit of a capacitor and resistor, as shown in the equivalent circuit in Fig. 16. For the calculation of the droplet's capacitance, we assume that the droplet capacitance having a spherical shape can be defined as the amount of electrical charge that must be added to an isolated droplet to raise its electrical potential by one volt [85]. In addition, we make another assumption that the shape change of the droplet would not change the capacitance significantly and it will not be violated within the regime that the shape change is minimal by the frequency [86]. Following the assumption, the capacitance of the three different droplet volumes is also calculated in Table 5.

Table 5. Capacitances of dielectric layer, droplet, and the EWOD chip at receiver for three different droplet volumes when the contact angle is 120°. All capacitance units are in pF.

Droplet size µl	Base area mm^2	C_d	C_w	C_{EWOD}
5	2.97	54.3	9.8	8.3
30	9.79	179	17	15.5
145	27.8	508	29	27.4

Since the droplet and the dielectric layer are connected in series, the total capacitance C_{EWOD} can be easily calculated as shown in Table 3. The total capacitance is much smaller than that of the installed capacitor (470 pF) that is connected in parallel to the EWOD chip. This implies that adding the EWOD chip would not change much the overall capacitance of the receiver, and thus would maintain the resonant frequency at the receiver as it is. As a result, the effect of the droplet size would be minimal since the capacitance of the EWOD chip is much smaller than that of the external capacitor. These predictions are experimentally confirmed, as shown in Fig. 29.

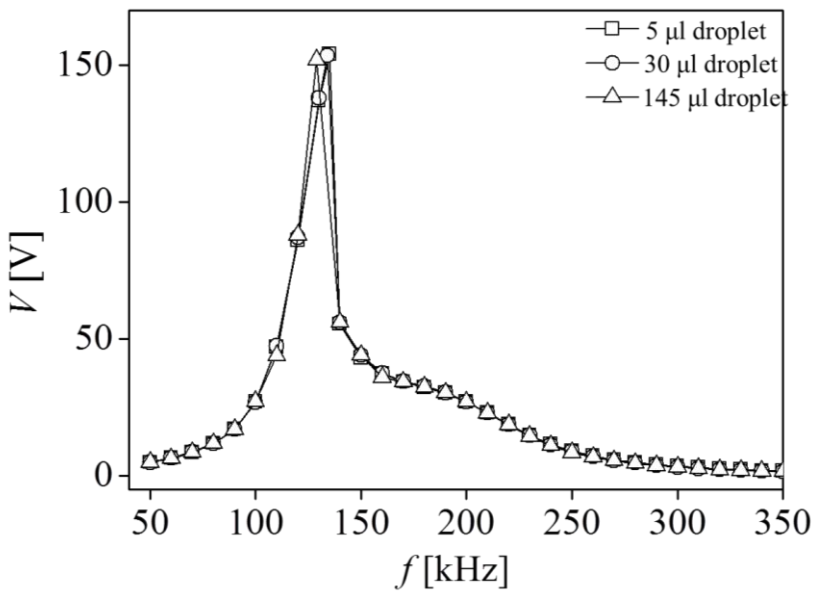

Figure 29. Voltage at the receiver (V_{tr}=24.9 V) when the EWOD chip including a droplet is installed in the receiver. The peak frequencies and voltages at the receiver is almost same with Fig. 27(a) regardless of the droplet volume.

Regardless of the droplet volume, the shift of the peak frequency is not significant. The peak frequencies are 135 kHz for the 5 µl droplet 134 kHz for the 30 µl droplet and 129 kHz for the 145 µl droplet. Compared to the wireless circuit without the EWOD chip, the frequency shift is also minimal. In addition, the voltage output at the receiver stays in a similar range regardless of the droplet volume. The voltages measured at each peak are 154, 153.5, and 152 V for 5, 30, 145 µl droplet volumes, respectively. These results imply that the present wireless circuit can be used for a wide range of droplet volume without necessarily adjusting the circuit parameters. As far as the overall capacitance of the EWOD chip including the droplet remains much smaller than the capacitance of the receiver, the droplet can be wirelessly driven via EWOD without any significant frequency shift or adjustment.

This result is also verified by deliberately adding another external capacitor in parallel with the existing capacitor (470 pF) at the receiver. The circuit set-up for this experiment is

shown in Fig. 30. The EWOD chip is replaced with additional capacitors and the behaviors of frequency are measured by changing the capacitance.

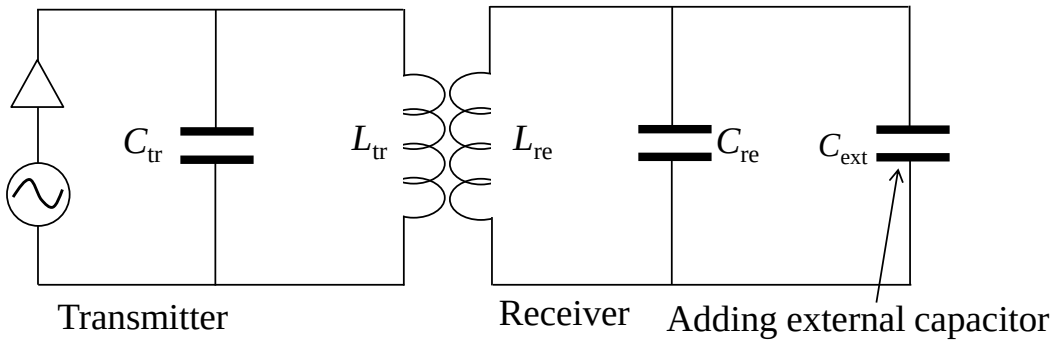

Figure 30. The wireless circuit set-up by adding external capacitor in place of EWOD with droplet. L_{tr}=0.055 mH, L_{re}=2.93 mH, C_{tr}=22000 pF, and C_{re}=470 pF, respectively.

No significant peak frequency shift is observed as far as the additional capacitance is much smaller than the external capacitor, for example, regions (a) and (b) in Fig. 31. When adding a capacitance similar to the capacitance of the present EWOD chip including the droplet, the frequency shift is minimal. The triangles denote the peak frequencies with the three droplets, as shown in Fig. 29. However, we can observe a significant frequency shift from 140 kHz when the additional capacitance is comparable to the existing capacitance, for example, point (c) in Fig. 31, the significant peak frequency shift begins to occur within this experiment set up when an additional capacitor is 470 pF which is equal to the existing external capacitor. The frequency shift is further observed when 1000 pF is added. These results are in good agreement with the results observed in Fig. 29. Since this circuit (especially for the receiver) is designed to have higher impedance at each *L* and *C* component than that of EWOD, the induced voltage at the receiver can be fully used without significant voltage loss for droplet manipulation.

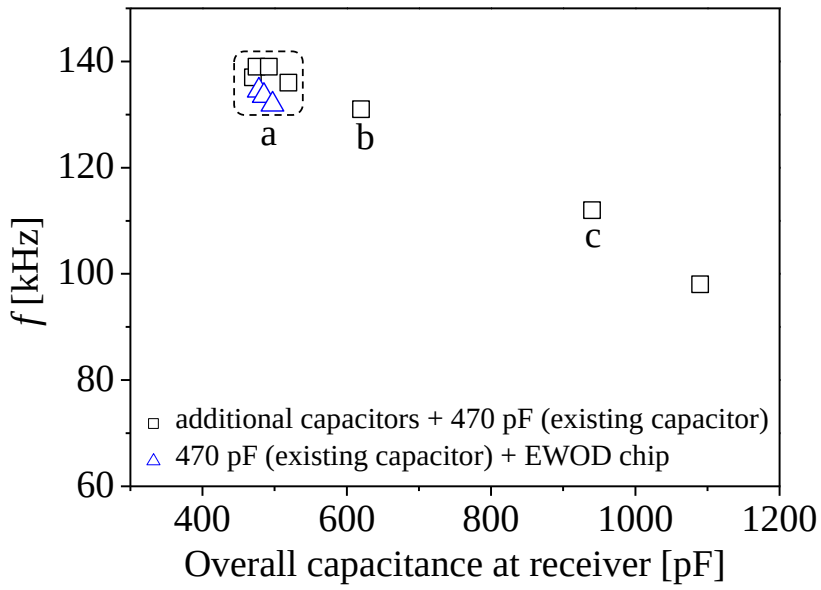

Figure 31. The shift of the resonant frequency in comparison with the data shown in Fig. 29 when an additional capacitor is added in the receiver in parallel to the existing external capacitor (470 pF).

3.2.3.3 Contact Angle Measurement and Voltage Drop across Droplet

A DI water droplet of 5 μl in volume is sitting on the dielectric layer (parylene layer of 4.8 μm in thickness), and the change in the contact angle is measured by changing the input voltage, accordingly the output at the receiver.

Figure 32 gives the measurement results. As the voltage at the receiver increases, the contact angle decreases. Here again, the overall voltage (V_t) denotes the voltage across the EWOD chip including the sessile droplet. The contact angle is saturated at 68^o when the overall voltage is over 300 V, and at a higher voltage than 300 V, the contact angle remains at the saturated angle. The initial contact angle measured with no voltage applied is 119^o, which means the span of the contact angle is 51^o. The corresponding droplet shape and its contact angles are shown in Fig. 32 (b).

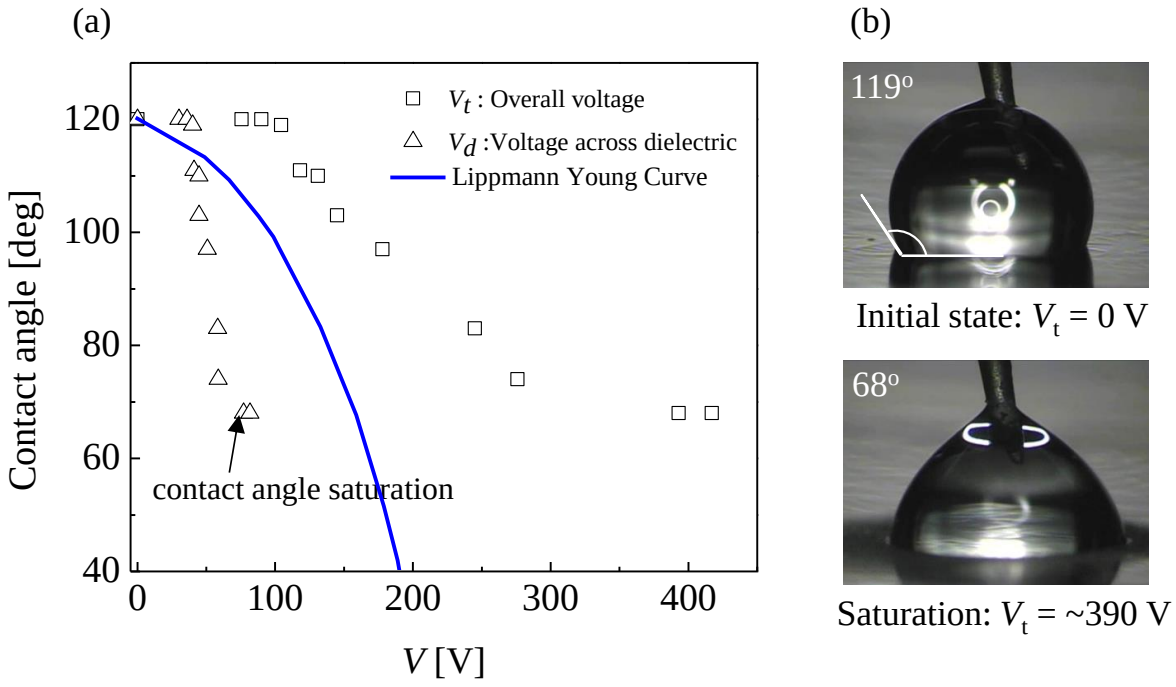

Figure 32. (a) Conact angle measured at 137 kHz. Square denotes the overall applied voltage to EWOD and triangle denotes the voltage only at dielectric layer. (b) and (c) are the corresponding droplet's shape and contact angle reading at initial and saturation state respectively.

We calculate the V_d (voltage across the dielectric layer), not V_t (overall voltage to EWOD) and its result also shown in Fig. 32(a) (triangle shapes). To find V_d, the overall circuit of the EWOD chip is modeled as a serial circuit of the droplet and the dielectric layer. Since the droplet and the dielectric layer are connected in series, the voltage across the dielectric layer can be calculated by using the transfer function. A significant voltage drop occurs across the droplet, not across the dielectric layer. As a consequence, the voltage across the dielectric layer is smaller than the overall voltage. This implies that for wireless EWOD operations the overall voltage produced at the receiver should be much higher than the typically required EWOD voltage. For example, at the onset of saturation, V_t is over 300 V but V_d is only about 80 V according to the data plot given in Fig. 32(a). The overall voltage is more than three times the voltage across the

dielectric layer. In addition, the blurred contact line at the saturation voltage can be also clearly observed from Fig. 32(b) photo which results from the ohmic losses over the droplet at high voltage application.

3.2.3.4 Droplet Oscillation with Wirelessly Transmitted Signal

Since the wireless transmission frequency (137 kHz) is much higher than the critical frequency of the droplet ω_{cri} (< 1 kHz), the droplet cannot oscillate at the transmission frequency but remains at a fixed contact angle. As mentioned earlier, however, droplet oscillation, in particular, at the natural frequency provides many useful functions. In order to oscillate a droplet at the natural frequency, the wireless transmission signal is amplitude-modulated.

A DI water droplet of 10 µl placed on a hydrophobic layer is driven by AM signal which is transmitted by the wireless powering set-up. The experiment set-up is exactly same as the Fig. 25 except that AM signal is generated from the function generator. The carrier frequency is fixed at 137 kHz. By changing the envelope frequency from 1 to 10^3 Hz, we could find that the maximum oscillation occurs at 122 Hz.

The snapshots of droplet oscillation within 5 ms of the enveloping signal are shown in Fig. 33(a). The snapshots were taken using the high-speed camera. The corresponding AM signal measured at the receiver is presented in Fig. 33(b). Since the high-speed camera was not synchronized with the enveloping signal, the phase at which each photo was taken is not known. However, we believe that the most left photo on top ($t = t_o$) in which the contact angle is greatest among the 6 photos corresponds to the time when the amplitude of the enveloping signal is close to the minimum whereas the time between time (t_o+4) ms and (t_o+5) ms in which the contact angle is lowest corresponds to the time when the amplitude of the enveloping signal is close to the maximum.

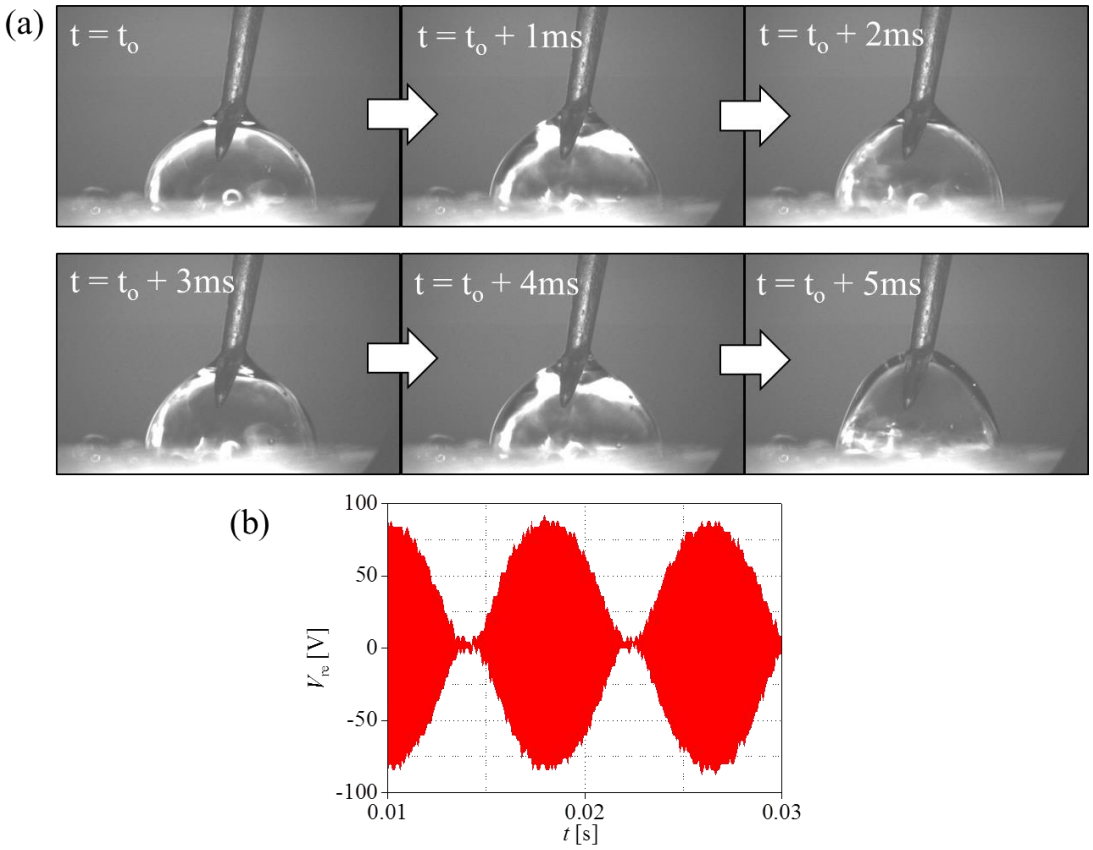

Figure 33. (a) High speed camera images of droplet (10 µl) oscillating with AM (122 Hz) signal transmitted at 137 kHz of carrier frequeny. (b) Corresponding signal applied to the droplet.

3.2.3.5 Transporting Droplet via Wireless EWOD

Finally, we demonstrate droplet transportation using AM signal at the enveloping frequency of 10 Hz and the carrier frequency of 137 kHz. The experimental set-up and AM signal at each circuit is given in Fig. 34.

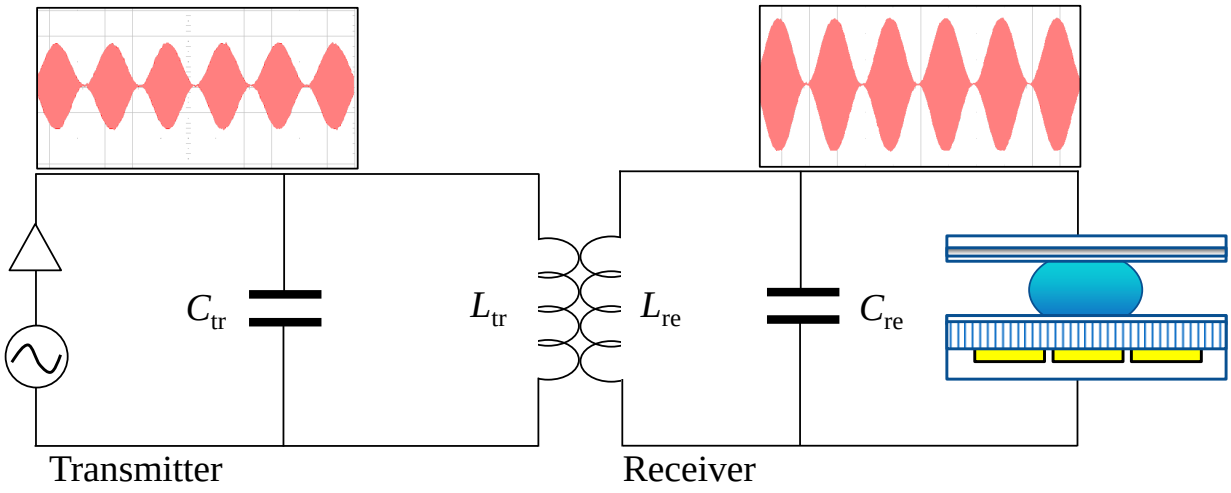

Figure 34. Wirelessly transmitted AM signal **(**10 Hz of envelope and 137 kHz of carrier frequency) is applied to EWOD to transport 2.5 µl of DI droplet.

The sequential snapshots of transporting of the droplet (2.5 µl in volume) are presented in Fig. 35. The wirelessly transmitted signal sequentially shifts from one electrode to the next in the linear array of electrodes to generate step-by-step transportations of the droplet. While in transportation, it is clearly observed that the droplet oscillates at 10 Hz.

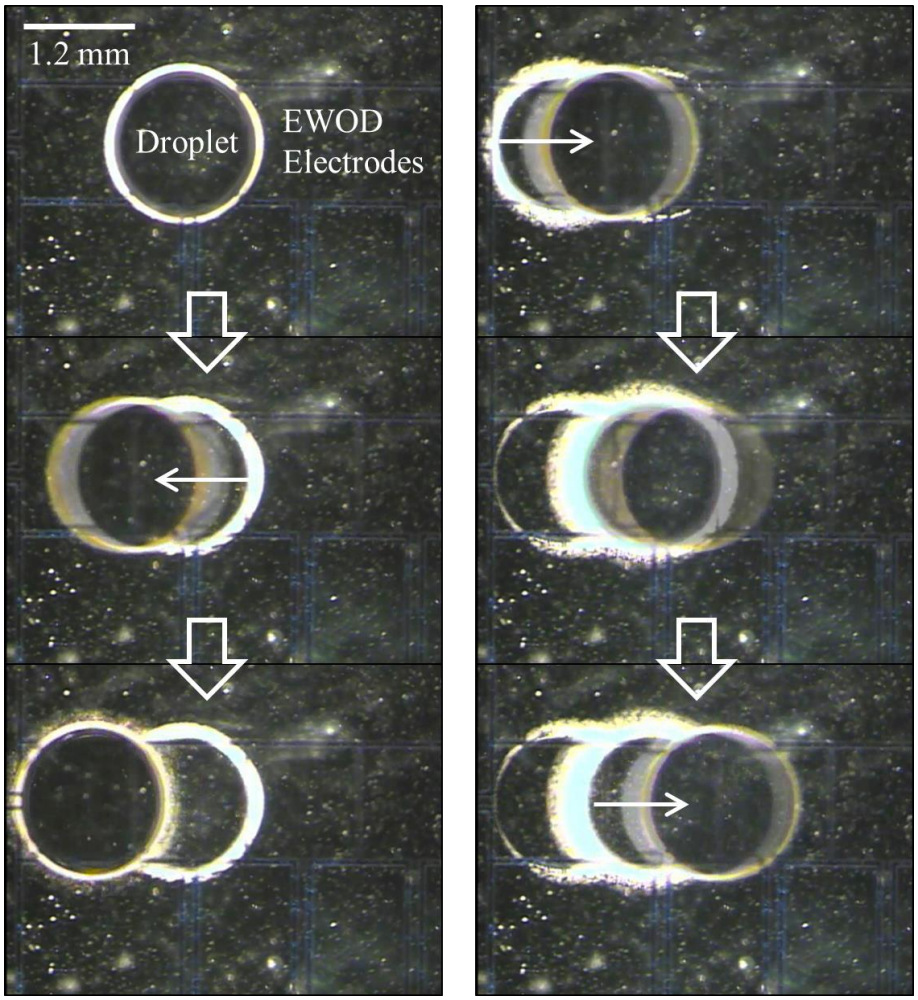

Figure 35. Snapshots of droplet transportation on EWOD electrodes. The droplet is actuate by wireless AM signal. The EWOD electrodes are activated sequentially from the right to the left (left column), and from the left to the right (right column). Each EWOD driving electrode has a square shape of 1.2×1.2 mm^2.

3.2.4 Summary and Conclusion

For wireless EWOD, a resonant L-C circuit based on inductive coupling was developed and investigated. When the transmitter as well as receiver circuits were set to resonate at the same frequency (137 kHz) by adjusting the coils and capacitors, high voltages (up to 390 V) at the receiver were achieved, which were sufficient to actuate droplets by EWOD. The overall

voltages obtained at the receiver should be much higher than the typical required EWOD voltage. We could not observe any significant voltage drop or resonance frequency shift at the receiver when droplets of 5, 30, 145 μl in volume were tested in the EWOD chip. This means that the circuit can be used for driving a wide range of droplet size without any circuit adjustment. In this case, however, the external capacitor at the receiver should be set to be much higher than the overall capacitance of the EWOD chip including the droplet. The presented transmission frequency (137 kHz) is too high to oscillate a droplet. Moreover, inductive coupling inherently has low efficiency at the low transmission frequency signal so that it may not be suitable for full droplet actuation. However, by embedding AM in the transmission signal, we achieved successful EWOD droplet oscillations of low frequency (< 1 kHz). Finally, using an array of EWOD electrodes, droplet transportation (which corresponds to pumping in the continuous microchannel microfluidics) was accomplished.

3.3 WIRELESS POWERING VIA PLANAR COILS

In this chapter, wireless receiver circuits are prepared and patterned on PCB. Due to lower *L* than the coils presented in the previous chapter, the transmission frequency is increased up to few MHz range. First, the wireless circuit without the demodulation circuit is investigated. Voltage measurements at the receiver circuits, separation distance vs. voltage output, contact angle measurements, and droplets oscillation with AM signal are provided. In another circuit set-up with addition of the external demodulation circuit, droplet's lateral transportation is demonstrated on testing EWOD devices fabricated on SiN wafer.

3.3.1 Experiments without External Demodulation Circuit

Overall schematic view of planar wireless EWOD is shown in Fig. 36(a). The upper part includes micro-fabricated receiver coils for wireless powering and EWOD electrodes for the droplet actuation. The dimensions being designed and fabricated are 7.5×6 cm^2 with 1.5 mm of board thickness. Each planar receiver coil has a rectangular shape with outer diameter no greater than 2.3 cm. The spool-type transmitter coils are prepared by winding the coils around a ferrite ring having outer diameter of 2.3 cm. These coils are placed underneath the planar wireless EWOD device and center to center alignment between the corresponding receiver and transmitter coils are maintained.

The droplet actuation model is also sketched in Fig. 36(b). The integrated device (bottom plate) is composed of 4 planar receiver coils and EWOD electrodes prepared on the PCB. A water droplet is pipetted on the EWOD electrode. Then, the top ground plate is placed over the bottom plate with about a 300 μm gap. A double-sided tape is used for a spacer between the top

and bottom plates to maintain the gap. As a result, the droplet is squeezed between the top and bottom plates and actuated by the wirelessly transmitted signal.

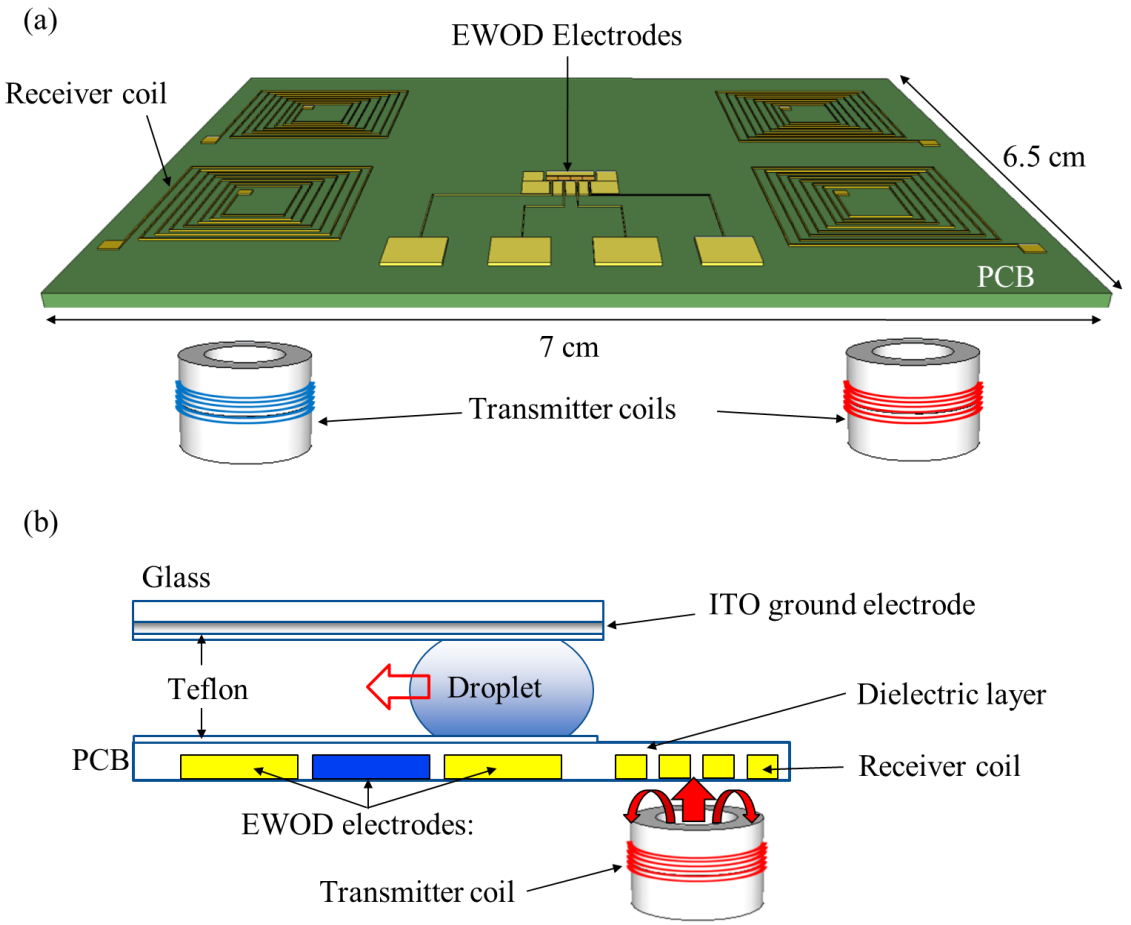

Figure 36. (a) An schematic of planar wireless device (coils) and EWOD electrodes. Transmitter coils are also located below each receiver coil in which center to center alignment is achieved. (b) Planar wireless EWOD system for droplet actuation.

3.3.1.1 Fabrication of Planar Wireless EWOD Device

The wireless EWOD device including planar receiver coils and EWOD electrodes (1.2×1.2 mm^2 square shape) are fabricated from PCB (15 µm thick of Cu layer) using standard photolithography process. The fabrication processes are capable of producing the wireless and

EWOD devices simultaneously in a simple and inexpensive manner with minimal dependence on facilities thereby the compact planar wireless EWOD devices can be easily realized. As a dielectric layer, parylene-C is chemically deposited on the PCB using the SCS (PDS 2010) parylene coater system.

The overall fabrication process illustrated in Fig. 37(a) is similar with that of testing EWOD device preparation in 3.2.2 except that both wireless coils and EWOD electrodes are simultaneously prepared. Fig. 37(b) also shows a photo of the fabricated device (7.5×6×0.15 cm^3) after completion of all fabrication processes. For the top plate for the grounding, the transparent and conductive ITO glass plate is prepared and coated with a 0.5% Teflon solution. The transmitter coils are prepared by winding the Cu wire (250 μm in diameter, 5 winding-turns) manually around a ring shaped air-core ferrite having the outer diameter of 2.3 cm. The photo of the transmitter coils is also shown in Fig. 37(d).

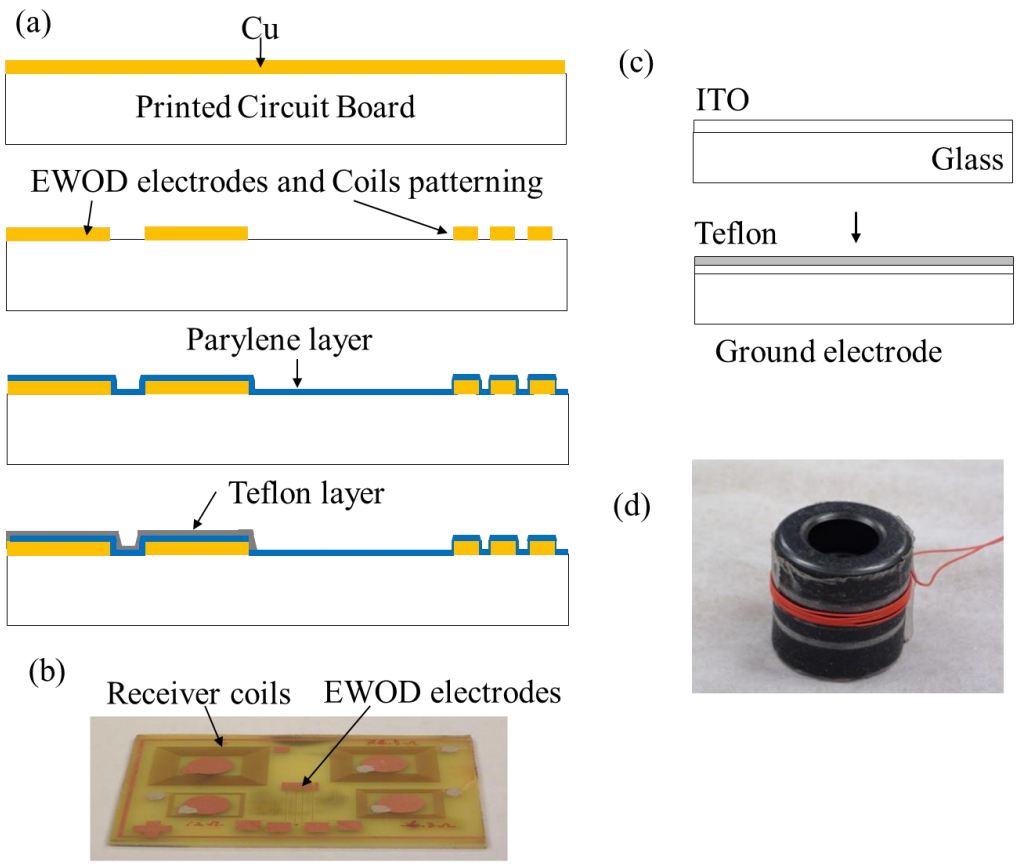

Figure 37. (a) Microfabrication process of planar wireless EWOD device. Cu layer (15 µm thickness) on top of 1.5 mm of PCB and patterning of receiver coils and EWOD electrodes.Deposition of 3.1 µm parylene layer and coating of hydrophobic Teflon layer. (b) Photo of microfabricated planar wireless EWOD device.(C) Top grounding electrode preparation on ITO coated by 0.5% Teflon. (d) Photo of transmitter coil having 5 winding-tuns around ferrite ring.

3.3.1.2 Wireless Circuit Set-up

An equivalent electric circuit in planar wireless powering is shown in Fig. 38. The transmitter circuit is a parallel L-C circuit composed of a function generator (Agilent 33220A), a power amplifier (Trek 2100 HF Driver), four transmitter coils and a capacitor (10000 pF) in parallel connection. Each transmitter coil has the inductance of 5.5~6 µH (measured by Agilent LCR meter 4285A). The receiver circuit also has an L-C circuit composed of a microfabricated planar

receiver coils, a parasitic capacitor, and EWOD chip. The capacitor in receiver circuit can be removed as the EWOD chip with droplet itself serves as a capacitor, particularly when the carrier frequency is very high (order of MHz). Four planar coils (two of 42 winding-turns and two of 50 winding-turns) are connected in series and each receiver coil is aligned with the corresponding transmitter coils underneath in which the center-to-center alignment is maintained. The measured inductance values are in the range of 30~42 μH for 42~50 winding-turns of the planar receiver coils.

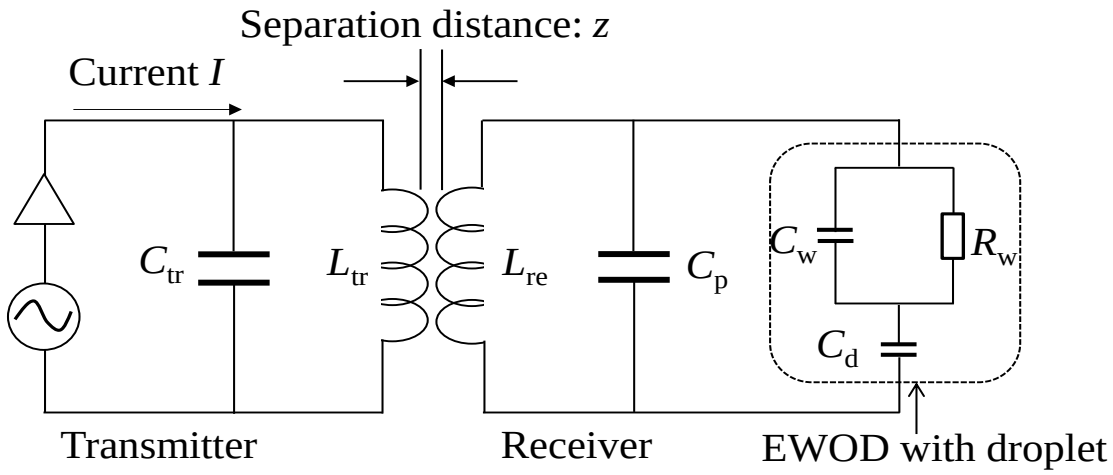

Figure 38. An equivalent electric circuit using magnetic induction for planar wireless EWOD. The EWOD part (dielectric C_d including a droplet, C_w and R_w) is connected to the receiver coil in parallel. L_{tr} and C_{tr} is the inductance and capacitance of the transmitter, L_{re} and C_p is the inductance and parasitic capacitance of the receiver.

Table 6. The measured *L* and *R* values for planar reciever coils and spool-type transmitter coil by LCR meter (Agilent 4285A).

	PCB coils (Receiver)		Transmitter coil
Number of turns	42	50	5
L [μH]	~30	~42	~5.8
R [Ω]	94.5	151.5	0.7

3.3.1.3 Voltage Output Measurement

After the wireless circuit set-up, the voltage output is measured at the two terminals of the receiver coil. Fig. 39(a) shows the induced voltage at the receiver over the frequency and the maximum attainable voltage is 237 V at 2.6 MHz without a droplet installation when transmitter coils and receiver coils are in contact distance. Since 4 receiver coils are in serial connection each other, the overall voltage attained is a summation of the voltage from the each single receiver coils' terminal. The corresponding waveforms are also given in Fig. 39 (b). The general peak behavior of this circuit is similar to Fig. 27(a) that is acquired at tuned circuit but having broad peak range. As listed in Table 5, the receiver coils fabricated on the PCB have a higher resistance and lower inductance values resulting in low quality factor. This implies that the selection of the transmission frequency is flexible and wide by a simple change of circuit devices (e.g. externally installed capacitors at the receiver circuit or transmitter circuit as well).

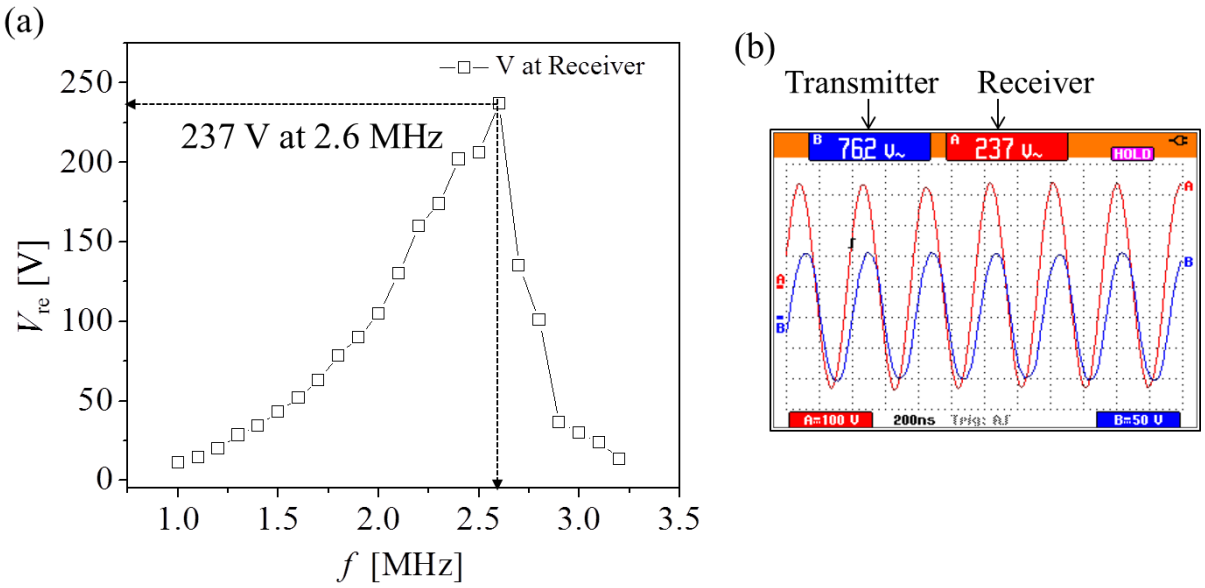

Figure 39. (a) Induced voltage at the receiver without droplet. (b) Corresponding waveforms at the transmitter (blue curve) and receiver (red curve).

Figure 40 also shows the relation of the receiver voltage to the separation distance between the transmitter and receiver coils measured at 2.6 MHz. As the separation distance between two coils is increased, the measured voltage at the receiver decays exponentially. Up to 2 cm of the separation distance, the decay is more rapid while the decay beyond 2 cm is gradual. In all cases, the distance should be maintained smaller than 2 cm in order for the voltage at the receiver to be higher than 50 V.

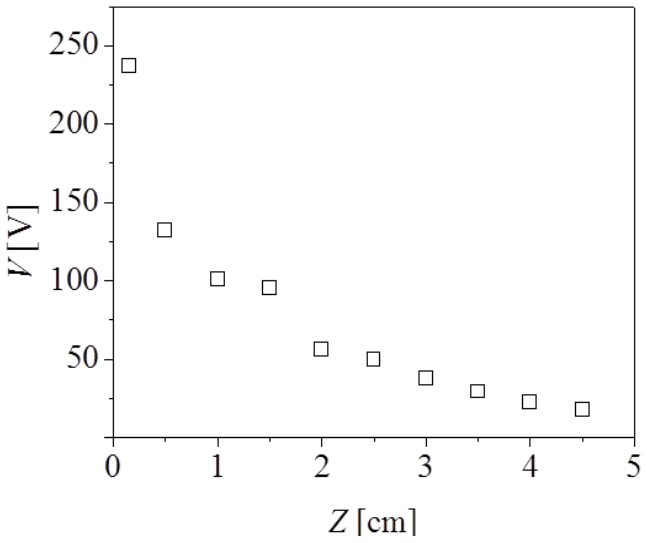

Figure 40. Separation distance between transmitter and planar receiver coils vs. induced voltage at the receiver (transmission frequency is fixed at 2.6 MHz).

3.3.1.4 Contact Angle Measurement

The measurement of the apparent contact angle change is performed with 5 μl of sessile liquid droplet. The liquid droplet having the conductivity σ=1413×10^{-4} S/m (measured at 22.9^{o}C by Orion 3-Star pH meter) is sitting on the EWOD chip, and the change in the contact angle is measured by changing the voltage from the function generator. The EWOD chip is prepared on Si wafer cleaved in small pieces (2×2 cm^2) having the dielectric layer (parylene-C) of 3.1 μm in thickness. 2% Teflon (~0.9 μm) AF is also coated over the entire area of samples to increase hydrophobicity. Instead of the top ground plate, a sharp tip is immersed into the droplet.

Figure 42 shows the measurement results performed at 1.75 MHz and the results are compared with Lippmann-Young's curve (solid curve in the same figure). The transmission frequency having the maximum voltage output has been shifted from 2.6 MHz to 1.75 MHz after the droplet installation on the EWOD chip while the contact angle measurement. Since the EWOD chip with the droplet also plays a role as additional capacitor connected in parallel with

the receiver coils, the overall capacitance is increased and thus the transmission frequency is lowered with the droplet installation.

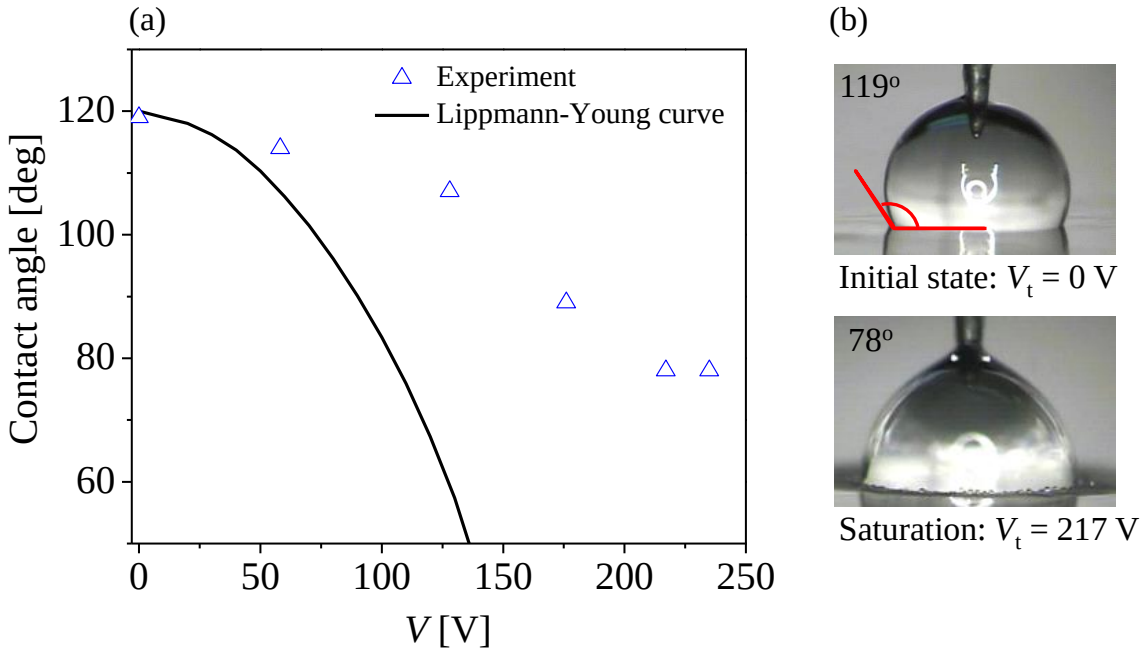

Figure 41. Measurement of 5 µl sessile droplet contact (σ=1413×10^{-4} S/m) angle vs. voltage at the receiver wirelessly transmitted at 1.75 MHz. The theoretical (solid) line is obtained from Lippmann-Young equation. (b) The initial contact angle is 119^{o} and the contact angle is 78^{o} when V_t=217 V. The contact angle saturation is observed at 78^{o}.

Compare to Lippmann-Young's curve in the Fig. 41(a), overall contact angle behaviors are similar, which is as the voltage at the receiver increases, the contact angle decreases. However, due to the significant voltage drop across the droplet at this transmission frequency, the overall applied voltage to the EWOD chip cannot fully contribute to the dielectric layer resulting in the smaller span of contact angle. The contact angle is saturated at 78^{o} when the overall voltage is 217 V, and at a higher voltage than 217 V, the contact angle remains at the

saturated angle. The initial contact angle is measured to be 119^{o} when no voltage is applied to the EWOD. The span of the contact angle is 41^{o} from the initial state to the saturation. The photos of corresponding contact angle and shape change are shown in Fig. 41(b). At the saturation, the vigorous small droplets are produced at the contact lines due to high voltage application.

3.3.1.5 Droplet Oscillation

Overlaid snapshots of droplet oscillation at 100 Hz of the enveloping signal are shown in Fig. 42(a). A droplet of 5 µl having conductivity of 1413×10^{-4} S/m placed on a hydrophobic layer is driven by an AM signal which is transmitted by the wireless powering set-up. The carrier frequency is fixed at 1.75 MHz. The snapshots are taken using the high-speed camera. The corresponding AM signal (the high-speed camera was not synchronized with the enveloping signal) measured at the receiver is also shown in Fig. 42 (b).

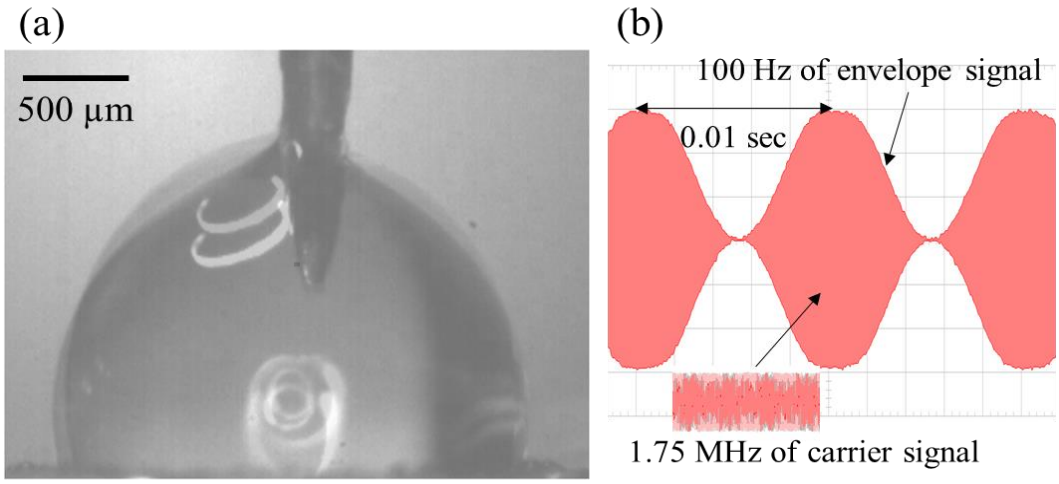

Figure 42. Droplet oscillation by wirelessly transmitted signal. (a) Overlaid high-speed camera images of droplet oscillation; 5 µl. (b) The envelope frequency is 100 Hz and the carrier frequency is 1.75 MHz.

3.3.1.6 Droplet Transportation on PCB EWOD Electrodes

From the contact angle measurement in previous section, the span of contact angle is 41^{o} with the conductivity of 1413×10^{-4} S/m, so it is expected that the droplet transportation or lateral motion on PCB EWOD electrodes can be achieved in the integrated planar wireless device. To demonstrate droplet's lateral motion on PCB EWOD electrodes, we also implement AM with the wirelessly transmitted signal (1.75 MHz).

A droplet of 2 µl having conductivity of 1413×10^{-4} S/m is placed on PCB EWOD electrode as shown in Fig. 43(a). Initially the clear oscillation is observed, and it is also observed that small droplet is generated along the contact line which makes the captured images blurred. While in one-step lateral motion (one step to left electrode (b), then one step to right electrode(c)), the loss of droplet volume becomes more significant as it appears in Fig. 44(c) ~ (f). No further lateral motion of the droplet is applicable. The corresponding waveform applied to EWOD is also given in Fig. 43(g). As it can be seen from the waveform applied to the EWOD, the signal contains the high frequency transmission component which makes the voltage drop across the droplet. As a result, ohmic losses within the droplet occur and make the mother droplet to produce the small droplets at the contact line. In addition, since the conductivity given in this experiment is ~4 orders of magnitude higher than DI water (which means more ionized molecules in the present droplet), the more vigorous small droplets are produced.

Unlike the wireless circuit prepared with spool-type coils in previous section, the planar coil has the physical size limit, inherently both the transmission frequency and induction voltage at the receiver are limited. Thus, in order for the present wireless circuit to be functional with the droplet's smooth lateral movement, the demodulation circuit needs to be added in which the high frequency components are effectively removed, and thus droplet will not see the high frequency

components after the demodulator resulting in significant reduction of the ohmic losses, accordingly no significant volume loss of the droplet is expected while in the lateral transportation. Thus, the further discussion is presented via the external demodulation circuit installed in the current planar wireless circuit set-up.

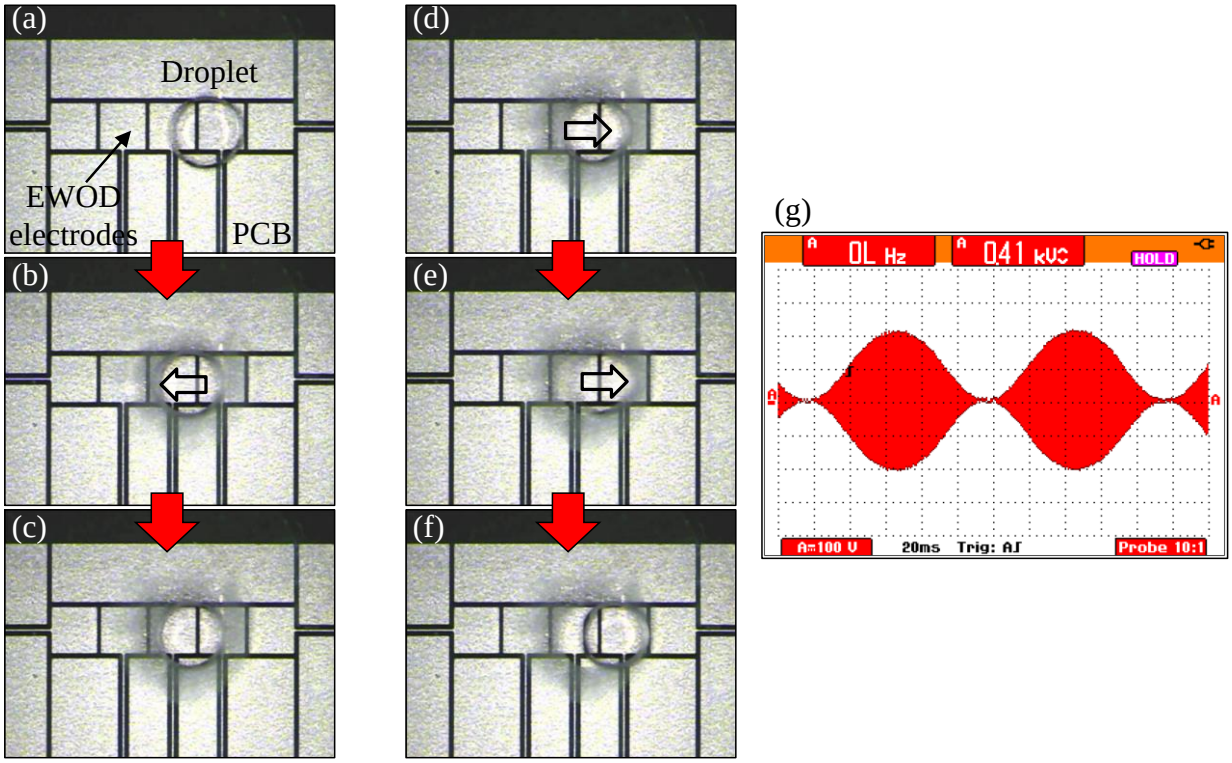

Figure 43. Droplet's lateral transportation (2 µl having σ of 1413×10^{-4} S/m on PCB EWOD electrodes a ~ f) at 1.75 MHz of carrier frequency with 10 Hz AM signal (g).

3.3.2 Experiments with External Demodulation Circuit

3.3.2.1 Addition of the Demodulation Circuit

The demodulation circuit composed of a diode and capacitor (1000 pF) is added in present receiver circuit. The circuit set-up with the demodulator is illustrated in Fig. 44. Since the droplet would not see any high frequency component by the demodulation circuit, the voltage drop across the droplet is possibly decreased resulting in the larger span of contact angle, which enables the droplet to transport without significant volume loss.

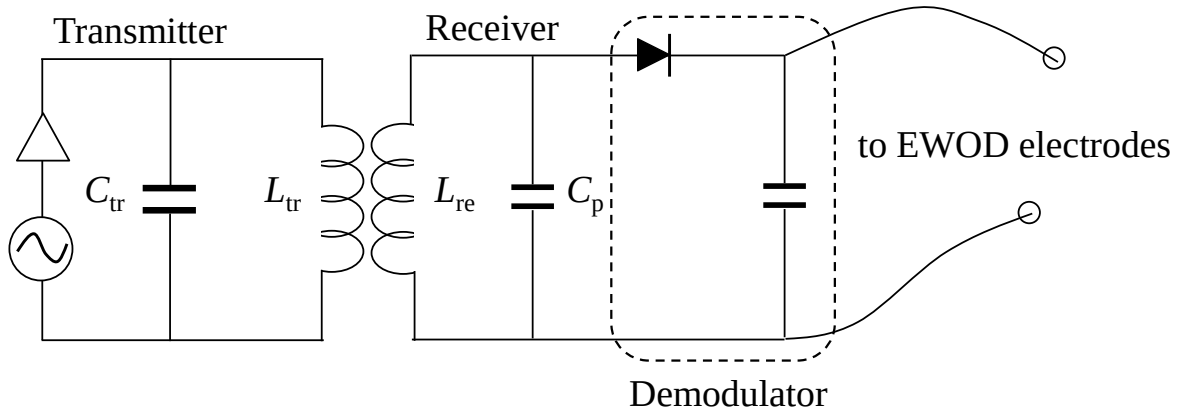

Figure 44. Addition of demodulation circuit in the current planar wireless circuit. The demodulation circuit composed of single diode (IN5399-E3/54) and capaciotr (10^{-8} F).

3.3.2.2 Droplet Transportation on PCB EWOD Electrodes

After the demodulation circuit is added, the droplet transportation experiment (2 μl having σ of 1413×10^{-4} S/m) is performed on PCB EWOD electrodes. The applied signal to the EWOD after the demodulator is presented in Fig. 45(g) only showing the low frequency envelope (10 Hz). As the captured images shown in Fig. 45(a) ~ (f), the first distinct feature is that the blurred images are no more observed while in motion as opposed to the images seen in Fig. 43. However, the

contact line of the droplet on the activated electrode, (e.g. the contact line in (b) and (d) in the figure 45, marked red-dash line), the droplet is stuck on the electrode, the contact line becomes wide and thus the further movement is hindered.

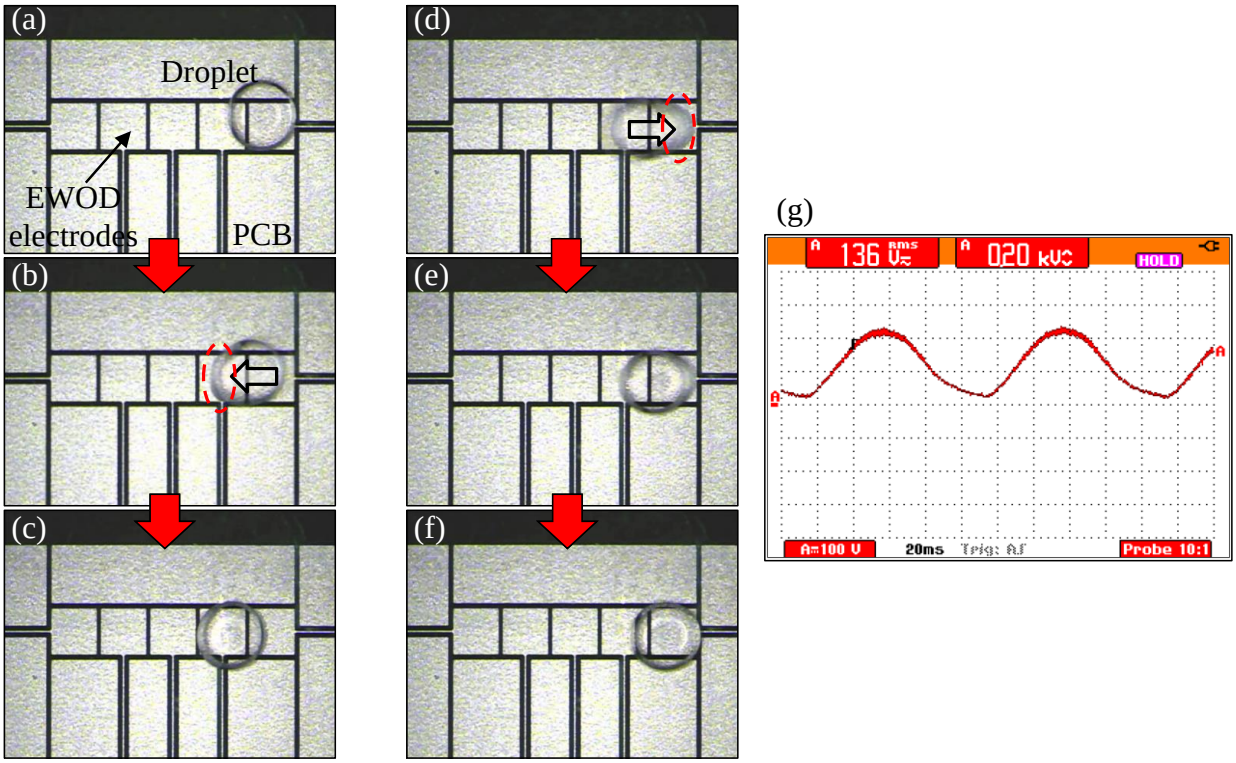

Figure 45. The lateral transportation of droplet (2 μl having σ of 1413×10^{-4} S/m driving by 2.15 MHz of carrier frequency with 10 Hz of envelope) one-step next electrode after the demodulator (a ~ f). The size of single EWOD electrode is 1.2×1.2 mm^2. (g) The demodulated signal is applied to the EWOD.

The one possible reason of the limited movement could be the surface condition of the PCB EWOD electrodes. Surface roughness, defects and wettability at a separation line are known to affect the contact angle and contact angle hysteresis [87, 88]. If there are sufficient numbers of defects or surface is not even, the droplet might not be able to move even in the application of the electric potential. We have prepared three EWOD electrodes in different

substrates and electrode materials conditions. PCB electrode (~15 µm of Cu thickness) in (a), Al electrode (~100 nm thick) fabricated on SiO_2 wafer in (b), and Au electrode (~100 nm thick) fabricated on glass substrate in (c) are illustrated in Fig. 47. Out of three samples, the EWOD electrode fabricated on PCB expresses the roughest surface condition compared with other two electrodes in which droplet's lateral transportation on PCB EWOD electrodes is limited.

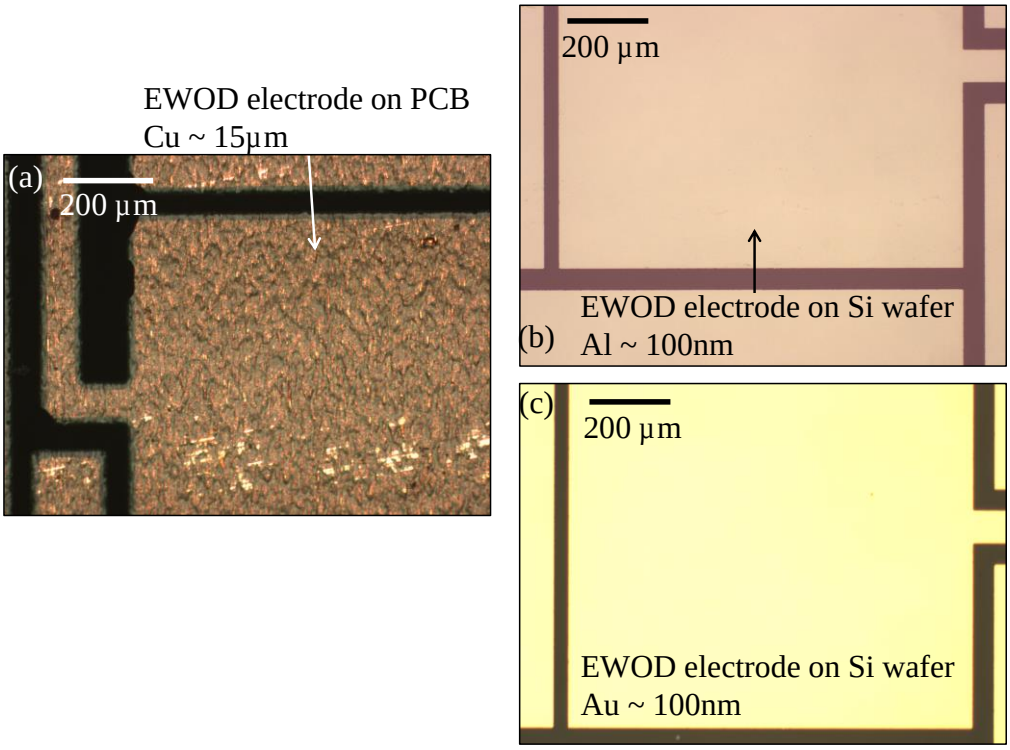

Figure 46. Three different EWOD electrodes prepared on PCB (a), Al on Si (b), and Au on Si (c).

By comparison with Al EWOD electrodes fabricated on Si wafer, we could observe more smooth and continuous transportation of the droplet. The droplet's lateral transportation captured in Fig. 47 is performed under the same applied potential given in Fig. 45(g) except for the EWOD electrodes condition. Initially the droplet's oscillation is observed (Fig. 47(a)), although

the image doesn't show the oscillation clearly, by the sequential activation to the next adjacent electrode, the smooth and continuous lateral movement is achieved.

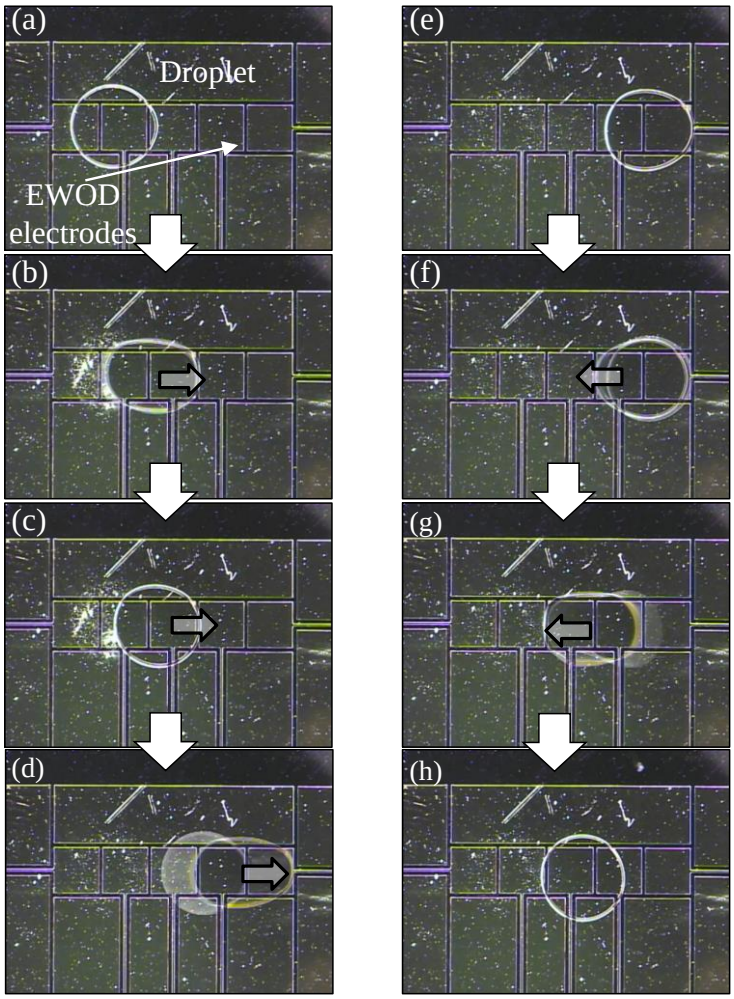

Figure 47. The sequential movement of the droplet (2 µl having σ of 1413×10^{-4} S/m) on Al EWOD electrodes on Si wafer at 2.15 MHz with 10 Hz AM signal. The applied signal is same as the one in Fig. 45(g).

3.3.3 Summary and Conclusion

In this chapter, the development and experimental verifications of planar wireless powering for EWOD actuation were presented and discussed. First, the wireless powering was achieved by

planar PCB coils (not by spool-type or commercial coils), resulting in seamless integration with EWOD array electrodes on a single and compact chip. The obtained voltage for wireless EWOD was over 230 V at 2.6 MHz without droplet installation, which is much higher than typically required EWOD voltages. Although the overall peak behavior was similar with the tuned circuit presented in the previous chapter, the more wide and broad range of peak behavior was obtained due to the intrinsic properties of the planar coil (low L and high R). As a consequence, the peak or transmission frequency was slightly shifted by addition of the droplets or external demodulation circuit. AM technique was also applied to the present wireless powering in order to oscillate droplets and we could observe the droplets oscillation even in the higher transmission frequency (~MHz range). For the efficient droplet's lateral actuation, we added the external demodulation circuit in front of the EOWD and we could demonstrate the lateral transportation of the droplet while in oscillation. It is obvious for the planar coils that the addition of the demodulation circuit is practically important due to the reduction of significant voltage division effect caused by the high transmission frequency.

4.0 APPLICATION OF PLANAR WIRELESS EWOD

In this chapter, applications of the planar wireless EWOD are presented. The planar structured wireless EWOD device is applied to the particle collection system and it is demonstrated by the droplet's lateral actuation while sweeping and collecting the particles. The planar wireless device is further applied to a mini-boat or floating object propulsion system, and the boat installed with the wireless devices is operated by the EWOD principle.

4.1 PARTICLE COLLECTING

4.1.1 The Concept of Particle Collecting

Potentially harmful particles existing in an airborne cloud of matter as a solid, liquid, or gas in environments can result in many adverse health effects such as asthma, infection, toxic reaction, hypersensitivity, and etc. To prevent exposure to harmful particles, many studies have been performed to find the better particles sampling methods [89, 90].

The particle collecting concept typically comprises two main steps: sampling (collecting) and analysis. Usually in a conventional sampling system, once the particles of interest are collected, they are analyzed in a laboratory scale which requires many analysis facilities. Unlike the conventional laboratory scale sampling and analysis performed so far, the lab-on-a-chip

based particle sampling has many advantages: automation, high throughput and short processing time. However, there still remains challenging issues such as many manual steps and large volume of the liquid [7].

In the previous studies performed by Zhao [91], theoretical and experimental works along with microfabricated testing devices were done and the underlying physics and optimal sampling conditions were investigated. Figure 48 represents the envisioned particles sampling system suggested by Zhao. The particles of interest are stopped on a filter membrane in the mean while air suction is applied through the filter membrane. Then a liquid droplet is transported around on the filter membrane by the EWOD principle [5], and the particles on the filter surface are collected into the droplet. The collecting of the particles from the surface is caused by the interfacial surface tension. Finally, the collected particles with the droplet are transported automatically to a lab-on-a-chip analysis system by EWOD actuation [7, 91].

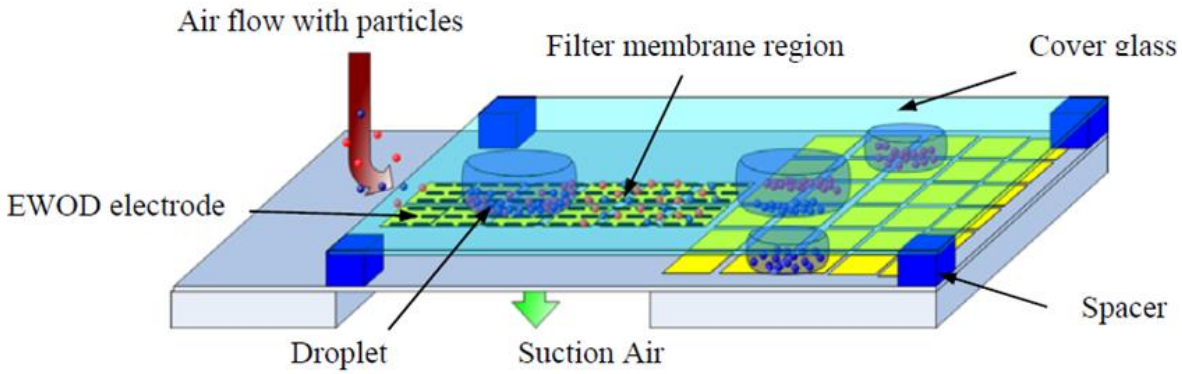

Figure 48. Airborne particle collection system integrated with digital microfluidics for sample analysis [91]. The droplets are transported by activating the array of electrodes by EWOD, collecting the particles on the filter membrane. The droplets containing the particles are automatically transported by EWOD to the next section for downstream on-chip analysis.

Although the idea of a lab-on-a-chip analysis by the droplet actuation based on EWOD has been enabled for the particle collecting and analysis to be simple, and thereby the scale of the analysis facilities are reduced with the small volume of the droplet [7, 91], the studies were performed in the cumbersome wiring between fragile Si filters and power circuitry. The complicate wiring structure and power circuitry still remains challenging tasks to overcome, while the EWOD with advanced analysis technique is struggling to find new area where the remote operation is necessary to extend its application.

As it is easily found in lab-on-a-chip EWOD, whether the system is open or closed, conventional EWOD system is designed on a planar structure electrodes to make the droplet's horizontal and lateral actuation easier while performing its function. One way to overcome the complicate and inconvenient electrical connection of current EWOD system, the application of the planar powering devices to conventional EWOD will contribute as a potential platform resulting in compact and reduced lab-on-a-chip system having more convenient sampling cycle with high robustness.

The sketch of suggested planar wireless EWOD device for the particle collecting system is illustrated in Fig. 49. The entire device mainly consists of two units on a horizontal plane: EWOD device for the particle collecting and the wireless powering device for the droplet actuation. The structure is much simpler than the conventional EWOD actuation system. The wirelessly delivered power activates the electrodes in which droplet can move laterally on the horizontal EWOD electrodes while collecting the particles. After collecting the particles, EWOD device with particles are easily detached from the main wireless platform for the further analysis while the wireless powering device is waiting for next EWOD device. Eventually this simple cycling by planar wireless platform would facilitate more rapid and accurate analysis.

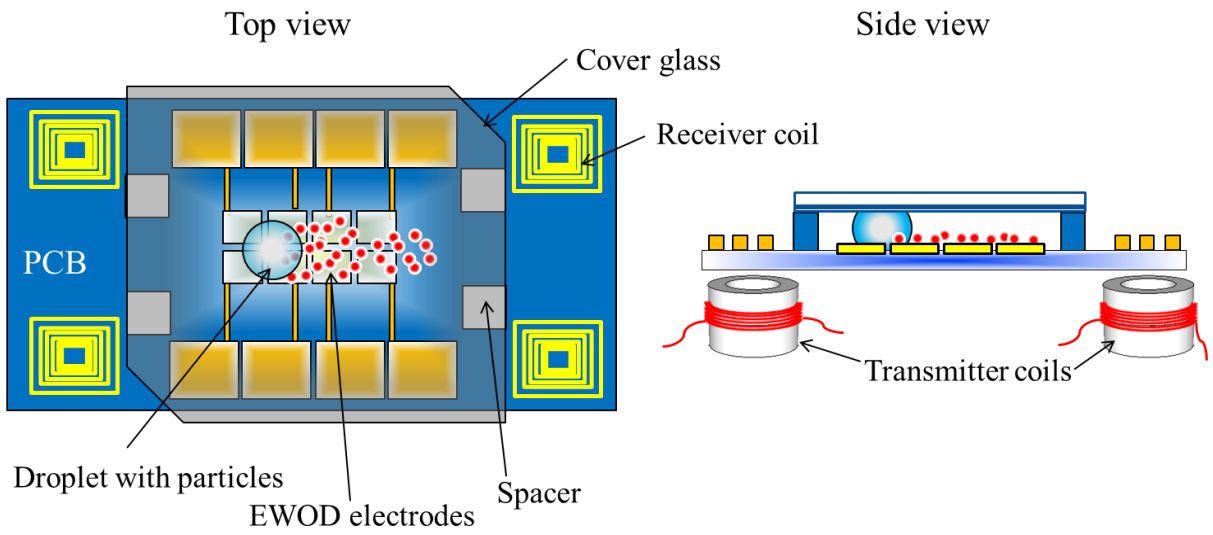

Figure 49. A schematic view of planar wireless EWOD for particle collecting. The upper integrated chip includes micro-fabricated receiver coils for wireless powering and EWOD electrodes for the droplet actuation.

4.1.2 Demonstration: Particle Collecting by Planar Wireless EWOD

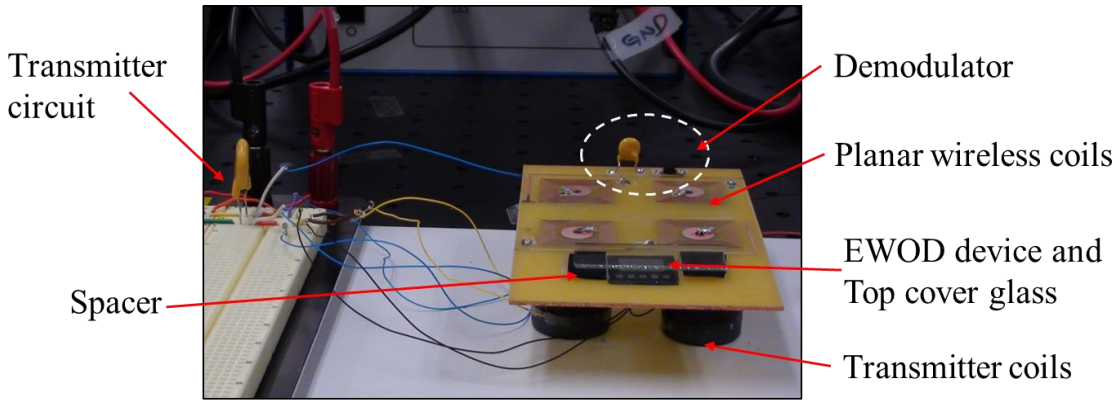

Figure 50. A schematic of the integrated wireless droplet actuation system. The system consists of the planar receivers and the demodulation circuit (capacitor+diode) with EWOD array electrodes on PCB (upper plate). Each receiver coil has a rectangular shape (outer dimension < 2.3 cm) and center-to-center aligned with homemade transmitter coils (bottom).

In order to demonstrate the particle collecting with the planar wireless device, a hydrophilic particle type that is borosilicate glass beads (40 μm in diameter, 9000 series, Duke Scientific Inc.) is selected. The circuit set-up is same as the one given in Fig. 44. The wirelessly transmitted AM signal (2.15 MHz of carrier and 100 Hz of envelope frequency) is demodulated and thus the droplet only meets the low frequency yet high voltage signal as given in Fig. 51(upper red waveform). The corresponding AM signal at the transmitter circuit is also given in Fig. 51 (bottom blue waveform).

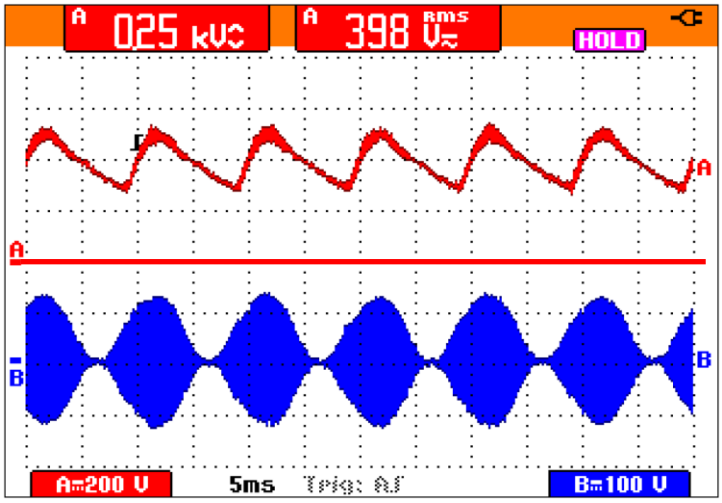

Figure 51. The wirelessly transmitted signal to the EWOD in red (upper) after the demodulation and the corresponding transmitter signal in blue (bottom) having 2.15 MHz of carrier and 100 Hz of envelope frequency.

The demonstration of sequential motion (captured images) is shown in Fig. 52. An array of the driving electrodes is patterned in a way that the droplet moves in a lateral path. The particles are deposited on the electrodes with care and the distribution of particles is improved by manually and gently tapping the margin area of the EWOD device. By sequential activation of the EWOD electrodes, the droplet sweeps and collects the particles inside the droplet while in lateral transportation simultaneously. The electrodes on which the droplet has passed become

clear indicating that the particles rarely remain on the path. Finally, the collected particles are suspended inside the droplet. After collecting the particles, the top glass plate is removed to enhance evaporation. About 10 minutes later the water droplet is completely evaporated, as shown in the last photo in Fig. 52, leaving a stack of the collected particles.

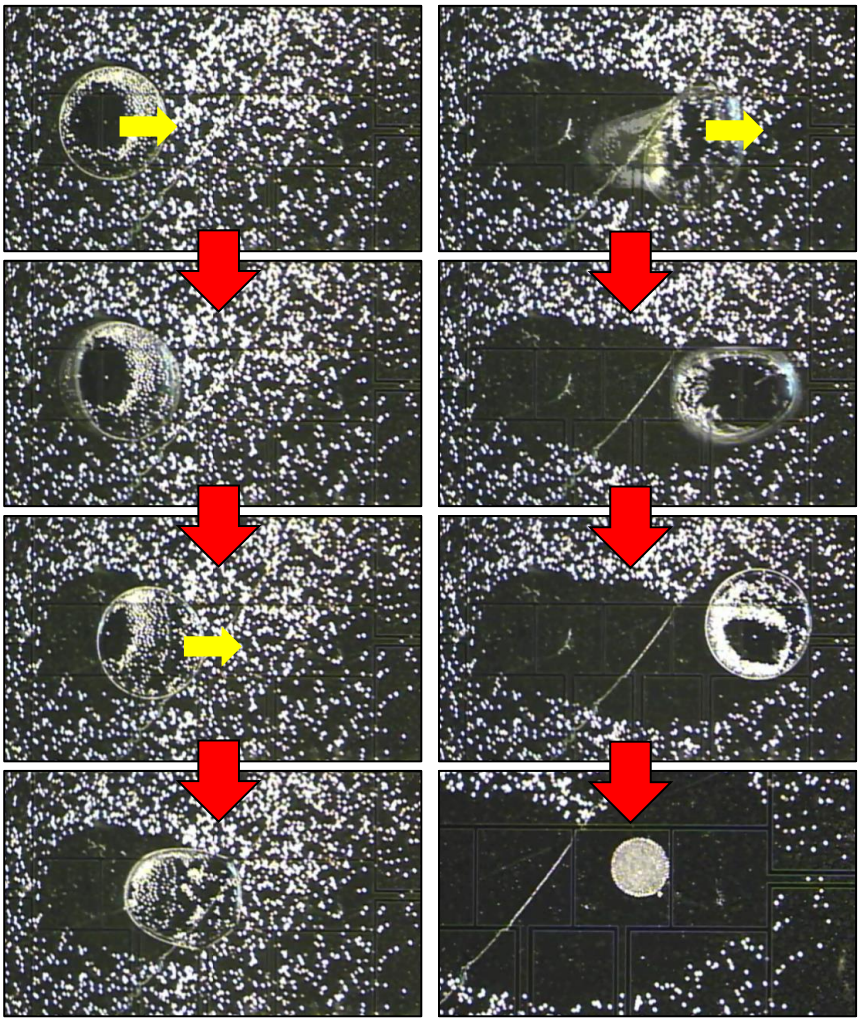

Figure 52. Demonstration of particle collecting by wirelessly transmitted signal (2 µl of DI water droplet). The transmission and envelope frequency is 2.15 MHz and 100 Hz respectively. The sequential motion of droplet colleting the 40 µm of glass beads. The final photo shows a stack of collected particles after the evaporation.

4.2 MINI-BOAT PROPULSION BY WIRELESS EWOD

4.2.1 The Concept of Mini-Boat Propulsion by EWOD

Vertical oscillation at the three-phase contact line operated by AC EWOD can be utilized to propel the mini-boat or floating object (few cm in size). EWOD electrode installed on the mini-boat is partially immersed in water and thereby net streaming flow is generated by contact line oscillation activated by AC signal [92, 93]. Except for the controllable parameters, such as AC frequency, signal voltage, dielectric layer thickness, and water conductivity, that may affect the propulsion speed, since the propulsion force is very small (several tens of micro-Newton), some other external factors, such as environment air flow and force from bended connection wires, can also strongly influence the propulsion. The water floating objects system can be potentially applied to environment monitoring systems and surveillance security systems.

In conventional boat propulsion system as illustrated in Fig. 53, the mini-boat devices have been powered by thin copper wires (typically ~30 μm in diameter) to minimize the effects of wire bending to the direct boat motion, which might be able to limit the propulsion of the boat. Instead of employing the thin wire in the mini-boat propulsion system, the wirelessly operated system would prevent the adverse effect from the propulsion. The boat equipped with wireless device propelling by EWOD principle without thin wires is described in Fig. 54.

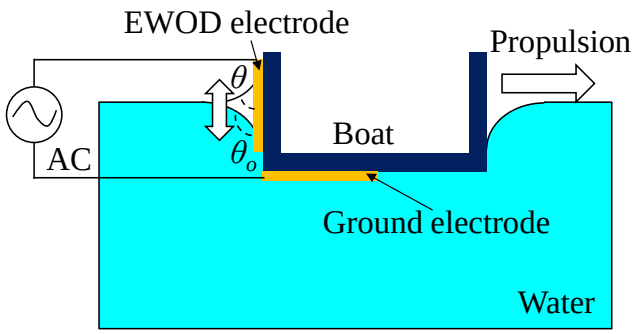

Figure 53. Typical mini-boat propulsion system by EWOD principle.

For the successful wireless operation, there are several factors to be considered. Since the propulsion speed reaches the peak at around 100 Hz and monotonically decreases to zero at around 1 kHz, the wirelessly transmitted high frequency signal (up to MHz range) cannot be directly applied to EWOD electrodes. To apply a low frequency signal from the wirelessly obtained high frequency yet high voltage signal, the AM (envelope frequency <1 kHz) needs to be implemented followed by demodulation circuit for the vertical oscillation at the interface. The air/water interface area plays a critical role for the vertical oscillation driven by the AC electrowetting. If the total weight of the wireless boat propulsion system (boat and wireless receiver unit) is too heavy, the interface area would be increased accordingly. As a result, the drag force (not by the electrowetting) will be also increased. Thus, the weight of the boat and wireless system needs to be minimized to satisfy the EWOD driven boat propulsion.

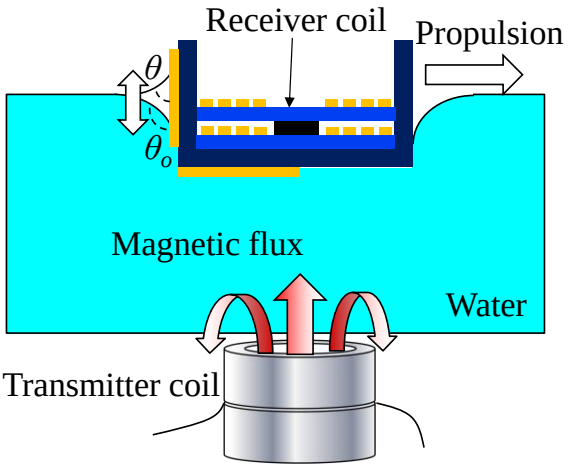

Figure 54. The wireless mini-boat propulsion system.

4.2.2 Demonstration: Wireless EWOD Mini-Boat Propulsion

A transparent box-type mini-boat with an open top (3.8×3.2×1 cm^3) is prepared. Two planar receiver coils having 20 and 42 winding-turns are connected and stacked in series. The fabrication process is illustrated in Fig. 55(a). For EWOD electrodes as shown in Fig. 55(b), two flexible Cu sheets (18 μm of Cu thickness) coated with the parylene (2.5 μm of thickness) are glued on the sidewall of the boat in Fig. 55(c) and Teflon layer is also coated on top of the parylene layer. The ground (aluminum) electrode is also installed on the bottom side of the boat. The total weight of the wireless boat is approximately 7.1 gram after all the devices and electrodes installation. The photo of the wireless EWOD boat is shown in the Fig. 55(d).

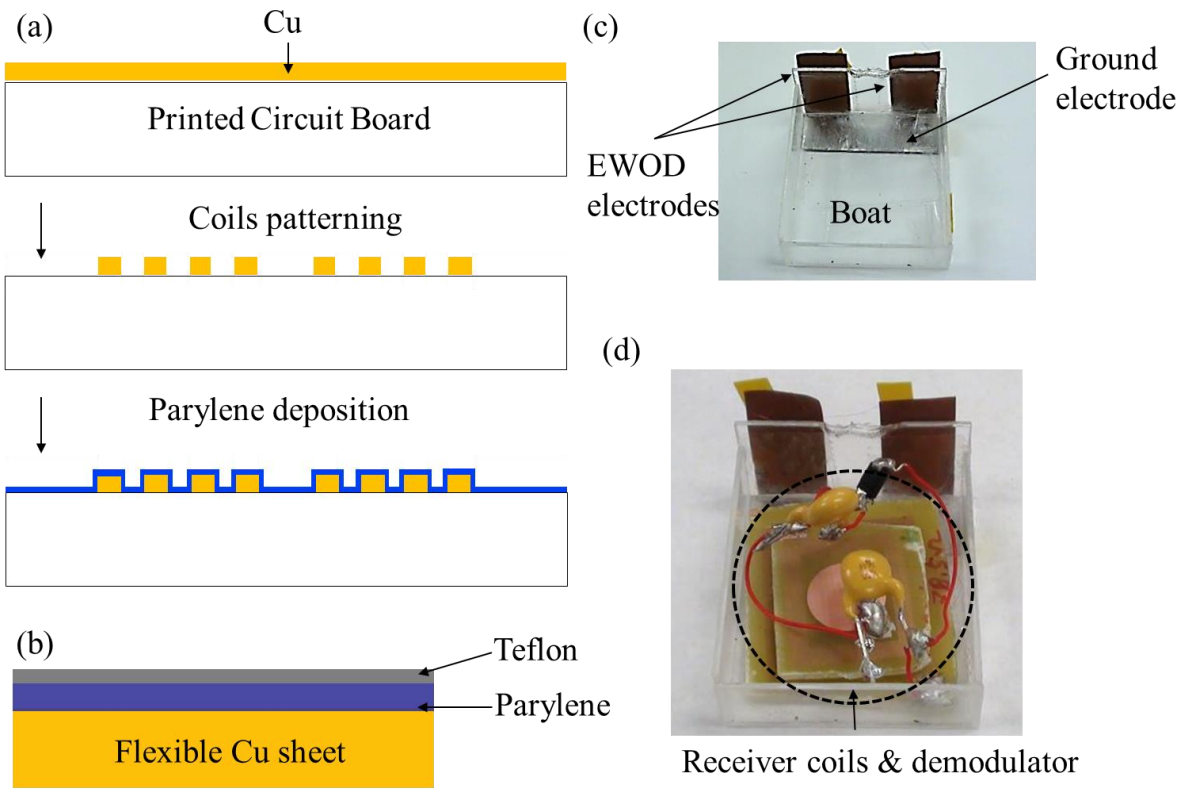

Figure 55. Microfabrication process of wireless EWOD boat: (a) Patterning of receiver coils (line width70 µm and spacing 50 µm) on Cu (15 µm) on PCB. (b) EWOD electrode (18 µm of Cu sheet.) (c) EWOD electrode and ground electrodes installed on boat. (d) Photo of wireless EWOD boat (overall dimension 3.8×3.2×1 cm^3).

An equivalent electric circuit in wireless boat is sketched in Fig. 56. The transmitter coil (similar to that of shown in Fig. 37(d)) is circular shape of 2.3 cm outer diameter and has the inductance of ~0.5 µH with 1.5 winding-turns around a ring shaped air-core ferrite, and it is connected with a capacitor (C_{tr} = 4700 pF) in parallel. The receiver circuit is composed of two planar coils in series (20 turns of L_1 = ~12 µH and 42 turns of L_2 = ~30 µH), a capacitor (C_{re} = 22 pF), and a demodulation circuit, which eventually transmits the low frequency yet high voltage to the EWOD electrodes. The demodulation circuit consists of the diode (IN5399-E3/54, Vishay General Semiconductor) and ceramic capacitor (1500 pF).

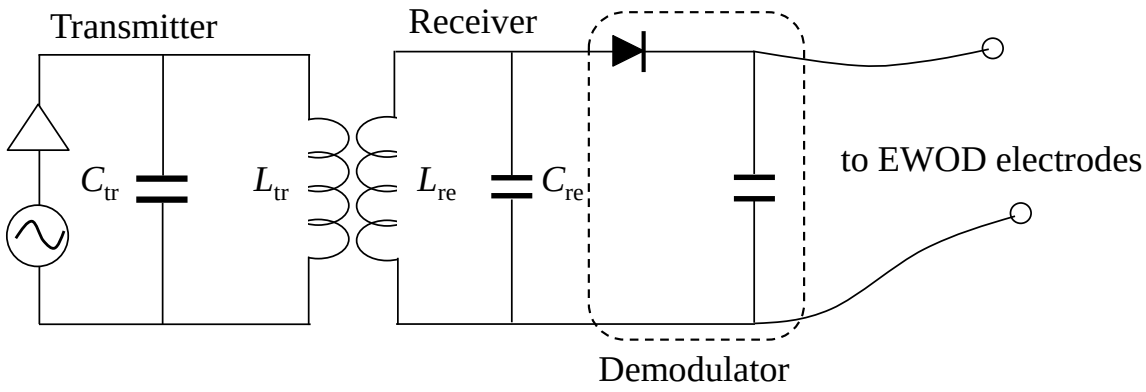

Figure 56. An equivalent electric circuit using magnetic induction. L_{tr} and C_{tr} is the inductance and capacitance of the transmitter, L_{re} and C_{re} is the inductance and capacitance of the receiver. Finally, demodulation circuit (diode and capacitor) is also installed with the wireless powering devices to transmit the low frequency yet high voltage signal to EWOD electrodes.

The overall experimental set-up for the wireless boat propulsion system is pictured in Fig. 57. The transmitter coil sitting on the position controller is directly located the bottom of the water pool and the water container is filled with ~10 mm water. The digital camera is positioned on top of the water pool to monitor the propulsion in real time. The position of transmitter coil is controlled manually while boat propulsion.

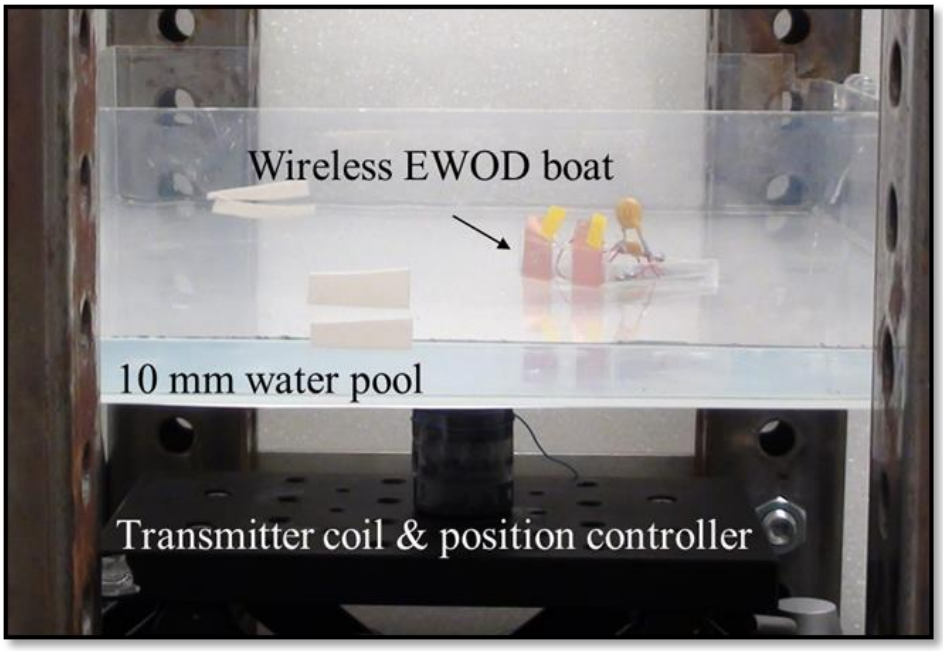

Figure 57. A photo of wireless boat propulsion set-up.

The voltage output is measured at the two terminals of the planar receiver coils after the wireless circuit installation. Fig. 58(a) shows the induced voltage at the receiver terminals over the frequency. The attainable induction voltage is 166 V at 2.7 MHz. Fig. 58(b) also shows that the separation distance (between transmitter coil and wireless receiver coils) versus the induced voltage at the receiver coil measured at 2.7 MHz. By increasing the input voltage from the function generator, the maximum attainable voltage could be increased up to 237 V when the two coils are in contact distance. Note that the measurement is performed not in the water pool but in ambient air. The induction voltage of ~100 V can be obtained up to ~1 cm of the separation distance between the transmitter coil and planar receiver coil while in center-to-center alignment.

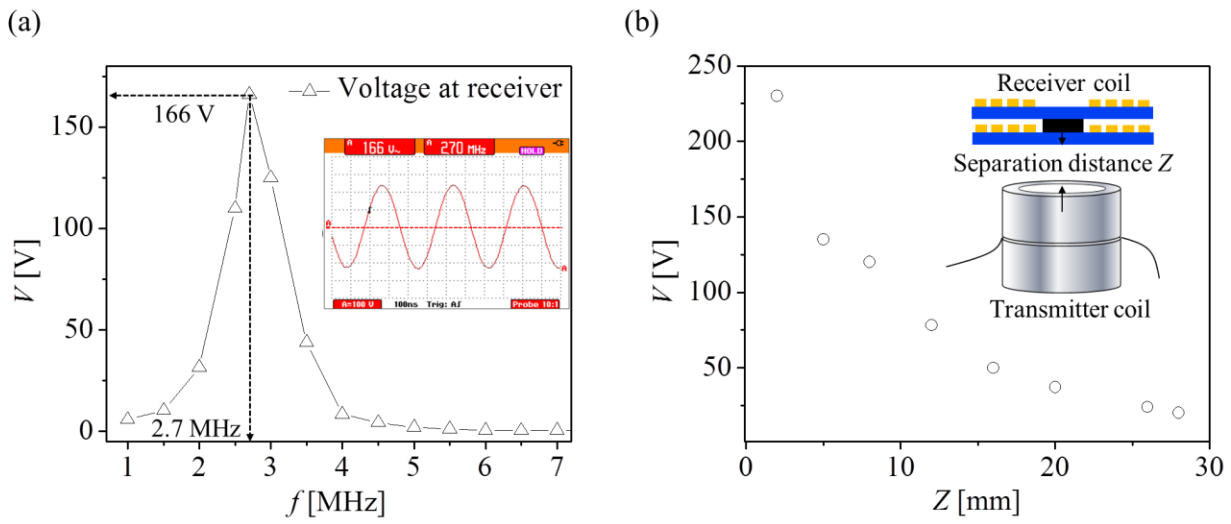

Figure 58. (a) Induced voltage at the receiver without droplet vs. the transmitting frequency. (c) Separation distance between (transmitter and planar receiver coils) on the induced voltage at the receiver (frequency=2.7 MHz).

The sequential snapshots of the boat propelled wirelessly in the water container are demonstrated in Fig. 59(a). The transmitted wireless signal (3.5 MHz of carrier frequency) is amplitude modulated with the 50 Hz of envelope. The AM signal is demodulated as the waveform shown Fig. 59(b) and eventually applied to the wireless boat. The wireless boat propels and moves forward at approximately ~5 mm/s. While in propulsion, the strong ripples on back side of boat generated by vertical oscillating at the contact line is clearly observed as shown in Fig. 59(c).

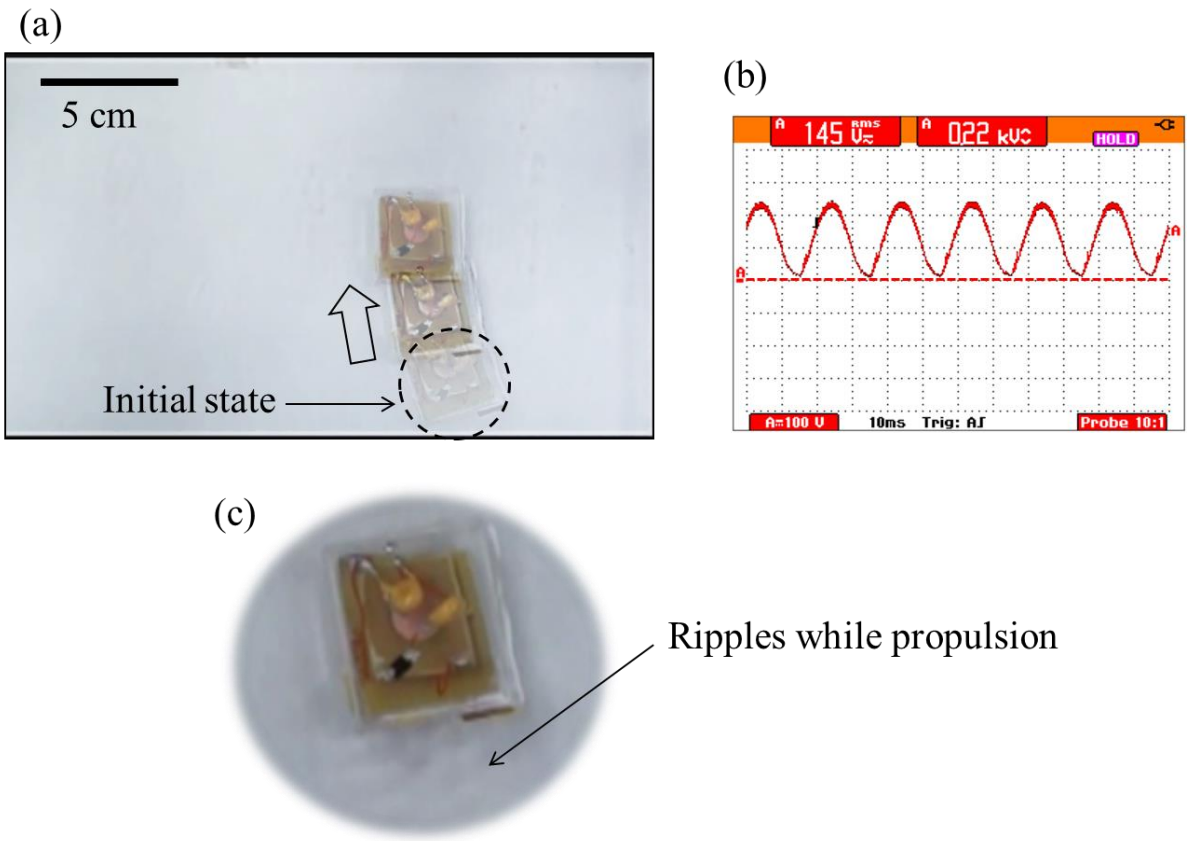

Figure 59. The sequential snapshots of wireless boat propulsion (a). The corresponding waveform after demodulation (b) 50 Hz of envelope frequency. The captured ripples on back side of boat while in propulsion (c).

5.0 CONCLUSION REMARKS

The wireless EWOD operation of droplets actuation has been experimentally demonstrated via magnetic induction. The magnetic induction which essentially utilizes AC input signal has advantages for wireless EWOD operation since EWOD responds not only DC but also AC applied signal and droplets oscillation can be easily achieved by embedding AM in the transmission signal. The higher transmission frequency is desirable to increase the induction efficiency at the receiver, however, droplet would not show any contact angle change due to voltage division over the droplet with EWOD area. As a consequence of the higher transmission frequency, the voltage at the receiver accordingly to the EWOD has to be higher than typically required EWOD voltages. This implies that the transmission frequency has to be incorporated with the given EWOD system. The inductance value that is strongly dependent of the coil's geometry is the key parameter to determine the transmission frequency. The addition of the external capacitor at the receiver circuit can be possibly avoided for simple and compact wireless EWOD in particular at the higher transmission frequency since the EWOD with droplet itself act as a capacitor.

In the mean-time, it is found that the droplet in certain condition has a function to directly respond to the low frequency envelope signal in the application of AM. This function is similar to the demodulation process. AM demodulation is an indispensable step to recover the low frequency envelope signal that is embedded in the high frequency carrier signal, however, it is

theoretically and experimentally verified that the EWOD droplet itself has the functionality of inherent AM demodulation. This means, the droplet oscillation can be achieved without addition of any artificial demodulation circuit. In practical point of view, the addition of the external demodulation circuit could be beneficial by incorporating with the magnetic induction. With the addition of the external, the EWOD can be operated with the low frequency (<1 kHz) yet high voltage.

The presented notion of wireless EWOD is possibly further extended to the area where the EWOD operation is essentially required yet seemingly believed to be hard-to-reach, to facilitate the remote and simple control of EWOD.

BIBLIOGRAPHY

[1] S.-Y. Teh, R. Lin, L.-H. Hung and A. P. Lee, Droplet microfluidics, Lab on a Chip, 8 (2008) 198-220.

[2] V. Srinivasan, V. K. Pamula and R. B. Fair, An Integrated Digital Microfluidic Lab-on-a-chip for Clinical Diagnostics on Human Physiological Fluids, Lab on a Chip, 4 (2004) 310-315.

[3] J. W. Hong and S. R. Quake, Integrated nanoliter systems, Nature Biotechnology, 21 (2003) 1179.

[4] M. G. Pollack, R. B. Fair and A. D. Shenderov, Electrowetting-based actuation of liquid droplets for microfluidic applications, Applied Physics Letters, 77 (2000) 1725-1726.

[5] S. K. Cho, H. Moon and C.-J. Kim, Creating, transporting, cutting, and merging liquid droplets by electrowetting-based actuation for digital microfluidic circuits, Journal of Microelectromechanical Systems, 12 (2003) 70-80.

[6] C.-C. Chang and R.-J. Yang, Electrokinetic mixing in microfluidic systems, Microfluidics and Nanofluidics, 3 (2007) 501-525.

[7] Y. Zhao and S. K. Cho, Microparticle sampling by electrowetting-actuated droplet sweeping, Lab on a Chip, 6 (2006) 137-144.

[8] H. Moon, S. K. Cho, R. L. Garrell and C.-J. C. J. Kim, Low voltage electrowetting-on-dielectric, Journal of Applied Physics, 92 (2002) 4080-4087.

[9] D. Y. Kim and A. J. Steckl, Electrowetting on Paper for Electronic Paper Display, ACS Applied Materials & Interfaces, 2 (2010) 3318-3323.

[10] T. Krupenkin, S. Yang and P. Mach, Tunable Liquid Microlens, Applied Physics Letters, 82 (2003) 316-318.

[11] J. W. Hong and S. R. Quake, Integrated nanoliter systems, Nature Biotechnology, 21 (2003) 1179.

[12] S. C. Jakeway, A. J. de Mello and E. L. Russell, Miniaturized total analysis systems for biological analysis, Fresenius' Journal of Analytical Chemistry, 366 (2000) 525-539.

[13] P. Paik, V. K. Pamula and R. B. Fair, Rapid droplet mixers for digital microfluidic systems, Lab on a Chip, 3 (2003) 253-259.

[14] L. Yeo, and H. C Chang, Electrowetting, Micro/Nanophysics Research Laboratory, Department of Mechanical Engineering, Monash University, (2008) 600-605.

[15] Y. Mita, Y. Li, M. Kubota, S. Morishita, W. Parkes, L. I. Haworth, B. W. Flynn, J. G. Terry, T. B. Tang, A. D. Ruthven, S. Smith and A. J. Walton, Demonstration of a Wireless Driven MEMS Pond Skater that Uses EWOD Technology, Solid-State Electronics, 53 (2009) 798-802.

[16] Y. Li, W. Parkes, L. I. Haworth, A. A. Stokes, K. R. Muir, P. Li, A. J. Collin, N. G. Hutcheon, R. Henderson, B. Rae and A. J. Walton, Anodic Ta2O5 for CMOS compatible low voltage electrowetting-on-dielectric device fabrication, Solid-State Electronics, 52 (2008) 1382-1387.

[17] S. Berry, J. Kedzierski and B. Abedian, Low voltage electrowetting using thin fluoroploymer films, Journal of Colloid and Interface Science, 303 (2006) 517-524.

[18] Y. Fouillet, D. Jary, C. Chabrol, P. Claustre and C. Peponnet, Digital microfluidic design and optimization of classic and new fluidic functions for lab on a chip systems, Microfluidics and Nanofluidics, 4 (2008) 159-165.

[19] L. Yifan, R. Y. Fu, D. Winters, B. W. Flynn, B. Parkes, D. S. Brodie, L. Yufei, J. Terry, L. I. Haworth, A. S. Bunting, J. T. M. Stevenson, S. Smith, C. L. Mackay, P. R. R. Langridge-Smith, A. A. Stokes and A. J. Walton, Test Structures for Characterizing the Integration of EWOD and SAW Technologies for Microfluidics, Semiconductor Manufacturing, IEEE Transactions on, 25 (2012) 323-330.

[20] L. Malic, D. Brassard, T. Veres and M. Tabrizian, Integration and detection of biochemical assays in digital microfluidic LOC devices, Lab on a Chip, 10 (2010) 418-431.

[21] M. G. Lippmann, Relations entre les phénomènes electriques et capillaires, Ann. Chim.Phys., 5 (1875) 494-549.

[22] J. Lee, H. Moon, J. Fowler, T. Schoellhammer and C.-J. Kim, Electrowetting and electrowetting-on-dielectric for microscale liquid handling, Sensors and Actuators A: Physical, 95 (2002) 259-268.

[23] A. R. Wheeler, Putting Electrowetting to Work, Science, 322 (2008) 539-540.

[24] B. Berge, Electrocapillarity and wetting of insulator films by water, Comptes Rendus de l'Academie des Sciences Serie II, 317 (1993) 157-163.

[25] M. Vallet, B. Berge and L. Vovelle, Electrowetting of water and aqueous solutions on poly(ethylene terephthalate) insulating films, Polymer, 37 (1996) 2465-2470.

[26] E. Seyrat and R. A. Hayes, Amorphous fluoropolymers as insulators for reversible low-voltage electrowetting, Journal of Applied Physics, 90 (2001) 1383-1386.

[27] W. J. J. Welters and L. G. J. Fokkink, Fast Electrically Switchable Capillary Effects, Langmuir, 14 (1998) 1535-1538.

[28] F. Mugele and J. Buehrle, Equilibrium drop surface profiles in electric fields, Journal of Physics Condensed Matter, 19 (2007) 375112.

[29] K. Adamiak, Capillary and electrostatic limitations to the contact angle in electrowetting-on-dielectric, Microfluidics and Nanofluidics, 2 (2006) 471-480.

[30] T. B. Jones, An electromechanical interpretation of electrowetting, Journal of Micromechanics and Microengineering, 15 (2005) 1184.

[31] K. H. Kang, How Electrostatic Fields Change Contact Angle in Electrowetting, Langmuir, 18 (2002) 10318-10322.

[32] J. Berthier and K. Brakke, Physics of Microdroplets, Wiley, Somerset, NJ, USA, 2012.

[33] A. Diana, M. Castillo, D. Brutin and T. Steinberg, Sessile Drop Wettability in Normal and Reduced Gravity, Microgravity Sci. Technol., 24 (2012) 195-202.

[34] J. Berthier, Micro and Nano Technologies : Micro-Drops and Digital Microfluidics (2nd Edition), William Andrew, Bighamton, NY, USA, 2012.

[35] V. Bahadur and S. V. Garimella, Electrowetting-Based Control of Static Droplet States on Rough Surfaces, Langmuir, 23 (2007) 4918-4924.

[36] in "Multiscale Dissipative Mechanisms and Hierarchical Surfaces" (Springer Berlin Heidelberg, 2008) p. 153-167.

[37] V. Bahadur and S. V. Garimella, Electrowetting-Based Control of Droplet Transition and Morphology on Artificially Microstructured Surfaces, Langmuir, 24 (2008) 8338-8345.

[38] N. Cañas, M. Kamperman, B. Völker, E. Kroner, R. M. McMeeking and E. Arzt, Effect of nano- and micro-roughness on adhesion of bioinspired micropatterned surfaces, Acta Biomaterialia, 8 (2012) 282-288.

[39] M. K. Chaudhury and G. M. Whitesides, How to Make Water Run Uphill, Science, 256 (1992) 1539-1541.

[40] R. Barber and D. Emerson, in "Microdroplet Technology", edited by Day, P., Manz, A. and Zhang, Y., Springer, New York (2012) pp. 77-116.

[41] M. P. A. Kumar, B. Cross, J.-C. Baret, and F. Mugele, Finite conductivity effects and apparent contact angle saturation in AC electrowetting, Materials Research Society, (2006).

[42] J. Berthier, P. Dubois, P. Clementz, P. Claustre, C. Peponnet and Y. Fouillet, Actuation potentials and capillary forces in electrowetting based microsystems, Sensors and Actuators A: Physical, 134 (2007) 471-479.

[43] J. Z. Chen, S. M. Troian, A. A. Darhuber and S. Wagner, Effect of contact angle hysteresis on thermocapillary droplet actuation, Journal of Applied Physics, 97 (2005) 014906-014909.

[44] F. Mugele and J.-C. Baret, Electrowetting: from basics to applications, Journal of Physics Condensed Matter, 17 (2005) 705-774.

[45] C. W. Extrand and Y. Kumagai, An Experimental Study of Contact Angle Hysteresis, Journal of Colloid and Interface Science, 191 (1997) 378-383.

[46] L. Gao and T. J. McCarthy, Contact Angle Hysteresis Explained, Langmuir, 22 (2006) 6234-6237.

[47] D. Schneider, A Critical Look at Wireless Power, IEEE Spectrum, (2010).

[48] A. Kurs, A. Karalis, R. Moffatt, J. D. Joannopoulos, P. Fisher and M. Soljačić, Wireless Power Transfer via Strongly Coupled Magnetic Resonances, Science, 317 (2007) 83-86.

[49] J. Hu, F. Xu, A. Q. Huang and F. G. Yuan, Optimal design of a vibration-based energy harvester using magnetostrictive material (MsM), Smart Materials and Structures, 20 (2011) 015021.

[50] S. R. Alten, Recording and Producing Audio for Media, Course Technology/Cengage Learning, Boston, MA, USA, 2011.

[51] L. S. J. Phee and M. Rasouli, Energy sources and their development for application in medical devices, Expert Review of Medical Devices, 7 (2010) 693+.

[52] A. Karalis, J. D. Joannopoulos and M. Soljačić, Efficient wireless non-radiative mid-range energy transfer, Annals of Physics, 323 (2008) 34-48.

[53] A. E. Umenei, Understanding Low Frequency Non-radiative Power Transfer, Fulton Innovation, (2011).

[54] Y. Ick-Jae and L. Hao, Investigation of Near-Field Wireless Power Transfer Under Multiple Transmitters, Antennas and Wireless Propagation Letters, IEEE, 10 (2011) 662-665.

[55] W. Fu, Zhang, B, Qiu, D and Wang, W., Analysis of Transmission Mechanism and Efficiency of Resonance Coupling Wireless Energy Transfer System, International Conference Electrical Machines and Systems, pp.2163-2168, (2008).

[56] in "McGraw-Hill Concise Encyclopedia of Science and Technology" (McGraw-Hill, 2006).

[57] Y. H. Kim, Kang, S. Y., Lee, M.L., Yu, B.G., and Zyung, T., Optimization of Wireless Power Transmission through Resonant Coupling, IEEE 6TH International Conference-Workshop Power Electronics Electrical Drives Automation and Motion, pp.1069-1073, (2010).

[58] J. R. Brauer, Magnetic Actuators and Sensors, John Wiley and Sons, Milwaukee, Wisconsin, USA, 2006.

[59] E. F. Fuchs and M. A. S. Masoum, Power Quality in Power Systems and Electrical Machines, (Elsevier).

[60] C. D. Meyer, S. S. Bedair, B. C. Morgan and D. P. Arnold, High-Inductance-Density, Air-Core, Power Inductors, and Transformers Designed for Operation at 100~500 MHz, Magnetics, IEEE Transactions on, 46 (2010) 2236-2239.

[61] F. S. Crawford, Mutual inductance M: An elementary derivation, American Journal of Physics, 60 (1992) 186-186.

[62] R. Puers, K. Schuylenbergh, M. Catrysse and B. Hermans, in "Analog Circuit Design", edited by Steyaert, M., Huijsing, J. H. and van Roermund, A. H. M. (Springer Netherlands, 2006) p. 395-414.

[63] in "Low Power VCO Design in CMOS", edited by Itoh, K., Lee, T., Sakurai, T., Sansen, W. C. and Schmitt-Landsiedel, D. (Springer Berlin Heidelberg, 2006) p. 39-54.

[64] N. Pamme, Magnetism and microfluidics, Lab on a Chip, 6 (2006) 24-38.

[65] H. L. Kao and T. Chang, Integrated the inductors on ultra-thin Si substrate to improve the RF performance for low-noise amplifier applications, Microwave and Optical Technology Letters, 52 (2010) 1576-1579.

[66] H. Contopanagos and A. G. Nassiopoulou, Integrated inductors on porous silicon, physica status solidi (a), 204 (2007) 1454-1458.

[67] C. Tung-Sheng, J. D. S. Deng, L. Chih-Yuan and K. Chin-Hsing, Improved performance of Si-based spiral inductors, Microwave and Wireless Components Letters, IEEE, 14 (2004) 466-468.

[68] Our Thanks to Reviewers IEEE Transactions on Advanced Packaging, Advanced Packaging, IEEE Transactions on, 32 (2009) 709-710.

[69] S. S. Mohan, M. del Mar Hershenson, S. P. Boyd and T. H. Lee, Simple accurate expressions for planar spiral inductances, Solid-State Circuits, IEEE Journal of, 34 (1999) 1419-1424.

[70] J. M. Oh, S. H. Ko and K. H. Kang, Shape Oscillation of a Drop in ac Electrowetting, Langmuir, 24 (2008) 8379-8386.

[71] F. Li and F. Mugele, How to make sticky surfaces slippery: Contact angle hysteresis in electrowetting with alternating voltage, Applied Physics Letters, 92 (2008) 244108-244103.

[72] Y. Nanayakkara and D. Armstrong, A liquid drop RC filter apparatus for detection, Analytical and Bioanalytical Chemistry, 401 (2011) 2669-2678.

[73] D. Klarman, D. Andelman and M. Urbakh, A Model of Electrowetting, Reversed Electrowetting, and Contact Angle Saturation, Langmuir, 27 (2011) 6031-6041.

[74] Y. S. Nanayakkara, H. Moon and D. W. Armstrong, A Tunable Ionic Liquid Based RC Filter Using Electrowetting: A New Concept, ACS Applied Materials & Interfaces, 2 (2010) 1785-1787.

[75] A. Quinn, R. Sedev and J. Ralston, Influence of the Electrical Double Layer in Electrowetting, The Journal of Physical Chemistry B, 107 (2003) 1163-1169.

[76] J. Hong, S. Ko, K. Kang and I. Kang, A numerical investigation on AC electrowetting of a droplet, Microfluidics and Nanofluidics, 5 (2008) 263-271.

[77] C. Decamps and J. De Coninck, Dynamics of Spontaneous Spreading under Electrowetting Conditions, Langmuir, 16 (2000) 10150-10153.

[78] T. B. Jones, J. D. Fowler, Y. S. Chang and C.-J. Kim, Frequency-Based Relationship of Electrowetting and Dielectrophoretic Liquid Microactuation, Langmuir, 19 (2003) 7646-7651.

[79] T. B. Jones, On the Relationship of Dielectrophoresis and Electrowetting, Langmuir, 18 (2002) 4437-4443.

[80] D. Chatterjee, H. Shepherd and R. L. Garrell, Electromechanical model for actuating liquids in a two-plate droplet microfluidic device, Lab on a Chip, 9 (2009) 1219-1229.

[81] D. Chatterjee, B. Hetayothin, A. R. Wheeler, D. J. King and R. L. Garrell, Droplet-based microfluidics with nonaqueous solvents and solutions, Lab on a Chip, 6 (2006) 199-206.

[82] M. G. Yoon, S. H. Byun and S. K. Cho, Inherent amplitude demodulation of an AC-EWOD (electrowetting on dielectric) droplet, Lab on a Chip, 13 (2013) 662-668.

[83] E. McCune, Practical Digital Wireless Signals, Cambridge University Press, Cambridge, GBR, 2010.

[84] M. S. Alencar and V. C. Rocha, Amplitude Modulation Communication Systems, Springer US, 2005.

[85] W. D. Greason, Electrostatic discharge in electronics, Research Studies Press, 1992.

[86] Y. L. Chow and M. M. Yovanovich, The shape factor of the capacitance of a conductor, Journal of Applied Physics, 53 (1982) 8470-8475.

[87] H. Rathgen and F. Mugele, Microscopic shape and contact angle measurement at a superhydrophobic surface, Faraday Discussions, 146 (2010) 49-56.

[88] R. Gupta, D. M. Sheth, T. K. Boone, A. B. Sevilla and J. Fréchette, Impact of Pinning of the Triple Contact Line on Electrowetting Performance, Langmuir, 27 (2011) 14923-14929.

[89] H. A. Burge, D. L. Pierson, T. O. Groves, K. F. Strawn and S. K. Mishra, Dynamics of Airborne Fungal Populations in a Large Office Building, Current Microbiology, 40 (2000) 10-16.

[90] S. Król, B. Zabiegała and J. Namieśnik, PBDEs in environmental samples: Sampling and analysis, Talanta, 93 (2012) 1-17.

[91] Y. Zhao, Microparticle sampling and separation enabled by droplet microfluidics, Swanson School of Engineering, Mechanical Engineering, University of Pittsburgh, (2008).

[92] S. K. Chung, K. Ryu and S. K. Cho, Electrowetting propulsion of water-floating objects, Applied Physics Letters, 95 (2009) 014107-014103.

[93] J. Yuan and S. Cho, Bio-inspired micro/mini propulsion at air-water interface: A review, J Mech Sci Technol, 26 (2012) 3761-3768.